An Investigation of the Tensile Strength and Stiffness of Unidirectional Polymer-Matrix, Carbon-Fiber Composites under the Influence of Elevated Temperatures

By
Brady M. Walther

Thesis submitted to the Faculty of the
Virginia Polytechnic Institute and State University
in Partial fulfillment of the requirements for the degree of
Master of Science
In
Engineering Mechanics

APPROVED

_____
Ken Reifsnider, Chairman

_____ _____
John J. Lesko David Gao

May 27, 1998
Blacksburg, Virginia

An investigation of the Tensile Strength and Stiffness of Unidirectional Polymer-Matrix, Carbon-Fiber Composites under the Influence of Elevated Temperatures

By
Brady M. Walther

(ABSTRACT)

Traditionally it was thought that the unidirectional strength in the fiber direction of fiber dominated composites was not influenced by the matrix material. As long as the fiber was not affected then the strength would remain. However this thesis will challenge that belief. The unidirectional strength in the fiber direction of fiber dominated composites is influenced by the matrix material.

Currently some companies in the industry that design with polymer-carbon fiber composites use a "knock down" factor on mechanical properties to account for the effect of environment or elevated temperatures. For example, the failure strength of a composite is reduced by some arbitrary factor such as ten percent for the adverse environmental condition that the system will encounter. If the composite must operate at elevated temperatures, then the design failure strength will reflect this condition with some arbitrary reduction. This reduction may be too aggressive or not aggressive enough for some composite systems and conditions, and does not reflect the details of the material or the situation.

To avoid grossly over or under designing with a "knock down" factor, many companies will invest money and time to determine the macro-mechanical response of a particular composite system under the expected service conditions. This is a large

investment because every specific material and each new system that is considered must be tested. However, if a general understanding of the effect of elevated temperatures on the tensile strength of polymer-carbon fiber composites can be developed, then this will save money and time because the physics and mechanics can be applied independently for all specific matrix materials and conditions.

This study investigated the micro-mechanical constituent properties that were thought to be affected by elevated temperatures. Then micro-mechanical equations were changed to reflect this effect and used to calculate the macro-mechanical tensile strength of the composite. These predictions were compared with macro-mechanical tensile strength data obtained under the influence of elevated temperatures. The composite systems in this study were unidirectional continuous carbon fibers in a polymer matrix.

The object of this study was to examine the quasi-static tensile strength of unidirectional polymer composites, and then use current analytic models to predict the experimental results. The strength and stiffness properties were measured in different temperature environments. The temperature environments ranged from -184.4 degrees Celsius to 220 degrees Celsius. New arguments were added to the current models to express the physics and mechanics of the tensile strength problem at different temperatures. The macro-mechanical and micro-mechanical effects were studied with different composite systems. However, all the systems had polymer matrixes with carbon fibers. The different matrix materials were polyphenylene sulfide (PPS), vinyl ester with two different fiber-matrix interface materials, and polyether ether ketone (PEEK). The different material systems were examined for comparisons to analytic models and to add to the database for these material systems.

As much information was obtained about the processing procedures of each of the material systems as possible. Then mechanical tests were preformed to determine the temperature response of the strength and stiffness of each material system. Finial observations were made about the behavior of material systems.

Current research and development has produced models for the prediction of the strength of unidirectional composites. These models are essential for the design and use for these types of material in the industry. The current micro-mechanical models describe the strength of a unidirectional polymer composite in the tensile direction. However, these models do not explicitly account for different temperature environments. Therefore, the models were developed to include the effect of elevated temperature on strength.

ACKNOWLEDGMENTS

The author would like to thank the following people for their involvement to this work:

- Dr. Ken L. Reifsnider, for all of the time and support he spent on this project. He is a true inspiration and role model for all young engineers.
- Dr. David Gao and Dr. John Lesko, for serving as committee members and for helping to edit this document.
- Dr. Scott Case, for all of his time and effort helping this work become complete.
- National Science Foundation and the Air Force, for the funding of this work and the educational opportunity.
- Members of the MRG at Virginia Tech, for the support and help in the lab.
- Mac McCord, for all the days that the lab equipment needed setting up.
- Danny Reed, for the open use of the fabrication lab.
- Shelia Collins, for the know how of getting things done under pressure.
- The authors parents, for all their help in keeping things possible.

Table of Content

List of Tables ..... **viii**

List of Figures ..... **x**

I. Introduction and Literature Review **1**
Literature Review 3
Strength 3
General Formulation of Strength Models 5
Model One 5
Model Two 17
Quantitative Differences between the Models 25
Temperature Effects on the Strength 25
Interfacial Shear Strength at Elevated Temperatures 30
Bulk Polymer Stiffness at Elevated Temperatures 33
Mechanical Properties for Materials 33

II. Experimental Procedures **35**
General Equipment 35
XPS 35
Fiber Volume Fraction Analysis 36
C-Scans 36
DMA 37
Quasi-static Tension Macro-Mechanical Test 37
Materials 39
Polyphenylene Sulfide (PPS) Composite 39
General Description 39
Processing 40
Specimen Preparation 40
Vinyl Ester Composite 42
General Description 42
Processing 43
Specimen Preparation 43
Polyether Ether Ketone (PEEK) Composite 44
General Description 44
Processing 45
Specimen Preparation 45

III. Experimental Results and Discussion 48
Polyphenylene Sulfide (PPS) Composite 48
Fiber Volume Fracture 48
XPS 48
DMA 49
Results of Macro-Mechanical Test 50
Fracture Modes 59
Vinyl Ester 61
Fiber Volume Fracture 61
Results of Macro-Mechanical Test 62
Fracture Modes 69
PEEK 74
Fiber Volume Fracture 74
Results of Macro-Mechanical Test 75
Fracture Modes 83
Summary of Experimental Results 83

IV. Model Development and Prediction of Experimental Results 85
Parametric Study 85
Changes to Model Parameters for Elevated Temperature 86
Model Predictions of Strength at Elevated Temperature 90

V. Summary, Conclusions, and Future Work 95
Summary of Method 95
Conclusions 95
Future Work 96

References 100

Appendix A: PPS RAW DATA 102

Appendix B: PEEK RAW DATA 108

Appendix C: VINYL ESTER RAW DATA 110

VITA 112

List of Tables

Table 1.01 Summary of mechanics parameter for AS-4 carbon fiber 34

Table 1.02 Properties of thermoplastics PEEK and PPS 34

Table 2.01 Sample quantity and testing temperature distribution: loading rate of 50 pounds per second..... 41

Table 2.02 Sample quantity and testing temperature distribution: loading rate of 40 pounds per second..... 41

Table 2.03 Sample quantity and testing temperature distribution: loading rate of 150 pounds per second..... 41

Table 3.01 Results of the fiber volume fracture measurements for PPS matrix composite 48

Table 3.02 Results from all PPS composite (PCI) tension tests- @ all loading rates 52

Table 3.03 Volume fracture measurements for vinyl ester matrix composite with an epoxy fiber-matrix interface..... 61

Table 3.04 Strength and stiffness results of vinyl ester composite with an epoxy fiber-matrix interface..... 62

Table 3.05 Strength and stiffness results of vinyl ester composite with a polyurethane fiber-matrix interface..... 63

Table 3.06 Results of fiber volume fraction test for PEEK matrix composite..... 74

Table 3.07 Strength and stiffness results for PEEK matrix composite 76

Table 4.01 Input variables for the micro-mechanical models for PPS composite 91

Table 4.02 Input variables for the micro-mechanical models for PEEK composite 91

Table 4.03 Model strength results for the PPS composite system 92

Table 4.04 Model strength results for the PEEK composite system 92

List of Figures

Figure 1.01 Batdorf Q-plot where composite failure occurs at the point of instability 8

Figure 1.02 Fiber fracture of unidirectional composites used by Gao and Reifsnider 10

Figure 1.03 Schematic of concentric cylinder model with a core of broken fibers with the neighboring fibers 18

Figure 1.04 Tensile strength as a function of local ineffective length 28

Figure 1.05 Unidirectional tensile strength as a function of temperature for two polymer carbon fiber composites 29

Figure 1.06 Interfacial shear strength as a function of temperature from single fragmentation test/ Epon 828 DU-700 32

Figure 1.07 Interfacial shear strength as a function of temperature from single fragmentation test/ Epon 828 mPDA 32

Figure 1.08 Bulk Epon 828 stress-strain curves at elevated temperatures 33

Figure 2.01 MTS with heater box set up with a specimen 38

Figure 2.02 Cryogenic chamber for quasi-static tension test 39

Figure 2.03 Drawing of a typical test specimens for PPS system 42

Figure 2.04 Drawing of a typical test specimen for vinyl ester system 44

Figure 2.05 Processing diagram for PEEK composite 45

Figure 2.06 Dimensional drawling of PEEK specimens 46

Figure 2.07 Photograph of PEEK specimens illustrating end tabs, extensometer tabs, and strain gage placement 47

Figure 3.01 DMA Result for PPS matrix composite system..... 49

Figure 3.02 Stress-strain calibration of extensometer with strain gage strain measurements..... 51

Figure 3.03 Stress-strain curve for PPS composite material..... 52

Figure 3.04 A plot of the strength values for the PPS composite material with their respective temperatures with standard deviations as error bars..... 53

Figure 3.05 Young's modulus for PPS composite system with all loading rates.. 54

Figure 3.06 A bar graph of the strength of PPS Composite (same data that makes up Figure 3.04)..... 55

Figure 3.07 A bar graph of Young's modulus for the PPS carbon fiber composite 55

Figure 3.08 The strength of PPS composite differentiating load rates of 40,50, and 150 pounds per sec 56

Figure 3.09 All strength data on PPS composite, data without strain measurements..... 57

Figure 3.10 A family of stress-strain curves for PPS composites at four different temperatures (30, 90, 110, and 130 degrees Celsius)..... 58

Figure 3.11 Strength of PPS composite at elevated temperatures and cryogenic temperatures 59

Figure 3.12 Fracture of PPS specimen at 31.1 degrees Celsius (Front and Side Views) 60

Figure 3.13 Fracture of PPS specimen at 229 degrees Celsius (Front and Side Views) 61

Figure 3.14 Stress-strain curve for vinyl ester with polyurethane interface 63

Figure 3.15 Stress-strain curve for vinyl ester with epoxy interface 64

Figure 3.16 Strength of vinyl ester composite as a function of temperature and two different interfaces..... 65

Figure 3.17 Stiffness of vinyl ester composite as a function of temperature and two different interfaces..... 66

Figure 3.18 A family of stress-strain curves for vinyl ester composite with an epoxy fiber-matrix interface at different temperatures (90, 140,35,110, and 130 Degrees C) 67

Figure 3.19 Strength for vinyl ester composite with both interfaces at elevated temperatures and cryogenic temperatures 68

Figure 3.20 Stiffness values of the vinyl ester composite with both fiber-matrix interfaces at elevated temperature and cryogenic temperatures 69

Figure 3.21 Fracture of a vinyl ester specimen with polyurethane fiber-matrix interface at 33.4 degrees Celsius (Front and Side Views)..... 70

Figure 3.22 Fracture of a vinyl ester specimen with polyurethane fiber-matrix interface at 149.7 degrees Celsius (Front and Side Views)..... 71

Figure 3.23 Fracture of a vinyl ester specimen with polyurethane fiber-matrix interface at -184.4 degrees Celsius (Front and Side Views) 72

Figure 3.24 Fracture of a vinyl ester specimen with epoxy fiber-matrix interface at 35 degrees Celsius (Front and Side Views)..... 73

Figure 3.25 Fracture of a vinyl ester specimen with epoxy fiber-matrix interface at 140 degrees Celsius (Front and Side Views)..... 74

Figure 3.26 C-Scan of PEEK matrix composite 75

Figure 3.27 Stress-strain curve for PEEK matrix composite at 150 degrees C 77

Figure 3.28 Stress-strain curve of a PEEK matrix composite at 100 degrees C ... 77

Figure 3.29 Stress-strain curve for PEEK matrix composite at 27 degrees C 78

Figure 3.30 A family of stress-strain curves for PEEK matrix at different temperatures (27, 90, and 170 Degrees C) 78

Figure 3.31 Strength values of PEEK matrix composite at elevated temperatures 80

Figure 3.32 Stiffness values for PEEK matrix composite measured with an extensometer..... 80

Figure 3.33 Stiffness of PEEK matrix composite measured with a strain gage.... 81

Figure 3.34 Average strength of PEEK matrix composite with standard deviations 82

Figure 3.35 Stiffness of PEEK matrix composite with standard deviations 82

Figure 4.01 Parametric study of the interfacial shear strength effect on strength of a composite 86

Figure 4.02 Approximation of the interfacial shear strength as a function of temperature for a PPS composite system 87

Figure 4.03 Approximation of the shear modulus as a function of temperature for the PPS matrix 88

Figure 4.04 Approximation to the interfacial shear strength as a function of temperature for PEEK composite system..... 89

Figure 4.05 Approximation of the shear modulus for PEEK as a function of temperature..... 90

Figure 4.06 Experimental data for PPS compared to model predictions of strength..... 92

Figure 4.07 Experimental data for PEEK composite compared to model predictions of strength..... 94

Figure 5.01 Processing for 350 degrees F cure cycle for toughened epoxy..... 98

Figure 5.02 Processing for 250 degrees F cure cycle for toughened epoxy..... 99

I. Introduction and Literature Review

In the past decade polymer based composites have provided a high strength to weight ratio. Many applications in the aerospace industry have benefited from these materials. However, in many cases the majority of the material has been placed in the structures as non-load-bearing members. In order to use composite materials as load-bearing members, the design parameters must be fully described. This description is very complex because of the nature of the composite system. Unlike steel or alloys, a composite system is anisotropic and heterogeneous material. In addition, the properties are sensitive to environmental conditions such as humidity, temperature, loading rates and aging.

However, much has been done in the area of describing such materials for design. One of the most important parameters for design is strength. This is generally defined by the condition where the material experiences a load and completely fails or fractures under that load. The micro-mechanics of this failure can be described to predict to the macro-mechanical failure strength. Two particular micro-mechanical models are described below. This paper focuses on the strength of composite systems under the effect of elevated temperature. In addition to strength, the stiffness of the system was

measured at elevated temperatures. The effects on the stiffness will be reported; however, the main focus was on the strength.

The literature review of this paper is intended to give the reader a general understanding of the strength of unidirectional composites. The major portion of the review describes the mathematical models used to predict the tensile strength of a composite system. These are not the only micro-mechanical models that exist.

These models evaluate the system at the micro-mechanical level, unlike traditional classical laminate theory. Some background information is given about the philosophy behind the models. However the background information is not extensive. This thesis focuses on using the existing models and comparing them to experimental data. The fundamental mathematics will not be changed in the models. However, the mathematical parameters, that are expected to be affected by elevated temperatures, will be developed to reflect this change.

The reporting of the experimental work will follow the literature review. Not only will these data serve to explore the theoretical models but will also add to the library of data for polymer composites and environmental effects. The next section is the development of the micro-mechanical models to allow for elevated temperatures in predicting strength. The micro-mechanical parameters are developed for the effect of elevated temperatures and strength predictions are made with these developments. The predictions are compared to the experimental data to test their validity.

Literature Review

Strength

Micro-mechanics models have evolved to predict the tensile strength of unidirectional composites. For the past two decades several researchers have studied tensile failure and strength. Weibull used the weakest link theory to predict the fracture of a single fiber. This theory was developed because Weibull discovered that the tensile strength of a single fiber was not uniform from point to point. Coleman, Rosen, and Hahn studied the fracture of a bundle of fibers [1]. Rosen calculated the bundle strength assuming that the statistical distribution of strength of the fibers governs the failure of each fiber. Therefore, the failure of the bundle of fibers is due to the statistical accumulation of fiber fractures in the system.

Zweben and Rosen related the failure of the fiber bundles in the company of the matrix material. They used the ineffective length to estimate the tensile strength. This was based on shear lag analysis. However, this model did not consider the effects of stress concentrations in the fibers adjacent to the broken fiber [1].

Batdorf showed that the stress concentrations in the adjacent fiber would lead to the accumulation of fiber fractures and this would lead to final (ultimate) failure of the composite [1]. His model uses the argument of the accumulation of a critical number of fiber fractures called “i-plets” leads to instability. The load level at which the instability occurs is the failure strength of the laminate.

These models lead us to the point that tensile strength of unidirectional composites is based on the ineffective length and stress concentration effects near fiber

fractures; both of these quantities are functions of the fiber and matrix elastic moduli. However, to this point the models do not consider the effects of the fiber-matrix interface. Resent experiments show that the strength can be improved considerably by changing the fiber matrix bonding.

Reifsnider postulated that the assumption of a perfect elastic matrix does not reflect the problem accurately. The high stress concentration in the matrix material near the broken fiber could lead to local matrix plasticity or debonding of the fiber matrix interface. Therefore, Reifsnider constructed a model that allows for elasto-plastic matrix deformation near fiber fractures. This model predicts an optimum interfacial strength value for which the tensile strength will be maximized [1].

When bonding between the fiber and the matrix is poor, there is an inefficient load transfer between the matrix and fiber. This may cause the matrix not to completely transfer the load to the fiber. If the load remains in the matrix the ultimate strength should decrease. Experimental results demonstrate this response; Madhukar and Drzal observed over a 10% decrease longitudinal stiffness going from an untreated fiber to a surface treated fiber [1]. This indicates that varying the interface can alter the longitudinal stiffness. The data indicated that if the transfer of load is 100% efficient then the experimental strength is comparable to the role of mixtures. However 100% transfer is theoretical.

In order to allow for this transfer effectiveness, Reifsnider introduces a new variable called “efficiency” to account for the interface interaction. This variable is determined by experimental results.

General Formulation of Strength Models

This section describes the formulation of two models that are based on the shear lag approach to tensile strength in the fiber direction. It is important to understand some of the assumptions that are made in the models. The first model is similar to that developed by Reifsnider and Gao (Model 1) and is included in MRLife10 (a life prediction code developed by the Materials Response Group at Virginia Tech) [2]. Reifsnider and Subramanian (Model 2) developed the second model [1]. For the most part, each of the models derived the strength representation with the same basic arguments. However, there are some minor differences between the two models. Let us take a look at each approach and the arguments made.

Model One

Gao and Reifsnider's model (Model 1) was derived for the unidirectional tensile strength of a polymer matrix composite material. It is based on the probability analysis that Batdorf used in 1982 [3]. Batdorf bases his analysis on the assumption that damage in the composite due to an applied load consists solely of breaks in the fibers. The composite is made of N fibers of length L that are held together by a matrix material. A single isolated break was called a singlet, pairs of breaks doublets, and in general an *i*-plet for all adjacent breaks of *i* fibers. Each of these breaks create a stress concentration factor c_i in the plane of the fiber break. That stress concentration is affected by the relative geometry of the unbroken fiber (fracture mechanics) and the material properties; however, this acts over a distance δ, called the ineffective length. Next, Batdorf assumes

that the fiber failure is governed by a two-parameter Weibull representation. When a stress is applied to a fiber of length L, the probability of the failure is given by

$$P_f(\sigma) = 1 - \exp\left[-\frac{L}{l_o}\left(\frac{\sigma}{\sigma_o}\right)^m \right] \quad \textbf{1}$$

P_f = The probability of failure
L = Fiber length
σ_o = Weibull characteristic value
m = Weibull modulus
l_o = Reference length
σ = The applied stress

However, if P_f is very small (<<1) then, Batdorf approximates the above equation by

$$P_f = \frac{L}{l_o}\left(\frac{\sigma}{\sigma_o}\right)^m \quad \textbf{2}$$

To calculate the number of singlets, Q_1, is multiplying the probability of failure given by Equation 3 so that

$$Q_1 = NP_f = N\frac{l}{l_o}\left(\frac{\sigma}{\sigma_o}\right)^m$$

$$Q_1 = \text{Number of singlets} \quad \textbf{3}$$

Next we assume that the stress concentration in the neighboring fibers varies with a linear behavior from c_1 to unity over a distance $\delta_1/2$, the ineffective length divided by two. This functional variation may be expressed as:

$$f(z) = c_1 + \frac{z}{\delta_1/2}(1 - c_1) \quad \textbf{4}$$

Reifsnider expressed the reliability of the fiber having a stress variation of this type given by:

$$R = \exp\left[-\left(\frac{\sigma}{\sigma_{ao}} \right)^{m} \right] \qquad \textbf{5}$$

where the variable σ_{ao} is defined by intergration over the length of the fiber.

$$\sigma_{ao} = \sigma_{o} \left(\int_{o}^{L} [f(z)]^{m} \, dz \right)^{\frac{-1}{m}} \qquad \textbf{6}$$

Now these relations can be combined in equation 4 to show that the probability of failure in the over-stressed region may be approximated by:

$$P_1 \approx \frac{\lambda_1}{l_o} \left(c_1 \frac{\sigma}{\sigma_o} \right)^{m} \qquad \textbf{7}$$

where the variable λ_1 contains the distance (ineffective length) and stress concentration.

$$\lambda_1 = \delta_1 \frac{c_1^{m+1} - 1}{c_1^{m} (c_1 - 1)(m+1)} \qquad \textbf{8}$$

Next the development considers the probability that a singlet becomes a doublet. If there are n_1 nearest neighbors, then this probability is given by:

$$P_{1 \to 2} = n_1 \frac{\lambda_1}{l_o} \left(c_1 \frac{\sigma}{\sigma_o} \right)^{m} \qquad \textbf{9}$$

Using equation 3, an estimate of the number of doublets is derived as:

$$Q_2 = \mathrm{Q}_1 n_1 \frac{\lambda_1}{\mathrm{l}_\mathrm{o}} \left(c \frac{\sigma}{\sigma_\mathrm{o}} \right)^m \qquad \textbf{10}$$

Repeating this process leads to a general model to estimate the number of i-plets:

$$Q_{i+1} = \mathrm{Q}_\mathrm{i} n_i \frac{\lambda_\mathrm{i}}{\mathrm{l}_\mathrm{o}} \left(c_i \frac{\sigma}{\sigma_\mathrm{o}} \right)^m \qquad \textbf{11}$$

or as

$$Q_i = \mathrm{N} \frac{\mathrm{L}}{\mathrm{l}_\mathrm{o}} \left(\frac{\sigma}{\sigma_o} \right)^{im} \prod_{j=1}^{i-1} c_j^m n_j \frac{\lambda_j}{l_o} \qquad \textbf{12}$$

The above equations are based by Batdorf (Equations 1-12). A log-log plot of Q_i versus stress (sigma) has a slope of im [2]. This is shown in Figure 1.01.

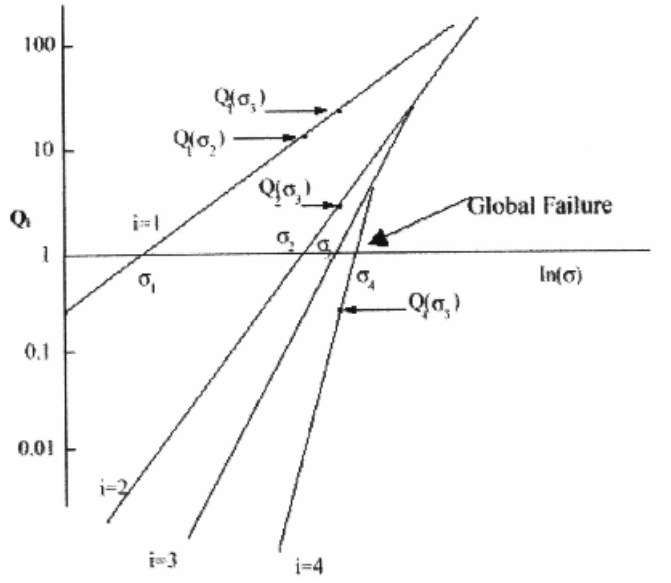

Figure 1.01 Batdorf Q-plot where composite failure occurs at the point of instability.

The failure stress is given by the lowest stress at which any unstable i-plet is formed. Therefore, the stress at which the envelope intersects the horizontal line $Q_i = 1$ or $\ln Q_i = 0$, is the failure stress. The only thing left to determine are the stress concentrations and the ineffective lengths for each number of adjacent fiber fractures. Gao and Reifsnider used a shear-lag model to determine these two values [3].

Gao and Reifsnider start by making an assumption that there is a central core of broken fibers as shown in Figure 1.02 [3]. The broken fiber are surrounded by unbroken fibers that are being strained. The core of broken fibers is assumed to be a homogeneous material whose Young's modulus is obtained by the rule of mixtures. The assumed circular cross sectional areas of the equivalent broken core is equal to the total area of the ith concentric cylinder of radius $r_f + d$.

$$\pi r_o^2 = i\pi(r_f + d)^2 = iA_f + iA_m$$
$$r_f = \text{the radius of the fiber}$$
$$d = \text{half of the width of matrix region} \qquad \textbf{13}$$

The variables correspond to the concentric cylinder model given in Figure 1.02 [4].

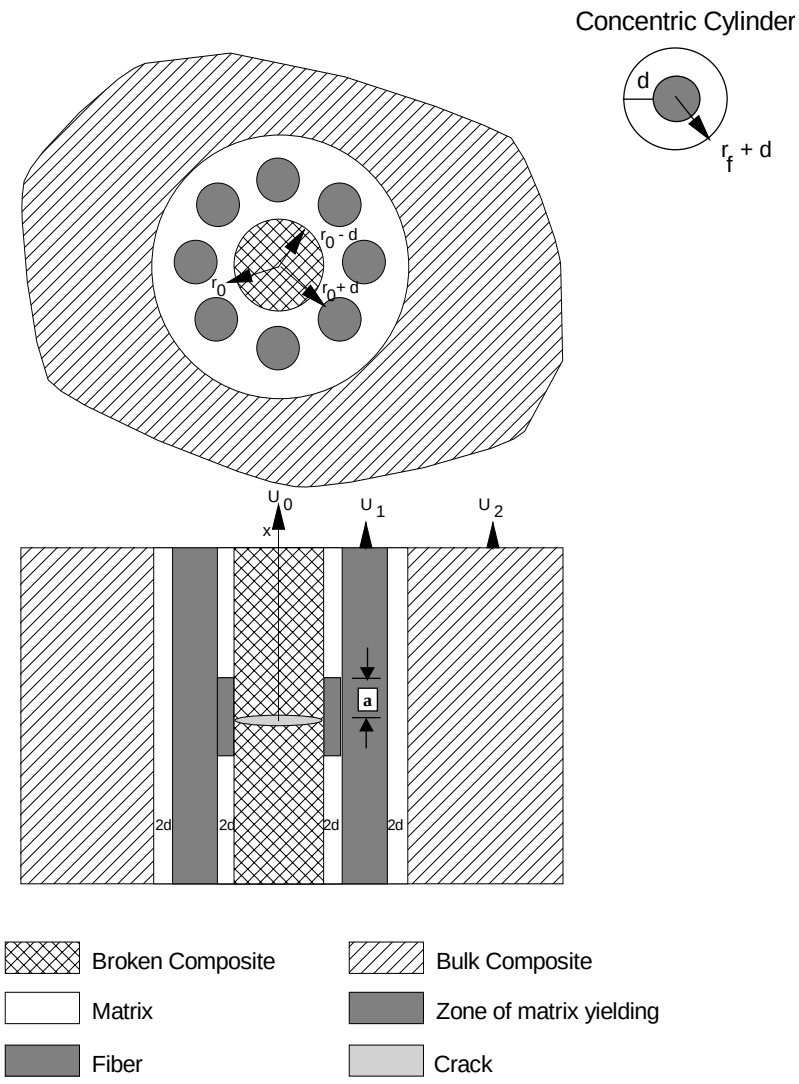

Figure 1.02 Fiber fracture of unidirectional composites used by Gao and Reifsnider.

The fiber area and matrix area are given by:

$$A_f = \pi r_f^2 \qquad \textbf{14}$$

$$A_m = \pi(\mathrm{r_f} + \mathrm{d})^2 - \pi r_f^2 \qquad \textbf{15}$$

The number of neighboring unbroken fibers, n_i, is dependent upon the number of broken fibers, i. The assumption is made that only the fibers carry the axial stress and the

matrix only supports shear (the classical shear lag assumptions). The distance measurement "*a*" gives the half-length of the region of matrix and/or interfacial yielding. The equilibrium equations for this region of the matrix and interfacial yielding are given as:

$$E\pi(r_o - d)^2 \frac{d^2U_o}{dx^2} - 2\pi r_o \eta \tau_o = 0$$

$$n_i A_f E_f \frac{d^2U_1}{dx^2} + 2\pi(r_o + 2d + 2r_f)\frac{G_m}{2d}(U_2 - U_1) + 2\pi r_o \eta \tau_o = 0$$

$$0 \le x \le a \qquad \textbf{16}$$

U_o = Displacements of the broken core
U_1 = Displacements of neighboring unbroken fiber
U_2 = Displacements of average composite
E_f = Young's modulus of the fiber
G_m = Shear modulus of the matrix
A_f = Area of the fiber
τ_o = Yielding stress of the matrix and interface
η = a shear parameter, efficiency factor

The efficiency factor parameter defines the efficiency nature of the shear transfer in the inelastic region. This parameter has the value between one and zero with zero being no shear stress transfer between broken fibers and their neighbors in the region. This is a representation of a complete fiber-matrix debonding of matrix cracking in the region.

Using the rule of mixtures, the Young's modulus of the broken core, E, is determined to be:

$$E = \frac{\mathrm{iA_f E_f} + \left[\mathrm{iA_m} - \pi(r_o^2 - (r_o - d)^2)\right]E_m}{\pi(\mathrm{r_o} - d)^2} \qquad \textbf{17}$$

where E_f and E_m are the Young's modulus for the fiber and matrix. Hence,

$$E\pi(r_o - d)^2 = \mathrm{iA_f E_f} + \left[\mathrm{iA_m} - \pi(r_o^2 - (r_o - d)^2)\right]E_m$$

$$= \mathrm{iA_f}E_f\left\{1 + \frac{\left[\mathrm{iA_m} - \pi(r_o^2 - (r_o - d)^2)\right]}{iA_f\ E_f}E_m\right\}$$

$$= iA_f E_f \beta \qquad \textbf{18}$$

where Beta is defined to be:

$$\beta = \left\{1 + \frac{\left[\mathrm{iA_m} - \pi(r_o^2 - (r_o - d)^2)\right]}{iA_f\ E_f}E_m\right\} \qquad \textbf{19}$$

Now the equilibrium equations (equation 16) are rewritten as:

$$iA_f E_f \beta \frac{\mathrm{d^2U_o}}{\mathrm{dx^2}} - 2\pi r_o \eta \tau_o = 0$$

$$n_i A_f E_f \frac{d^2U_1}{dx^2} + 2\pi(r_o + 2d + 2r_f)\frac{G_m}{2d}(U_2 - U_1) + 2\pi r_o \eta \tau_o = 0 \qquad \textbf{20}$$

For the region in which no interfacial yielding has occurred, the equilibrium equations are:

$$E\pi(r_o - d)^2 \frac{d^2U_o}{dx^2} - 2\pi r_o \frac{G_m}{2d}(U_1 - U_o) = 0$$

$$n_i A_f E_f \frac{d^2U_1}{dx^2} + 2\pi(r_o + 2d + 2r_f)\frac{G_m}{2d}(U_2 - U_1) + 2\pi r_o \frac{G_m}{2d}(U_1 - U_o) = 0 \quad \textbf{21}$$

$$a \le x < \infty$$

These equations now can be rewritten as:

$$iA_f E_f \beta \frac{\mathrm{d}^2 \mathrm{U}_o}{\mathrm{dx}^2} - 2\pi r_o \frac{G_m}{2d}(U1 - Uo) = 0$$

$$n_i A_f E_f \frac{d^2U_1}{dx^2} + 2\pi(r_o + 2d + 2r_f)\frac{G_m}{2d}(U_2 - U_1) + 2\pi r_o \frac{G_m}{2d}(U_1 - U_o) = 0 \quad \textbf{22}$$

Gao and Reifsnider assumed that the strain in the average composite is constant, therefore

$$U_2 = \frac{\sigma}{\mathrm{E}} x \quad \textbf{23}$$

where σ in this equation represents the remote fiber stress. Then, introducing the following normalization:

$$U_o = \sigma \mathrm{u}_o \sqrt{\frac{2dA_f}{E_f G_m r_o}}$$

$$U_1 = \sigma \mathrm{u}_1 \sqrt{\frac{2dA_f}{E_f G_m r_o}}$$

$$x = \zeta \sqrt{\frac{2A_f E_f d}{G_m r_o}}$$

$$\tau_o = \bar{\tau}_o \, \sigma \sqrt{\frac{A_f G_m}{2dE_f r_o}}$$

$$a = \alpha \sqrt{\frac{2A_f E_f d}{G_m r_o}} \qquad \textbf{24}$$

We can rewrite the equilibrium equations as

$$\frac{d^2 u_o}{d\xi^2} - \frac{2\pi}{i\beta} \eta \bar{\tau}_o = 0$$

$$\frac{d^2 u_1}{d\zeta^2} - \phi t u_1 + \phi(\eta \bar{\tau}_o + t\xi) = 0$$

$$0 \le \zeta < \infty \qquad \textbf{25}$$

with

$$\frac{d^2 u_o}{d\zeta^2} + \frac{2\pi}{i\beta}(u_1 - u_o) = 0$$

$$\frac{d^2 u_1}{d\zeta^2} - \phi(1+t)u_1 + \phi u_o = -\phi t \zeta \qquad \textbf{26}$$

$$\alpha \le \zeta < \infty$$

where

$$t = \frac{r_o + 2d + 2r_f}{r_o} \qquad \textbf{27}$$

$$\phi = \frac{2\pi}{n_i} \qquad \textbf{28}$$

In order to solve the second order differential equations, two boundary conditions must be applied. They are as follows:

$$\frac{du_o(0)}{d\zeta} = u_1(0) = 0$$

$$\frac{du_o(\infty)}{d\zeta} = \frac{du_1(\infty)}{d\zeta} = 1 \qquad \textbf{29}$$

The solution to the second order differential equation (equations 26) is as follows:

$$u_o = \frac{\pi\eta\bar{\tau}_o}{i\beta}\zeta^2 + A_1$$

$$u_1 = \frac{\eta\bar{\tau}_o}{t} + \zeta + A_2\exp(\zeta\sqrt{t\phi}) - (A_2 + \frac{\zeta\bar{\tau}_o}{\mathrm{t}})\exp(-\zeta\sqrt{t\phi}) \qquad \textbf{30}$$

The constants A_1 and A_2 will be determined from continuity conditions.

The solution to equations 27 can be written as follows:

$$u_o = \zeta + B_1(1 + t - \frac{\lambda_1}{\phi})\exp(-\sqrt{\lambda_1\zeta}) + B_2(1 + t - \frac{\lambda_2}{\phi})\exp(-\sqrt{\lambda_2\zeta})$$

$$u_1 = \zeta + B_1\exp(-\sqrt{\lambda_1\zeta}) + B_2\exp(-\sqrt{\lambda_2\zeta}) \qquad \textbf{31}$$

where B_1 and B_2 are constants with

$$\lambda_1 = \left\{ n_i + i\beta(1+t) + \sqrt{n_i^2\ 2\mathrm{i}\beta\mathrm{n}_\mathrm{i}(1-t) + (i\beta)^2(1+t)^2} \right\} \frac{\pi}{i\beta n_i}$$

$$\lambda_2 = \left\{ n_i + i\beta(1+t) - \sqrt{n_i^2\ 2\mathrm{i}\beta\mathrm{n}_\mathrm{i}(1-t) + (i\beta)^2(1+t)^2} \right\} \frac{\pi}{i\beta n_i} \quad \textbf{32}$$

The stress concentration on the unbroken fibers is expressed as;

$$C_i(\zeta) = \frac{du_1(\zeta)}{d\zeta} \quad \textbf{33}$$

and the dimensionless shear stress is expressed as:

$$\bar{\tau}(\zeta) = u_o - u_1 \quad \textbf{34}$$

The finial equation used to predict the strength of the composite is shown below.

$$X_t = \mathrm{V_f} \bullet \hat{\sigma}_\mathrm{c} + (1 - \mathrm{V_f})\mathrm{E_m} \bullet \frac{\hat{\sigma}_c}{\mathrm{E_f}}$$

$\mathrm{V_f} = \text{Fiber Volume Fraction}$ **35**
$\hat{\sigma}_\mathrm{c} = \text{Critical Stress}$
$\mathrm{E_m} = \text{Stiffness of Matrix}$
$\mathrm{E_f} = \text{Stiffness of Fiber}$

Case and Reifsnider have developed a computer code based on the above arguments for strength with a polymer matrix composite. This code (MRLife) is written in "C++" and the results from this code will be used to compare with the experimental results [2].

Model Two

The Subramanian and Reifsnider model is based on many of the same assumptions that model 1 is based on [1]. The broken fibers are assumed to form a central core with a layer of matrix material around the fiber. The broken fiber(s) is assumed to have the neighbors of fibers arranged in a concentric cylinder with the broken fiber(s) in the center, as shown in Figure 1.03. These assumptions are based on the work of Gao and Reifsnider described previously. The equilibrium equations for the central core of broken fibers and the adjacent fibers are written in the differential equation with the dependent variable of displacement in this form

$$E_{f1}\pi \, \mathrm{r}_{\mathrm{f1}}^{2} \frac{d^{2}u_{f1}}{dx^{2}} + 2\pi \, \mathrm{r}_{\mathrm{f1}}\tau_{\mathrm{m1}} = 0 \qquad \textbf{36}$$

$$n_i E_{f2}\pi \, \mathrm{r}_{\mathrm{f}}^{2} \frac{\mathrm{d}^{2}\mathrm{u}_{\mathrm{f2}}}{\mathrm{dx}^{2}} + 2\pi \mathrm{r}_{\mathrm{m}}\tau_{\mathrm{m2}} + 2\pi \, \mathrm{r}_{\mathrm{f2}}\tau_{\mathrm{m3}} = 0 \qquad \textbf{37}$$

where the shear stress is defined by

$$\tau_{m1} = \left(\frac{\mathrm{u}_{\mathrm{m2}} - \mathrm{u}_{\mathrm{m1}}}{\mathrm{b}} \right) G_m \qquad \textbf{38}$$

$$\tau_{m2} = \left(\frac{\mathrm{u}_{\mathrm{m1}} - \mathrm{u}_{\mathrm{m2}}}{\mathrm{b}} \right) G_m \qquad \textbf{39}$$

$$\tau_{\mathrm{m3}} = \left(\frac{\mathrm{u}_{\mathrm{c}} - \mathrm{u}_{\mathrm{m2}}}{\mathrm{b}} \right) G_m \qquad \textbf{40}$$

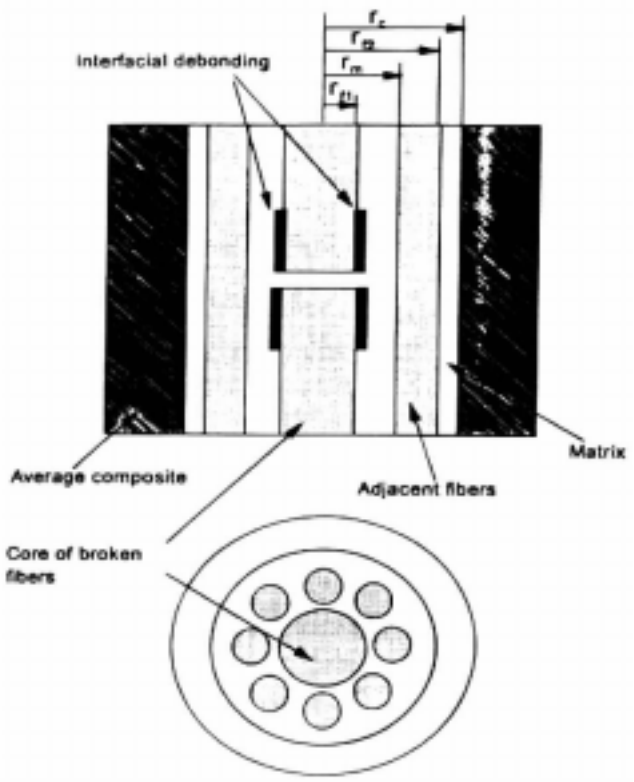

Figure 1.03 Schematic of concentric cylinder model with a core of broken fibers with the neighboring fibers.

These equations are based on the assumption that the displacement varies linearly in the radial direction in the matrix material. The fibers are also assumed to carry all the axial load with the matrix around the fibers acting only to transfer the load between the fibers through a shear transfer mechanism. Assuming that the displacement in the fiber and matrix at the fiber-matrix interface is discontinuous, and that the displacement in the average composite is uniform, the following expressions can be written

$$u_c = \frac{\sigma_a x}{E_x} \qquad \textbf{41}$$

$$u_{f1} = \eta u_{m1} \qquad \textbf{42}$$

$$u_{f2} = \eta \, u_{m2} \qquad \textbf{43}$$

Again, the efficiency factor is used to determine how well the load is transferred from the matrix into the fiber. If the value is one, then this indicates perfect bonding of the interface and a good load transfer. A value of zero indicates no transfer of load from the matrix into the fiber.

The equilibrium equations may then be rewritten as follows:

$$\frac{d^2 u_{f1}}{dx^2} + k_1 u_{f1} + k_2 u_{f2} = 0 \qquad \textbf{44}$$

$$\frac{d^2 u_{f2}}{dx^2} - k_3 u_{f2} + k_4 u_{f1} + k_5 x = 0 \qquad \textbf{45}$$

where

$$k_1 = -\frac{2 r_{f1} G_m}{b E_{f1} \eta \, r_{f1}^2}$$

$$k_3 = \frac{2 r_m G_m}{n_i b E_{f2} \eta \, r_{f2}^2} + \frac{2 r_{f2} G_m}{n_i b E_{f2} \eta \, r_{f2}^2}$$

$$k_4 = \frac{2 r_m G_m}{n_i b E_{f2} \eta \, r_{f2}^2}$$

$$k5 = \frac{2 r_{f2} G_m \sigma_a}{n_i b E_{f2} \eta \, r_{f2}^2 E_x} \qquad \textbf{46}$$

The following boundary conditions are used to solve the differential equations (44 and 45).

$$\left(\frac{du_{f1}}{dx}\right)_{x=0} = 0$$

$$(u_{f2})_{x=0} = 0 \qquad \textbf{47}$$

Solving the differential equations yields:

$$[D^4 + D^2(k_1 - k_3) - (k_2k_4 + k_1k_3)]u_{f2} - k_2k_5x = 0 \qquad \textbf{48}$$

The homogenous solution to the differential equation requires that

$$u_{f1} = C_1e^{-\alpha x} + C_2e^{-\beta x} + C_3x + C_4e^{\alpha x} + C_5e^{\beta x}$$

$$u_{f2} = D_1e^{-\alpha x} + D_2e^{-\beta x} + D_3x + D_4e^{\alpha x} + D_5e^{\beta x} \qquad \textbf{49}$$

where

$$\alpha, \beta = \left[\frac{(k_3 - k_1) \pm \sqrt{(k_1 + k_3)^2 + 4k_2k_4}}{2}\right]^{1/2} \qquad \textbf{50}$$

The following constants must be zero in order for the fiber strains to be finite at regions far away from the fiber fracture; C_4 , C_5, D_4, and D_5. Next the assumed displacement functions are substituted into the equilibrium equations and the remaining constants are determined.

$$C_3 = \frac{-k_2 k_5}{k_1 k_3 + k_2 k_4}$$

$$D_3 = -C_3$$

$$C_1 = \left(-\frac{k_2}{\alpha^2 + k_1} \right) D_1$$

$$C_2 = \left(-\frac{k_2}{\beta^2 + k_1} \right) D_2$$

$$D_1 = \frac{C_3}{\left[\frac{\beta k_2}{\beta^2 + k_1} - \frac{\alpha k_2}{\alpha^2 + k_1} \right]}$$

$$D_2 = -D_1 \qquad \textbf{51}$$

Now the solution to the displacements is obtained

$$u_{f1} = C_1 e^{-\alpha x} + C_2 e^{-\beta x} + C_3 x$$

$$u_{f2} = D_1 e^{-\alpha x} + D_2 e^{-\beta x} + D_3 x \qquad \textbf{52}$$

The strains and stresses in the central core and the adjacent fibers are derived using the strain-displacement and constitutive relationships of mechanics of materials.

$$\varepsilon_{f1} = \frac{du_{f1}}{dx}; \quad \sigma_{f1} = E_{f1} \varepsilon_{f1}$$

$$\varepsilon_{f2} = \frac{du_{f2}}{dx}; \quad \sigma_{f2} = E_{f2} \varepsilon_{f2} \qquad \textbf{53}$$

The stress concentration factor in the adjacent fiber for the elastic case is written as

$$C_i = (\sigma_{f2})_{x=0} / (\sigma_{f2})_{x\to\infty} \qquad \textbf{54}$$

In the elastic case, the ineffective length is obtained by determining the length over which the inner core recovers 99% of the applied stress [1].

$$\sigma_{f1}(x) = 0.99\,\sigma_a \qquad \textbf{55}$$

In the plastic case, the stress concentration factor Ci* and the ineffective length delta I* are obtained using the following approximation. It is assumed that the matrix exhibits an elastic-perfectly plastic behavior. If the average shear stress in the matrix exceeds the interfacial shear strength, the interface is assumed to debond. Once debonding occurs, the shear stress in the matrix is assumed to be constant over the region defined as the plastic ineffective length, and zero elsewhere [1]. The plastic stress concentration factor is estimated by calculating the average stress in the adjacent fiber as follows:

$$\overline{\sigma_{f2}} = \frac{1}{\delta}\int_0^{\delta} \sigma_{f2}\,dx$$

$$\overline{\sigma_{f2}} = \frac{E_{f2}}{\delta}[D_3\delta - D_1 - D_2]$$

$$C_i^* = \frac{\overline{\sigma_{f2}}}{E_{f2}D_3} \qquad \textbf{56}$$

For the elastic-perfectly plastic case, the stress concentration factor will be equal to one. The force balance argument is used to estimate the plastic ineffective length as follows:

$$\delta_i^* = \frac{\overline{\sigma}_{f1} r_{f1}}{2\eta \tau_i} \qquad \textbf{57}$$

where the average stress in the inner core is given by

$$\overline{\sigma}_{f1} = \frac{E_{f1}}{\delta} \int_0^{\delta} \varepsilon_{f1} dx$$

$$\overline{\sigma}_{f1} = \frac{E_{f1}}{\delta} (C_3 \delta - C_1 - C_2) \qquad \textbf{58}$$

When writing the force balance equation, it was assumed that due to interfacial debonding the shear stress in the matrix is not equal to the interfacial shear strength, but is multiplied by the efficiency factor. Once debonding has occurred the transfer of stress is done with a mechanism of friction. After debonding it is assumed that the stress transfer will not be perfect. The shear stress is multiplied by the efficiency factor to reflect this behavior [1].

Now that the stress concentration factor and the ineffective lengths have been derived for both cases of plastic and elastic local behavior for different fiber breakages, the tensile strength is predicted following Batdorf's analysis. As previously discussed, Batdorf showed that the stress level at which the first fiber fracture occurs is expressed as:

$$\sigma_1 = \left(\frac{1}{\mathrm{NL}}\right)^{1/m} \sigma_o$$

$N = total$ number of fibers in the specimen
L = normalized length of the specimen
m = Weibull strength shape factor for the fiber
σ_o = Weibull strength location parameter for the fiber

59

The stress level at which the next fiber fractures occur is given by

$$\sigma_i = \left(\frac{1}{NL\pi\, \mathrm{n}_{i-1}\lambda_{i-1}}\right)^{1/m} \sigma_o \quad \mathrm{i} = 2,3,...$$

60

and

$$\lambda_i = 2\delta_i \left[\frac{C_i^{m+1} - 1}{(C_i - 1)(m+1)}\right]$$

61

The average shear stress in the matrix region is estimated as follows

$$\overline{\tau_m} = \frac{1}{\delta}\int_0^{\delta}\left(\frac{u_{2m} - u_{1m}}{b}\right) G_m dx$$

$$\overline{\tau_m} = \frac{G_m}{\delta b \eta}\left[\frac{(D_1 - C_1)}{\alpha} + \frac{(D_2 - C_2)}{\beta}\right]$$

62

It is assumed that interfacial debonding occurs when the average shear stress in the matrix exceeds the interfacial shear strength. At each load level, calculations are made to see if the interfacial failure occurs. Once the interfacial failure occurs then the

plastic stress factor and ineffective lengths are used to predict fiber fractures. However, if there is no interfacial failure until instability occurs, then the final failure is classified as elastic failure. If the debonding occurs before the final failure, the failure is termed plastic.

Model 2 can be used to predict failure of an unidirectional laminate for tensile strength. A computer code that makes the looped calculations of this model is written in Pascal.

Quantitative Differences between the Models

As previously mentioned, both of the models are based on the classical shear lag arguments. However there are some differences between the two models. Model 1 assumes that the displacement in the fiber and matrix outside the yielding region to be continuos at the fiber-matrix interface. Model 2 admits displacement discontinuities between the fiber and matrix outside the yielding zone. Model 1 uses the maximum shear stress value in the matrix to determine if yielding occurs. Model 2 uses the average shear stress value in the matrix to determine if yielding occurs. Other differences maybe between the assumed geometry of the fiber matrix regions.

Temperature Effects on the Strength

Many researchers have tried to understand the effects of elevated temperatures on composite materials. Many questions still remain about the effect. For example, how does the temperature affect the material system with respect to creep recovery and visco-

elastic-plastic behavior. More important is how we express these behaviors in terms of known constitutive equations [5].

The approach to these questions has been to identify the failure mode(s) that control fracture, and to set up a boundary value problem that represents the micro-details in terms of the constituents and geometry. The simplest example of this is the rule of mixtures:

$$X_t = \mathrm{v_f X_f} + \mathrm{v_m X_m}$$

X_t = Composite strength **63**
$\mathrm{X_f}$ and $\mathrm{X_m}$ = Fiber and matrix strength
$\mathrm{v_f}$ and $\mathrm{v_m}$ = Fiber and matrix volume fraction

However this model is limited as a one-dimensional model and not considered sufficiently rigorous. An alternative model represents the tensile strength and performance of the constituents and the interphase regions between [5]. This model includes more of the physical factors and effects that control tensile strength:

$$X_t = \sigma^{\frac{\mathrm{m}}{\mathrm{m+1}}}\left(\frac{2\tau_0 L}{\overline{D}}\right)^{\frac{1}{m+1}}\left(\frac{2}{m+2}\right)^{\frac{1}{m+1}}\left(\frac{m+1}{m+2}\right)\frac{(1+m)^{\frac{1}{m}}}{[C_n^m + C_n^{m-1} + \ldots + 1]^{1/m}}$$

64

$\overline{D}$ = Fiber diameter
σ = Characteristic strength of the fibers
τ_o = Interfacial shear strength
L = Characteristic length of the material
C_n = Local stress concentration numbers when neighboring fibers are broken
m = Weibull shape parameter of the statistical distribution of fiber strengths

The above models are useful and if we examine them we can see that there are several parameters that are influenced by temperature. Reifsnider and Case state that the yield strength of the matrix (or interphase region between the fiber and the matrix) can be

expected to decrease with increasing temperature [5]. Also, the stiffness of the components will, in general, be a function of temperature. For a polymer matrix material, for example, the shear stiffness will often be strongly temperature dependent [5].

Furthermore, temperature also effects the ineffective length. As discussed, the ineffective length is created in the region of a fiber fracture. When a fiber breaks, the stress is transferred back into a neighboring fiber by the surrounding matrix in a manner that is controlled by the stiffness of the surrounding material. As the surrounding material becomes less stiff, the ineffective length becomes larger. If the ineffective length is large, then the fiber fracture regions will interact more easily and may connect together to cause complete failure [5]. However, if the matrix material and surrounding composite is very stiff, then the stress is transferred back into the fiber over a small distance and the ineffective length is small. In this case, the stress concentration in the material next to a fiber break is very high. This greatly increases the chance of one fiber fracture causing an unstable sequence of neighboring fiber fractures resulting in complete failure. A shear lag equation for the ineffective length is as follows:

$$\delta = \frac{1}{2}\left[\frac{1}{2}\left(\frac{1-\nu_f^{0.5}}{\nu_f^{0.5}}\right)\left(\frac{E_f}{G_m}\right)\right]^{\frac{1}{2}} \ln\left(\frac{1}{1-\phi}\right) \quad \textbf{65}$$

δ = Ineffective length
ν_f = Volume fraction of the fiber
G_m = Matrix stiffness
E_f = Stiffness of the fibers
ϕ = Efficiency factor for the stress transfer

Case and Reifsnider pointed out that elevated temperature reduces the stiffness of the matrix and with this reduction the ineffective length will increase. Under this

assumption, the strength equation should express what happens to the composite strength. If the increase in temperature causes the ineffective length to increase, then the composite strength may respond with an increase or decrease. The basic assumption is that as the temperature is elevated, the polymer matrix stiffness will reduce and with this phenomena the ineffective length will increase. The effect of the ineffective length on the strength is demonstrated in the following figure (Figure 1.04) [5].

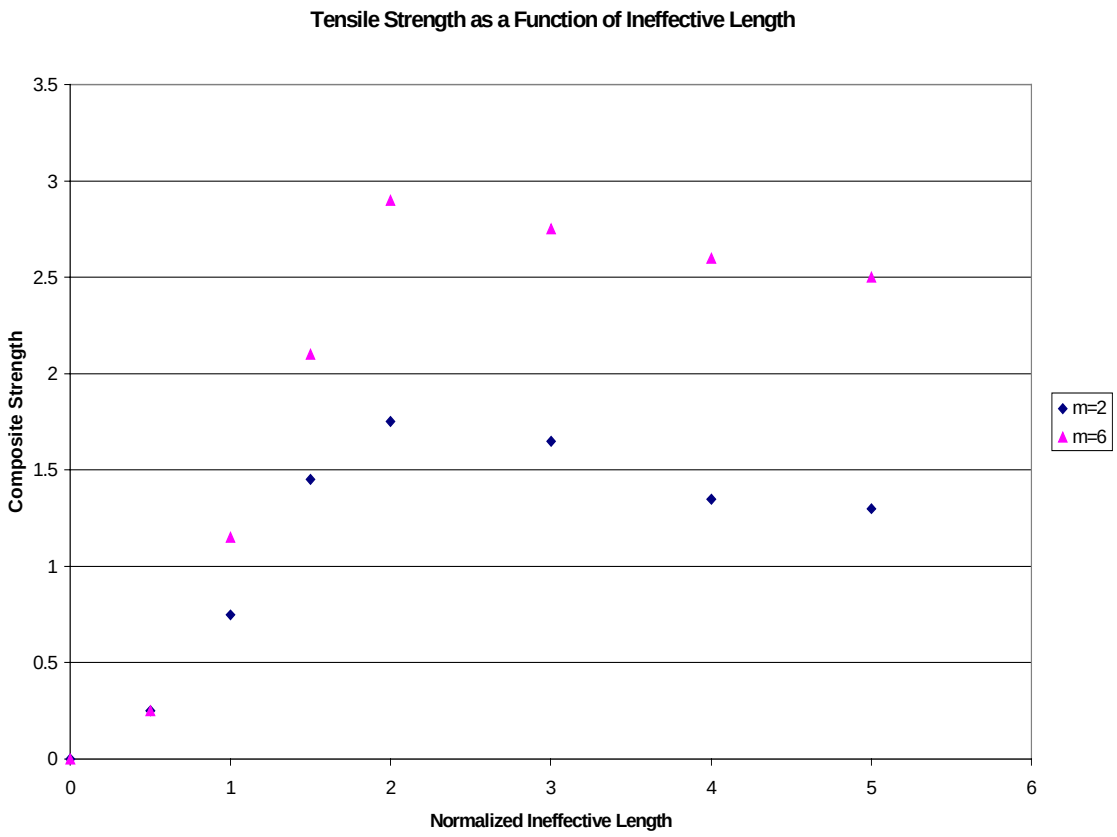

Figure 1.04 Tensile strength as a function of local ineffective length.

This figure (Figure 1.04) is generated for different ineffective length values with two different Weibull shape factors (m). Clearly, this figure indicates that there is a location were the strength is maximum. To the left of the maximum, strength is reduced

by a stress concentration due to the small ineffective length that causes a brittle fracture. To the right of the maximum, the strength is reduced by the greater ineffective length because of the coupling of fiber fracture zones. Therefore, as the elevated temperatures cause the ineffective length to change, the strength may increase or decrease based on the position of the value for the ineffective length [5].

Using some data we can demonstrate the strength increases and decreases with the change of elevated temperature (Figure 1.05). The IM7/K3B system was tested in our laboratory and the Graphite/Epoxy system was tested by Haskins [6].

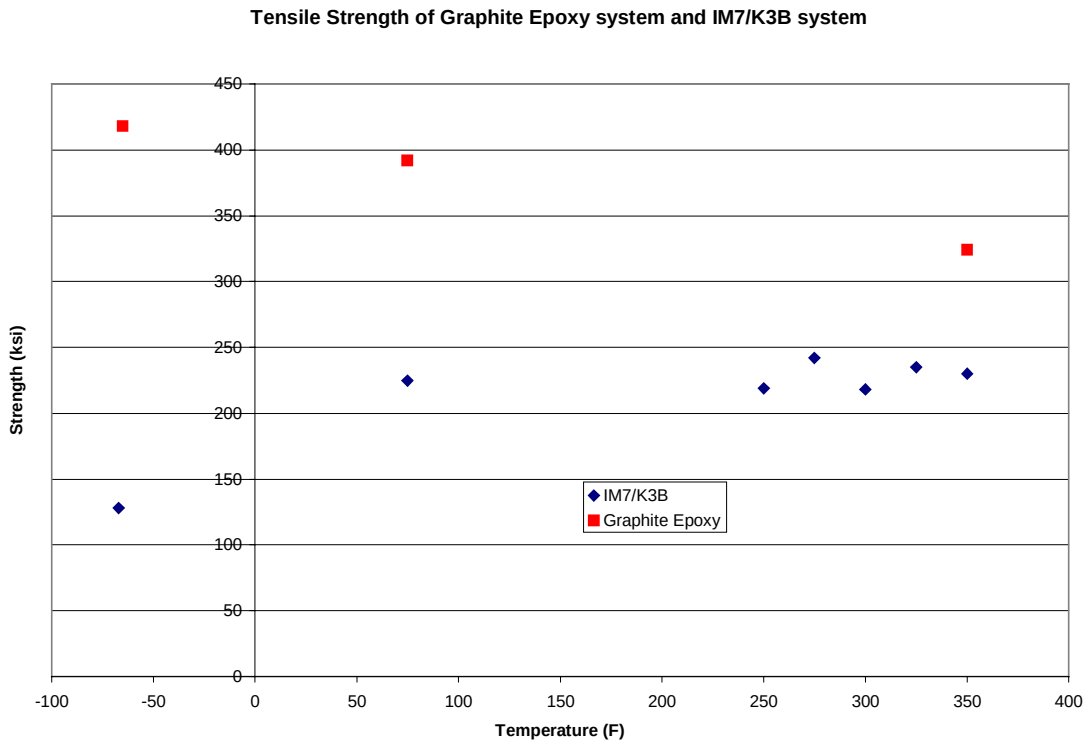

Figure 1.05 Unidirectional tensile strength as a function of temperature for two polymer carbon fiber composites.

This figure indicates that, depending on the matrix material, we can be to the left of the ineffective length temperature maximum or to the right of this maximum. Observing the Graphite/Epoxy system in Figure 1.05, the indication is that this system is to the left of the maximum in Figure 1.04. However the IM7/K3B system indicates that the strength is to the right of the maximum in Figure 1.04.

Interfacial Shear Strength at Elevated Temperatures

Both of the above models use the interfacial shear strength as a parameter in the formulation of the strength. Many researches have spent time investigating the fiber-matrix shear strength. The matrix polymer adhering to the fiber surface produces this strength. An investigation was performed on the interfacial adhesion on carbon fiber at elevated temperatures by H. Zhuang and J.P. Wightman [7]. This evaluation is also known as single fiber fracture testing.

The testing was conducted on various carbon fibers in a single "dog bone" specimens of epoxy matrix. Preparation of the single fiber composite was as follows: a silicone rubber mold with a dog-bone-shaped cavity was used to give the composite its shape during cure of the epoxy. A single fiber was fixed on both ends with the middle suspended in the mold. Epoxy resin was poured in the mold with the fiber embedded in the epoxy. The cure schedule was 75 degrees C for 2 hours and then 125 degrees C for another 2 hours. Then the specimens were allowed to cool overnight and removed from the mold [7].

The fragmentation test was preformed as follows: the single fiber specimens were mounted in a hand operated loading fixture one at a time. The specimens were observed with a transmitting-light microscope. The specimens were then pulled in tension at a

speed of 1 mm/min and the fiber fractures were observed during this process. The tension on the specimen was stopped after no further breaks were observed with increasing load. The fragment lengths then were measured with the aid of the microscope and recorded.

The same procedure was used for the elevated temperature fragmentation tests. However, the fixture was placed in a hot oil bath with the oil at the desired temperature. The specimens were given 10 minutes in the oil bath to allow for the heat transfer [7].

The equation used to determine the interfacial shear strength was as follows.

$$\tau = \frac{\sigma_f}{2}\frac{d}{l_c}$$

$\tau =$ interfacial shear strength **66**
$\sigma_f =$ fiber strength at the critical length
$d =$ fiber diameter
$l_c =$ critical length

Figure 1.06 and Figure 1.07 show the response of the interfacial shear strength as a function of temperature. Three different fibers were used to examine the adhesion process on the fibers for a single matrix material. The carbon fibers were AS-4, AU-4 and Panex 33 (S) and the epoxy was Epon 828. Two different curing agents were used on the epoxy. Figure 1.06 shows the response with the Jeffamine DU-700 curing agent and Figure 1.07 shows the response with mPDA curing agent [7].

The results show that the interfacial shear strength decreases as a function of temperature. The trend from one carbon fiber system to another system can vary, and the curing agent can also effect the strength value.

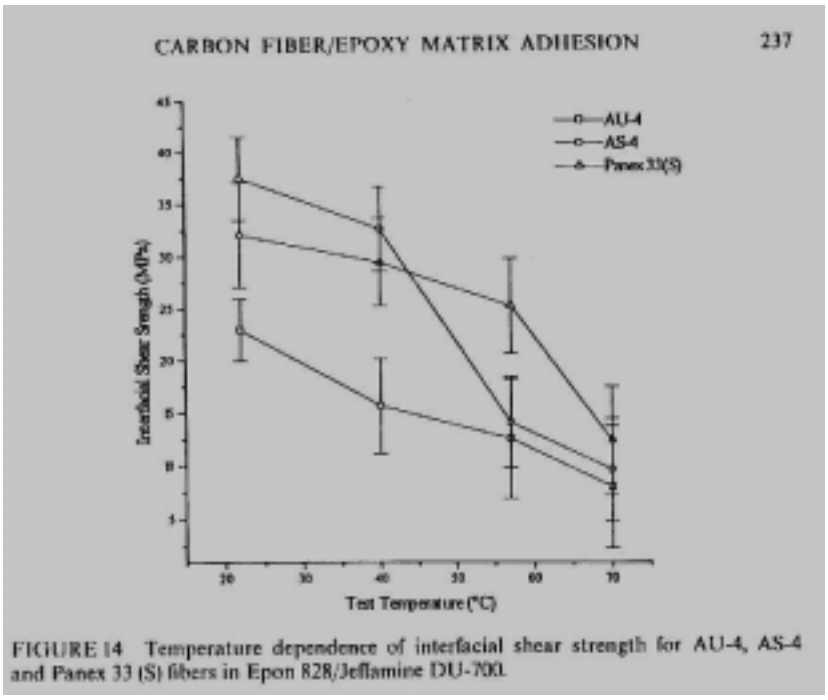

Figure 1.06 Interfacial shear strength as a function of temperature from single fragmentation test/ Epon 828 DU-700 [7].

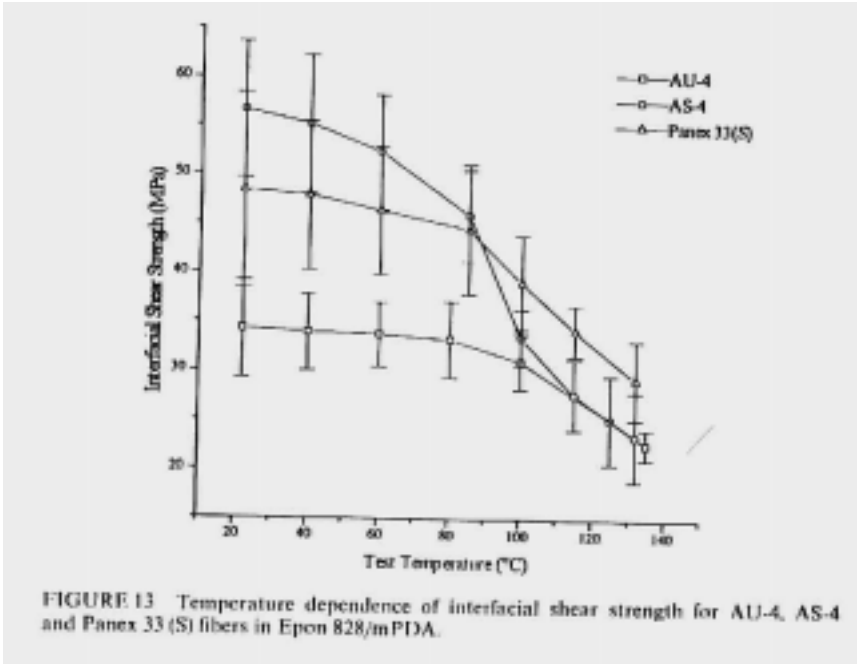

Figure 1.07 Interfacial shear strength as a function of temperature from single fragmentation test/ Epon 828 mPDA [7].

Bulk Polymer Stiffness at Elevated Temperatures

The other variable known to be affected by the elevated temperature is the matrix stiffness. Most polymers become less stiff as their temperature is increased because the polymer chains are given more freedom to move and bonding is reduced. At melt temperature, most polymers act as a fluid; therefore, as the temperature approaches the glass transition temperature of the polymer, the stiffness is effected. An example of this behavior is found in Figure 1.08 [8]. This figure is a collection of stress-strain curves for epon 828 epoxy.

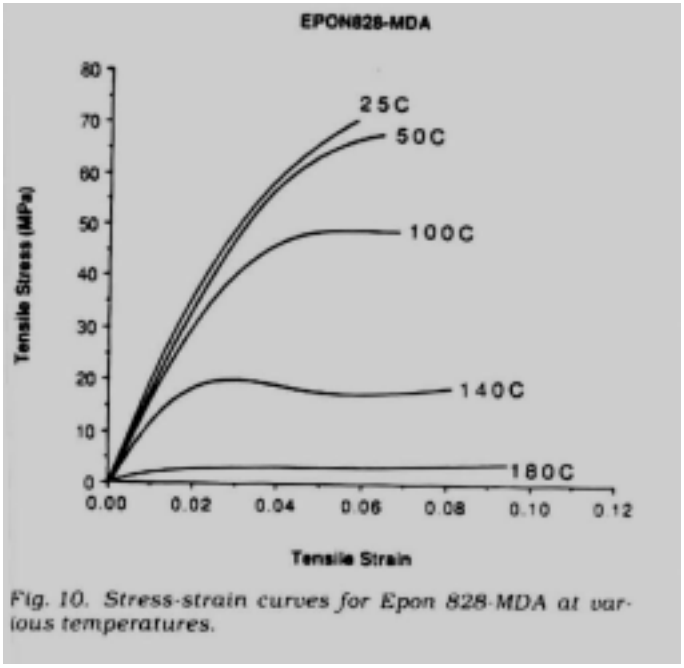

Figure 1.08 Bulk Epon 828 stress-strain curves at elevated temperatures [8].

Mechanical Properties for Materials

Mechanical properties for AS-4 carbon fiber are give in Table 1.01. The source of the property is also given in the table. In addition to the carbon fiber, properties of

PPS and PEEK polymers are given in Table 1.02. These properties will be used in the models.

Table 1.01 Summary of mechanics parameter for AS-4 carbon fiber.

AS-4 Carbon Fiber Properties	**Value**
Young's Modulus E_f [8]	241 (Msi)
Weibull location parameter [8]	5.25
Weibull shape factor [8]	10.65
Radius of a single fiber [8]	1.378x10-4 (in)
Fiber strength location Parameter [8]	786000 (psi)

Table 1.02 Properties of thermoplastics PEEK and PPS.

Property at 23 degrees C	**PPS**	**PEEK**
Tensile Modulus	480 (ksi) [9]	470 (ksi) [10]
Poisson's ration	0.35	0.40 [10]
Melt Temperature	285-290 (C) [9]	370-400 (C) [10]
Glass Transitional Temp.	88 (C) [9]	143 (C) [10]

II. Experimental Procedures

General Equipment

XPS

X-ray Photoelectron Spectroscopy (XPS) was used to determine the surface chemistry of material that was supplied in test form. XPS involves the bombardment of the specimen surface with mono-energetic X-rays in a high vacuum. As the photons travel through the material some are absorbed and their energy is transferred to electrons which can be ejected from the specimen. The spectrum, the electron intensity versus the binding energy of the electron to the atom, is obtained by pulse-counting techniques [11].

This test was used to supplement information about the composites' chemistry. The PPS system was the only system that was delivered ready to test and the company, Polymer Composite International (P.C.I.) did not disclose any processing information. Therefore it was necessary to use this test to obtain some information about the composite.

Fiber Volume Fraction Analysis

The fiber volume fraction for each material was determined by a buoyancy test. Several samples were taken from each material type. The dry weight of each sample was measured on an electronic balance. Then the samples were weighed submerged in isopropanol. Knowing the density of the resin, fiber, and isopropanol the fiber volume can be calculated with the following equations:

$$\rho_c = \frac{W_{air}}{W_{air} - W_{iso}} * \rho_{\text{iso}}$$

ρ_c = Density of Composite (g/cc)
W_{air} = Weight of Composite in air (g)
W_{iso} = Weight of Composite in Isopropanol
ρ_{iso} = Density of Isopropanol

$$V_f = \frac{\rho_c - \rho_{resin}}{\rho_{fiber} - \rho_{resin}}$$

V_f = Volume fraction of Fiber in Composite
ρ_{fiber} = Density of Fiber (g/cc)
ρ_{resin} = Density of Resin (g/cc)

C-Scans

A Scanning Acoustic Microscope C-Scan was preformed on the PEEK panels to detect flaws. This instrument uses sound waves to penetrate the panel and uses the returning sound wave to interrogate the material's make up. The panel was placed in a bath of water for a short period of time (10 minutes) while the C-Scan was preformed.

If the time of flight of the sound wave is different in some places of the material, the image will display this variation. This method is a nondestructive test that has limited use. The instrument can help detect a flaw in the panels, such as, a fiber rich region or a matrix rich region. If a flaw is detected then the defected section of the panel can be discarded to avoid experimental discrepancies.

DMA

A Dynamic Mechanical Analysis (DMA) was used to determine the glass transition temperature (T_g) for the composite systems. Many times the glass transition temperature of the composite system is different than the bulk polymer's glass transition temperature. This measurement was used only to get an approximate glass transition temperature and was not used to estimate any mechanical properties.

Quasi-static Tension Macro-Mechanical Test

The tension tests were conducted on a MTS hydraulic closed loop axial loading machine. The grip pressure was determined by running a few specimens and increased if slipping occurred. The final grip pressure was determined to be between 700 and 1000 pounds per square inch.

The elevated temperature environmental chamber was constructed from an electrical box that was cut in half. The specimen was loaded into the MTS and the extensometer was put in place. Figure 2.01 shows this step. Then the other half of the box was brought together with glider pins to enclose the environment. The two halves created a space for the specimen in the MTS grips. The heat was provided by an

industrial hot air blower and was controlled with an Omega Controller. The controller cycled the current to the every 2 seconds. The heat environment was placed around the specimen for a time period and was maintained until failure was achieved. A dummy strain gage was also placed in this environment to provide thermal compensation.

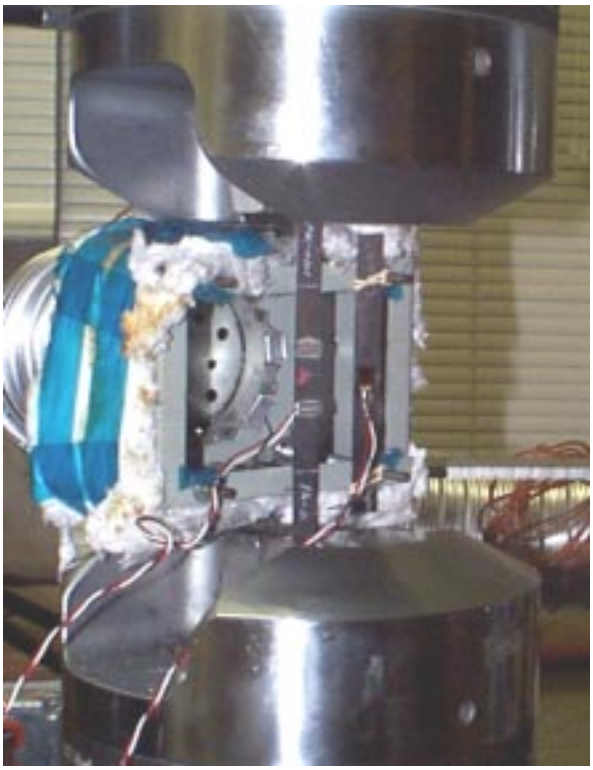

Figure 2.01 MTS with heater box set up with a specimen.

The majority of the tests were done with the elevated temperatures; however, some tests were conducted under the influence of cryogenic temperatures. The environmental chamber for these tests is shown in Figure 2.02. The temperatures were obtained by using liquid nitrogen that was pumped into the cell. The time that the

specimen experienced of the cryogenic temperature varied from test-to-test due to the limitation of the controller on the pump. However, once the temperature remained constant the test was conducted under the temperature until failure. This cell also contained the dummy thermal strain gage.

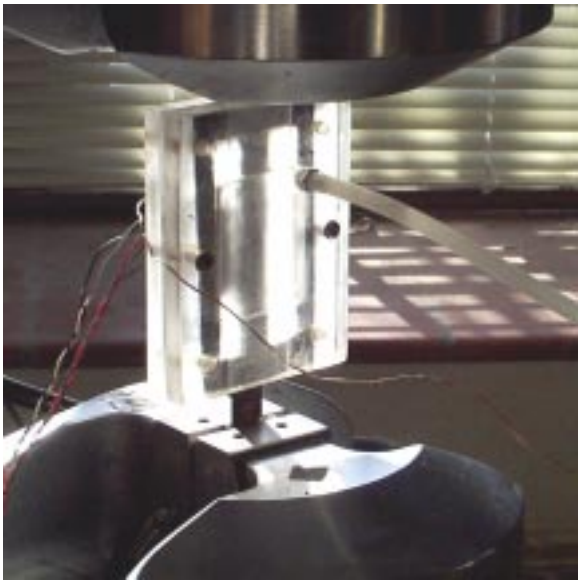

Figure 2.02 Cryogenic chamber for quasi-static tension test.

Materials

Polyphenylene Sulfide (PPS) Composite

General Description

This composite system had a resin matrix made of polyphenylene sulfide (PPS) polymer with carbon fiber in a unidirectional orientation. The carbon fiber was thought to be AS-4, however, this information was not supplied. PPS is a thermoplastic that has excellent heat resistance, excellent flame resistance, and moderate processability. It has no known solvents up to 200 degrees Celsius. Normally PPS is about 65% crystalline

and has a glass transition temperature of 85 degrees Celsius. [10]. The low Tg value is due to the flexible sulfide linkage between the aromatic rings [10].

Processing

Polymer Composite International (P.C.I.) manufactured the material on a spool with an average thickness of 0.025 inches and a width of 0.48 inches. Limited information was provided concerning the material's chemistry or manufacturing process.

Specimen Preparation

The specimens were cut to 8 inches from the spool. Each specimen was grit blasted using silicone on both ends one inch towards the center. One-inch fiberglass tabs were then placed with an adhesive on both ends with the composite sandwiched between them. The adhesive then was cured at 50 degrees Celsius for 2 hours. Figure 2.03 shows the dimensions of a typical specimen. If strain measurements were conducted in the test, extensometer tabs or strain gages were fixed in the middles on the surface. Strain gages were supplied by Micro-Measurements, Inc. and were of type CEA-06-125UW-350. Each gage was mounted on the specimen with M-Bond 600 using the directions supplied by the Micro-Measurements.

After tabbing the specimens, the following Tables 2.01-03 shows the testing temperatures and number of specimens tested. Each specimen was placed in the heater for 15 minutes to allow for the heat transfer.

Table 2.01 Sample quantity and testing temperature distribution: loading rate of 50 pounds per second.

Temperature (degrees C)	Number of Specimens Tested
60	4
70	4
80	4
90	4
100	4
110	4
120	4
130	4
140	4
150	4

Table 2.02 Sample quantity and testing temperature distribution: loading rate of 40 pounds per second.

Temperature (degrees C)	Number of Specimens Tested
24	4
30	4
60	3
70	3
80	3
90	3
100	3
110	3
120	3
130	3
140	3
150	3

Table 2.03 Sample quantity and testing temperature distribution: loading rate of 150 pounds per second.

Temperature (degrees C)	Number of Specimens Tested
30	8
60	4
70	4
80	4
90	4
100	4
110	4
120	4
130	4
140	4
150	4

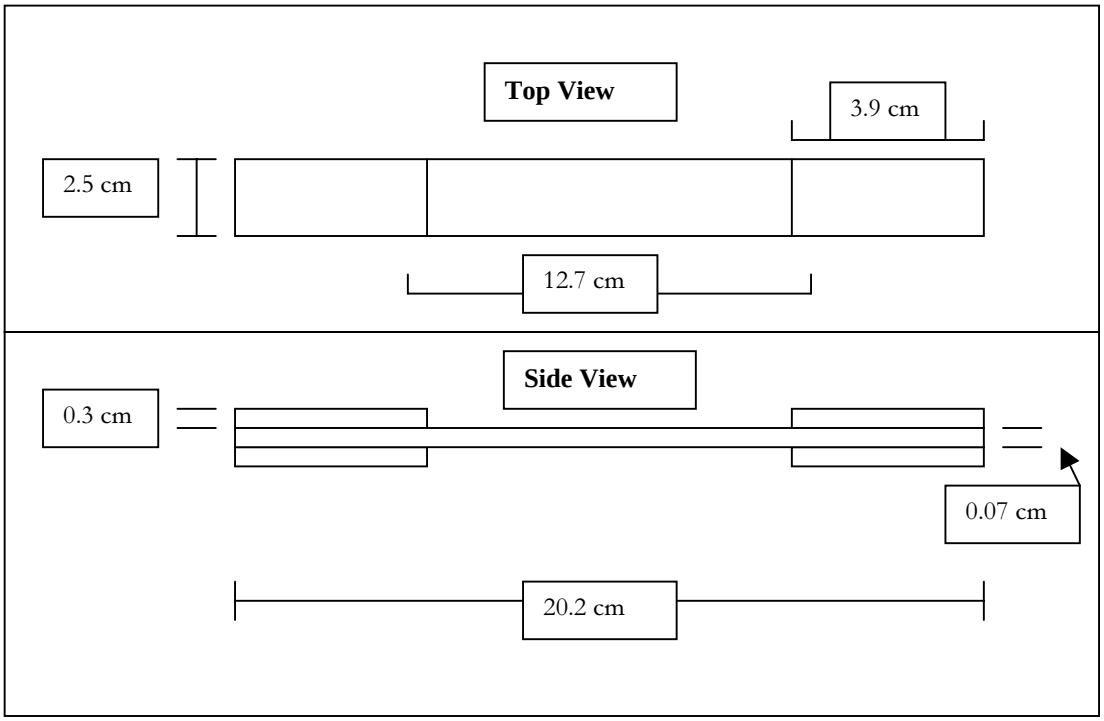

Figure 2.03 Drawing of a typical test specimens for PPS system.

Vinyl Ester Composite

General Description

This composite had a vinyl ester matrix with a carbon fiber. The carbon fiber was a Panex 33. In addition to the matrix polymer the composite had a polymer fiber-matrix interface of either polyurethane or epoxy. Vinyl ester is a thermosetting polymer and has many applications in the industry. It has excellent chemical resistance and tensile strength. However, it has a higher volumetric shrinkage (5-10%) than epoxy [10].

Processing

Dow Chemical Company supplied the vinyl ester matrix polymer. The matrix material consisted of 70 weight percent of pure vinyl ester and 30 percent of styrene monomer. The vinyl ester (T_g of 140 degrees C) had an average molecular weight (M_n) of 680 g/mol and was terminated by a methacrylate functional group. The fiber-matrix interface material was obtained from B.F. Goodrich and is refered to as SANCURE 2026 (polyurethane). The other fiber-matrix interface material was a priority Z' epoxy treated fiber.

The composite was manufactured by pultrusion at Strongwell, Inc. using their pilot scale pultruder. Spools of carbon fibers were placed in the creel rack for its processing. The individual tows were directed into the process on a teflon board. The fibers were dipped in the resin bath and cured at 150 degrees C.

Specimen Preparation

This material was in limited supply because it was being used on another project. However one 8-foot strip was supplied of each epoxy and polyurethane fiber-matrix interfaces. The strip was cut into twelve 8-inch specimens for each of the fiber-matrix interfaces. Aluminum end tabs with a steel screen system were employed. This system is not the traditional tabbing method based on ASTM Standards [12]. However, it was found to be an effective tabbing system that did not allow slipping or splitting.

Extensometer tabs were placed in the center of the specimen. The specimen was then placed in the MTS using a grip pressure of 750 (psi). The extensometer was calibrated and placed on the specimen. The heater chamber was placed around the

specimen and the desired elevated temperature was obtained. After the chamber was at the desired temperature, the specimen was left in the environment for 10 minutes before testing. The test was started with the specimen still in the environment. A typical specimen is shown in Figure 2.04.

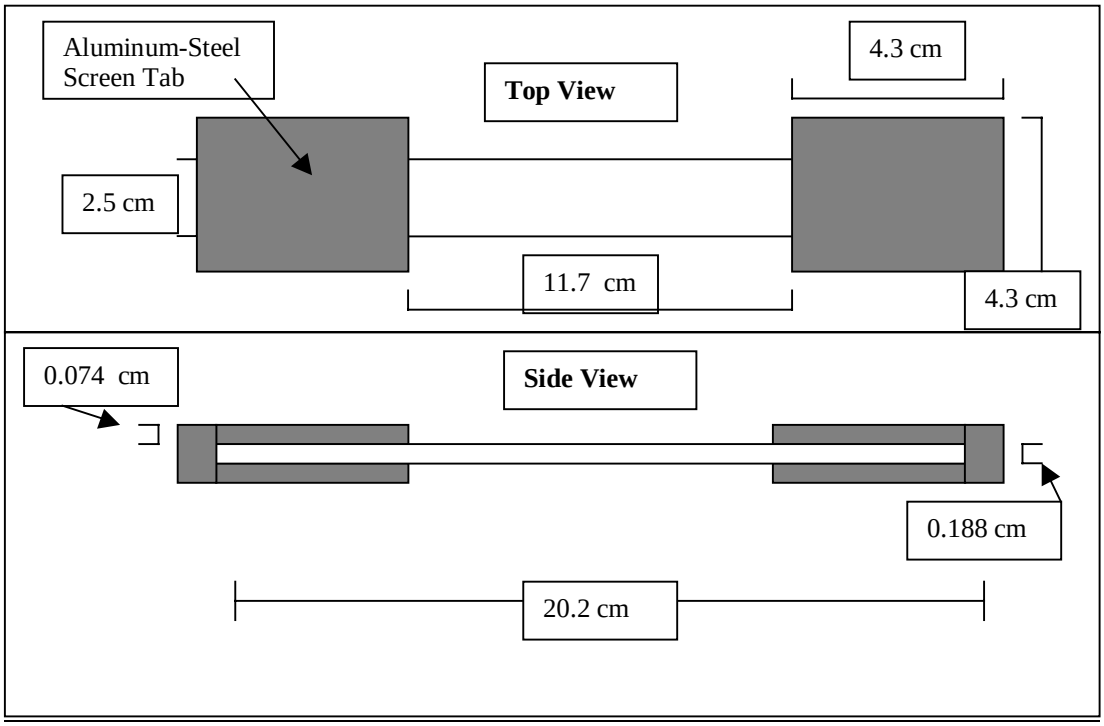

Figure 2.04 Drawing of a typical test specimen for vinyl ester system.

Polyether Ether Ketone (PEEK) Composite

General Description

This material was purchased from FiberRite Company in a prepreg form. The prepreg contained the PEEK resin and the AS-4 carbon fiber. Three 10 inch by 10 inch panels were produced in a hot platen vacuum press. The panels were all unidirectional

consisting of eight plies. PEEK is a themoplastic polymer and has many uses in structures. PEEK is a leading thermoplastic choice to replace epoxies in some aerospace industry applications. It has a high fracture toughness and a low water absorption [10].

Processing

As mentioned before, three panels were made from the prepreg material. Each panel was 10 inches by 10 inches and was fabricated in a vacuum hot press. Figure 2.05 shows the processing information of the panels. The figure indicates the processing temperature and the pressure values along with the time at each processing step.

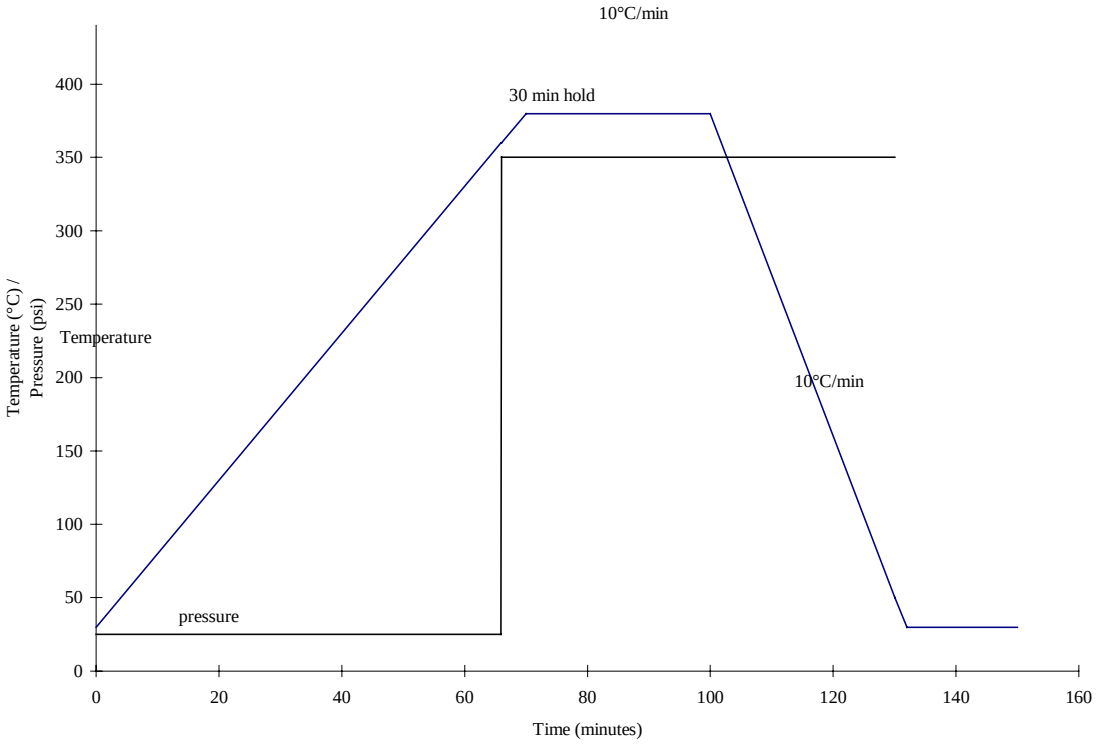

Figure 2.05 Processing diagram for PEEK composite.

Specimen Preparation

After the panel was fabricated, each panel was tabbed with the glass epoxy tabbing material. The 2.25-inch tabs were fixated to the panel with an epoxy adhesive on both ends with the composite sandwiched between them. The adhesive then was cured at 50 degrees Celsius for 2 hours. After the panel was tabbed, the 0.5-inch wide specimens were cut from the panel. A typical specimen is shown in Figure 2.06 and 2.07. Extensometer tabs and strain gages were then placed in the center of each specimen. The strain gages were supplied by Micro-Measurements Group, Inc. and were of type CEA-06-125UW-350. They were mounted on the specimens using M-Bond 600 by the directions given by Micro-Measurements. The specimens were then placed in the MTS grips and the heat environment was applied for 10 minutes before the test began.

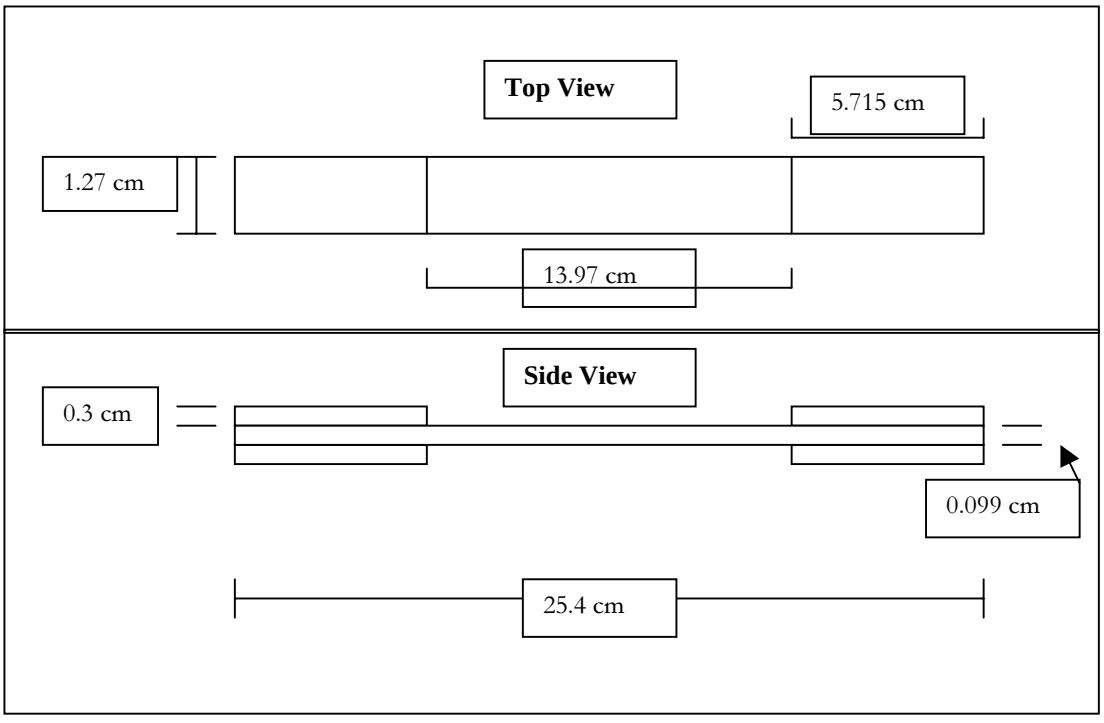

Figure 2.06 Dimensional drawling of PEEK specimens.

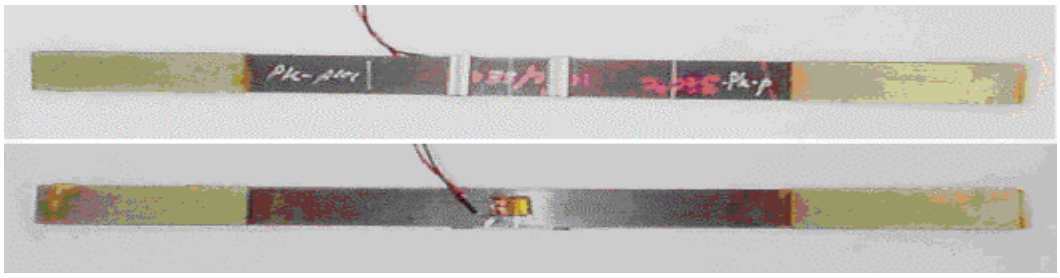

Figure 2.07 Photograph of PEEK specimens illustrating end tabs, extensometer tabs, and strain gage placement

III. Experimental Results and Discussion

Polyphenylene Sulfide (PPS) Composite

Fiber Volume Fraction

Table 3.01 Results of the fiber volume fracture measurements for PPS matrix composite.

Specimen #	Dry Weight (gr.)	Wet Weight (gr.)	Density of Composite	Volume Fraction of Fiber
1	0.3613	0.1748	1.5149	0.3975
2	0.2843	0.1370	1.5093	0.3848
3	0.3494	0.1684	1.5096	0.3853
4	0.3130	0.1511	1.5118	0.3905
5	0.4152	0.2008	1.5144	0.3963
6	0.2990	0.1444	1.5124	0.3918

As shown is Table 3.01, the fiber volume fraction for the PPS matrix composite was measured to be, on average 39 percent. This is the average value from the six independent specimens shown in Table 3.01.

XPS

The surface chemistry was analyzed with an X-ray Photoelectron Spectroscopy (XPS) presented the following elements: Carbon 1s 81.23%, Oxygen 1s 10.16%, Sulfur 2p 4.93%, Silicone 2p 2.11%, Sodium1s 0.33%, Nitrogen 1s 0.92%, Chloride 2p 0.31%. These are expected elements to be found in a PPS composite. Chloride is a typical element used in formulation of the PPS polymer.

DMA

The results from the DMA indicate that the glass transition temperature for the PPS composite is 128 degrees Celsius. This value is greater than the bulk PPS glass transition temperature of 88 degrees Celsius. However, a composite is different from the bulk matrix material because the carbon fibers can influence this test and the state of the matrix material. The results from the DMA are shown in Figure 3.01.

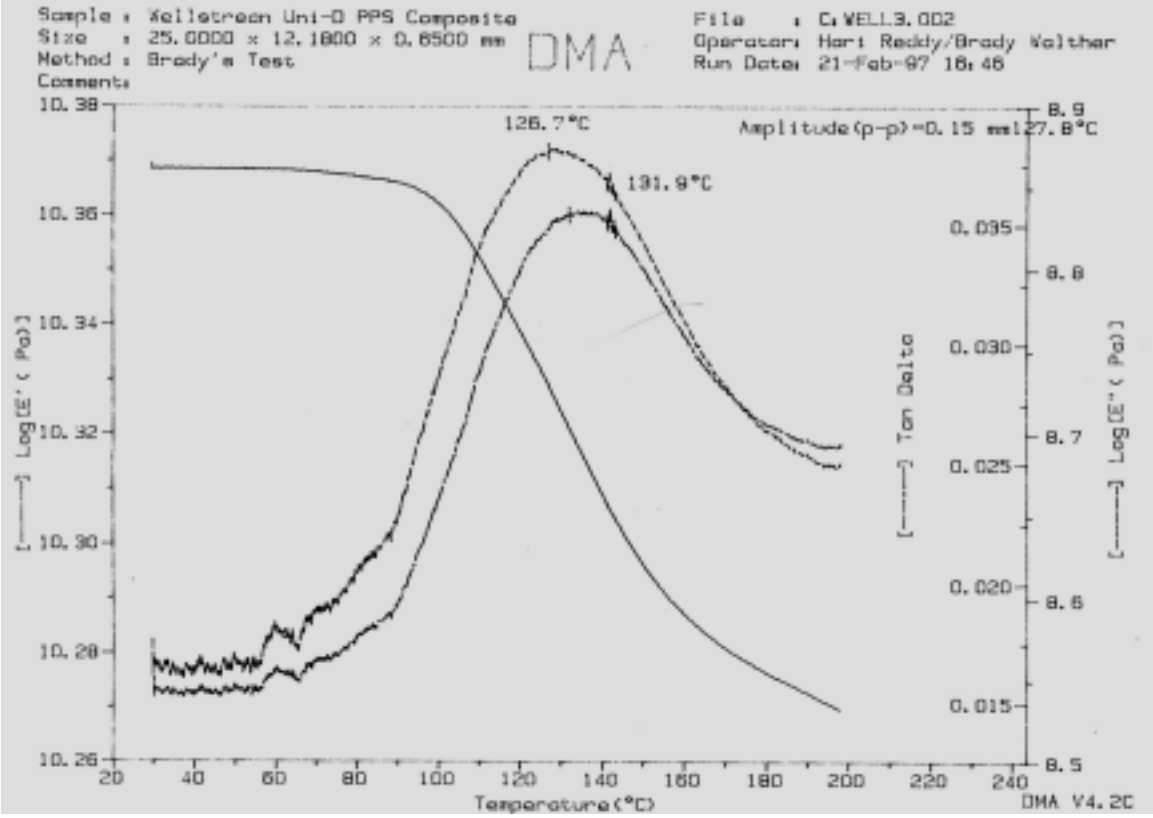

Figure 3.01 DMA Result for PPS matrix composite system.

Results of Macro-Mechanical Test

All one hundred and twenty six plus specimens were tested for ultimate strength on an MTS hydraulic closed loop axial loading machine with loading rates of 40 lbf/sec, 50 lbf/sec, and 150 lbf/sec. Each specimen had the same nominal cross sectional area.

Stress and strain were measured in the fiber direction. The stress was calculated by dividing the load by the cross-sectional area. The strain was measured, the majority of the time, using an extensometer supplied by MTS. MTS rated the extensometer to be calibrated to 300 degrees Fahrenheit (or 150 degrees Celsius). This was verified using an extensometer measurement on a piece of steel at the elevated temperatures. Strain gages were also used on some specimens to compare with the extensometer. The measured modulus of the steel was 31 (Msi). This is a little high from the standard value of 30 (Msi) for steel; however, this measurement was consistent in the temperature range. The load cell for this MTS may need to be calibrated.

Stress-strain curves were generated to determine young's modulus (stiffness) of the composite. The moduli were measured on the linear domain of the curve. This domain included approximently 40% or 50% of failure strength. Typical stress-strain curves, for the PPS composite system, are given in Figures 3.02 and 3.03.

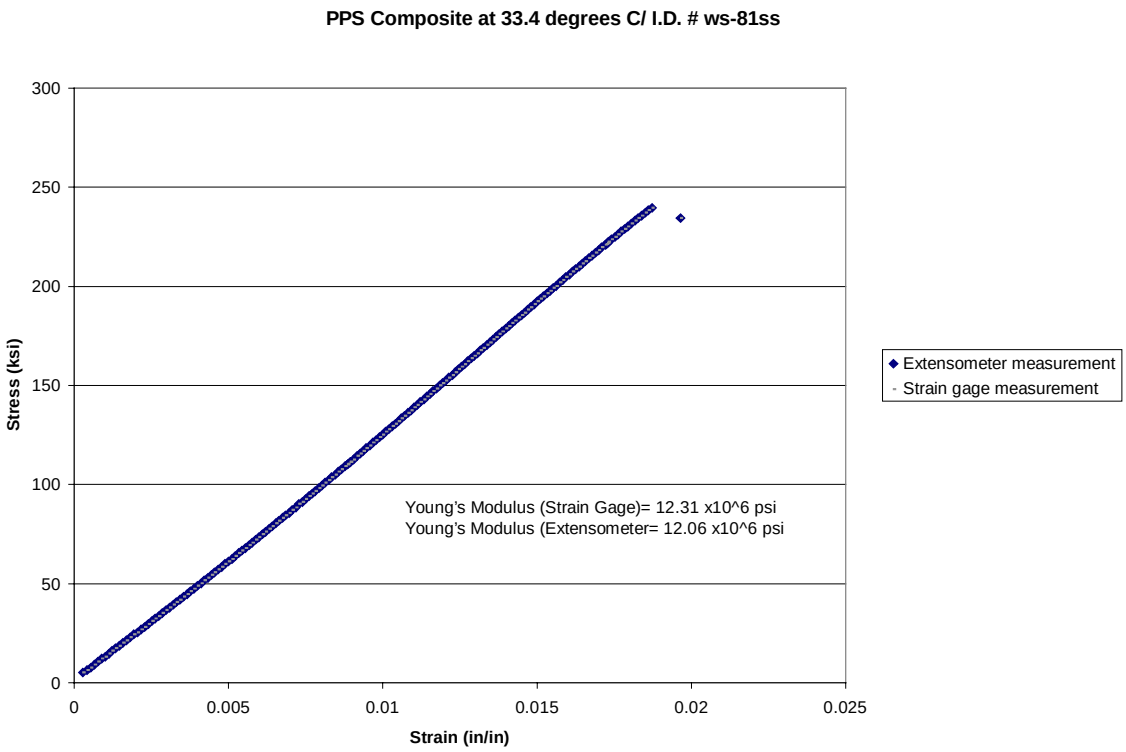

Figure 3.02 Stress-strain calibration of extensometer with strain gage strain measurements.

Figure 3.02 demonstrates the calibration efforts on the extensometer. On this particular specimen strain was measured in the fiber direction with both an extensometer and a strain gage. The strain gage produced a modulus of 12.31 msi; the extensometer produced a modulus of 12.06 msi. Furthermore, calibration tests were conducted measuring the strain with the extensometer on a piece of steel at elevated temperatures. The results of this particular calibration test do not appear in this work. However, the results of the calibration tests were satisfactory. Therefore, the extensometer is an appropriate device to measure the strain between the temperatures of 30^0 to 150^0 Celsius.

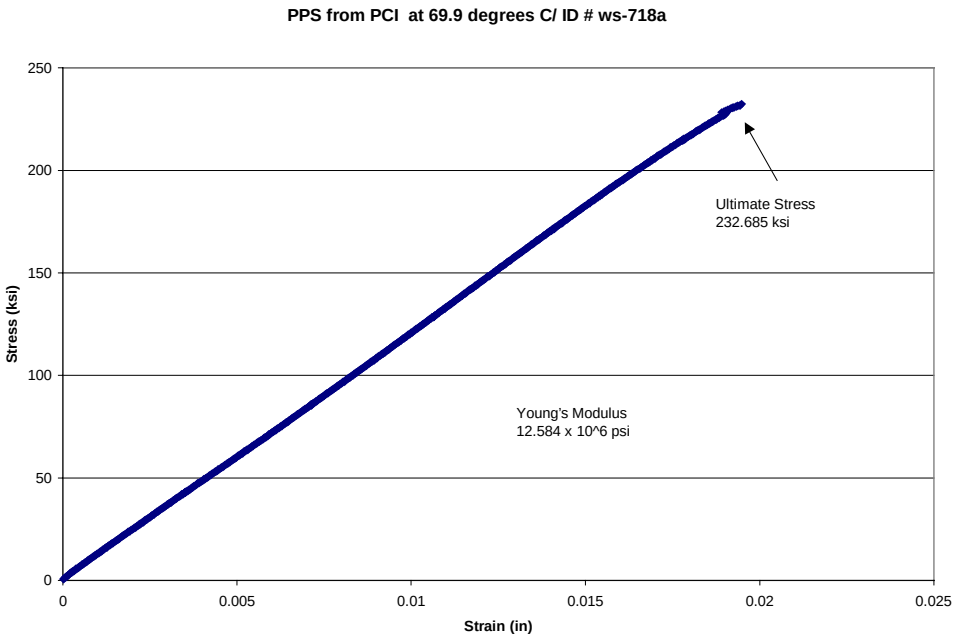

Figure 3.03 Stress-strain curve for PPS composite material.

Table 3.02 and Figure 3.04 give the statistical results for all tests run at that temperature. This includes all three major loading rates.

Table 3.02 Results from all PPS Composite (PCI) tension tests- @ all loading rates.

Test Temperature (C^0)	# of Specimens (All load rate)	Average Strength (ksi)	Standard Deviation for Strength	Average Young's Modulus (x10^6 psi)	Standard Deviation for Young's Modulus
30	15	240.8	6.9	12.588	0.530
60	12	222.7	19.0	12.255	0.198
70	12	220.3	13.9	12.411	0.736
80	14	220.9	13.9	12.330	0.695
90	18	219.9	13.6	12.258	0.524
100	12	214.9	12.4	12.096	0.292
110	13	211.3	15.4	12.028	0.270
120	12	211.5	11.7	12.001	0.382
130	12	199.7	16.5	11.617	0.669
140	12	198.1	13.6	12.266	0.418
150	10	201.9	12.1	12.551	0.726

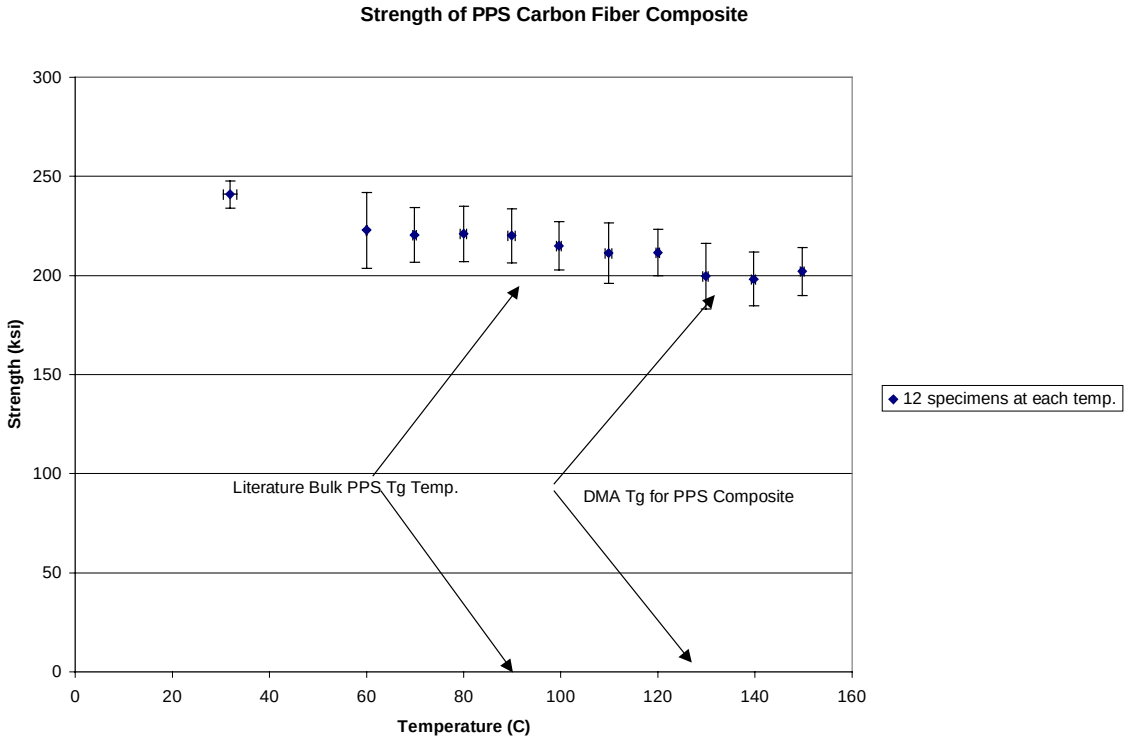

Figure 3.04 A plot of the strength values for the PPS Composite material with their respective temperatures with standard deviations as error bars.

As we can see (in Figure 3.04) the average strength of this composite can be expected to decline 17.7 percent from 30^0 to 140^0 Celsius. In addition to this decline in strength, the data indicate that the strength declines both at 90 and 130 degrees Celsius. These temperatures are unique to the material because 90 degrees Celsius is the literature value for the glass transitional temperature for bulk PPS, and 126 degrees is the measured (by DMA) glass transition temperature for the PPS composite system. Figure 3.04 indicates both of these transitions. One possible explanation to these two transitions is that the bulk matrix away from the fibers is changing at 90 degrees Celsius. Then the matrix material near the fibers is changed at 130 degrees Celsius.

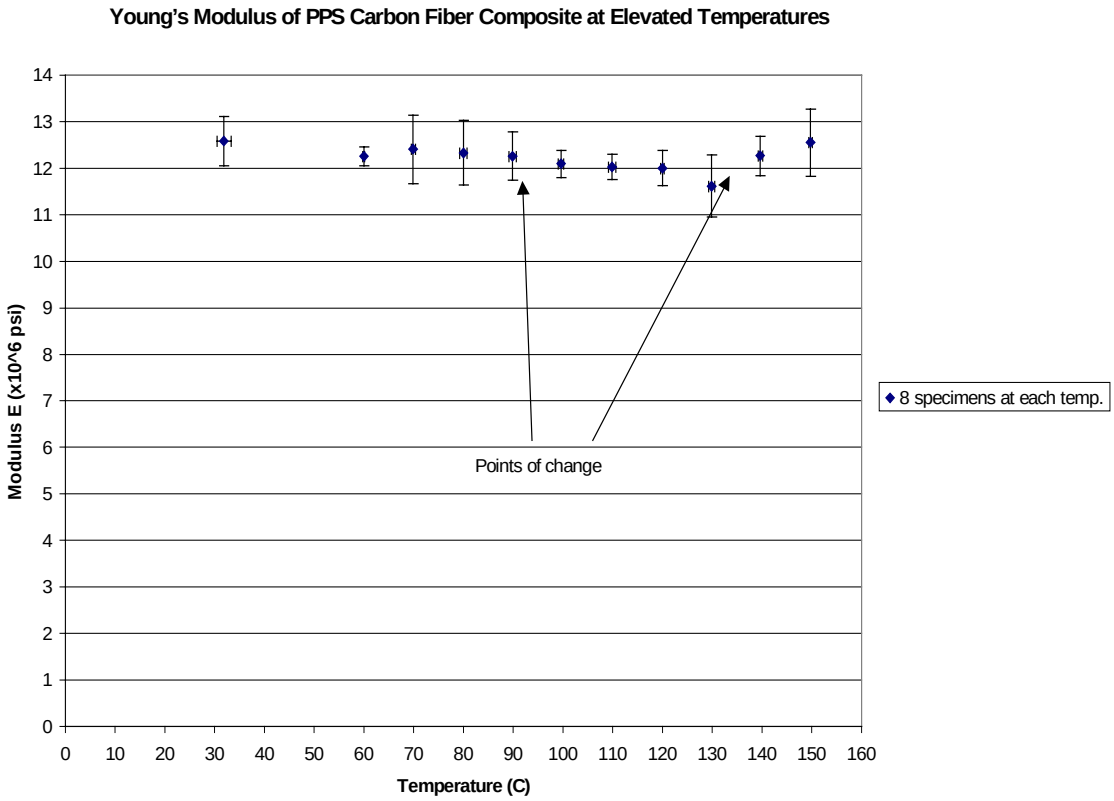

Figure 3.05 Young's modulus for PPS composite system with all loading rates.

However, the stiffness modulus only declined 7.7 percent between 30^0 and 130^0 Celsius. Furthermore, the modulus almost returned to its value at 30^0 at 150^0 Celsius. This result is represented by Figure 3.05 and in Table 3.02.

Figures 3.06 and 3.07 demonstrate the same plots (same data) as in Figures 3.04 and 3.05; however, the data are presented in a bar chart. These figures indicate the magnitude of the standard deviations of the strength values at the temperatures.

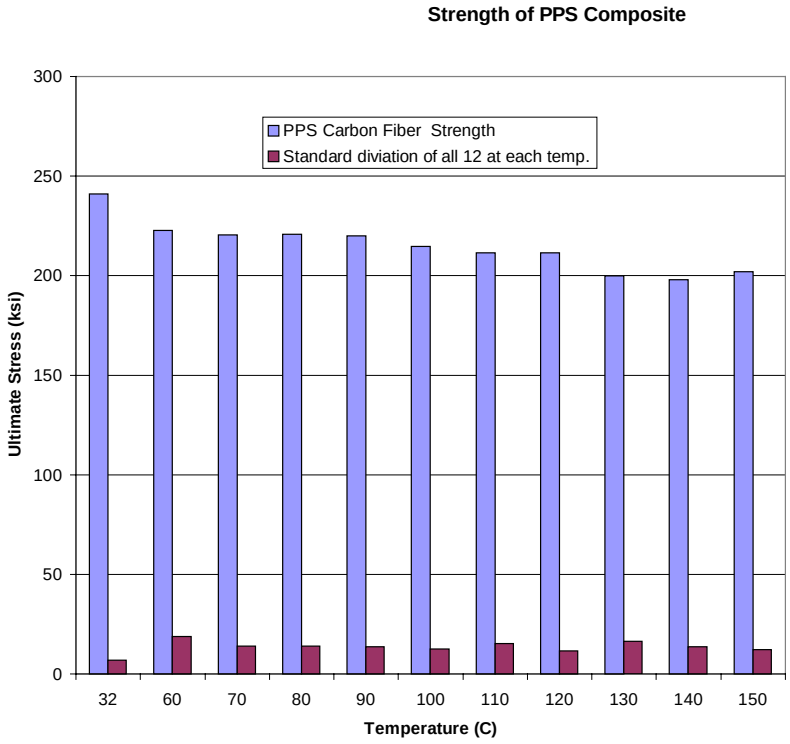

Figure 3.06 A bar graph of the strength of PPS Composite (same data that makes up Figure 3.04).

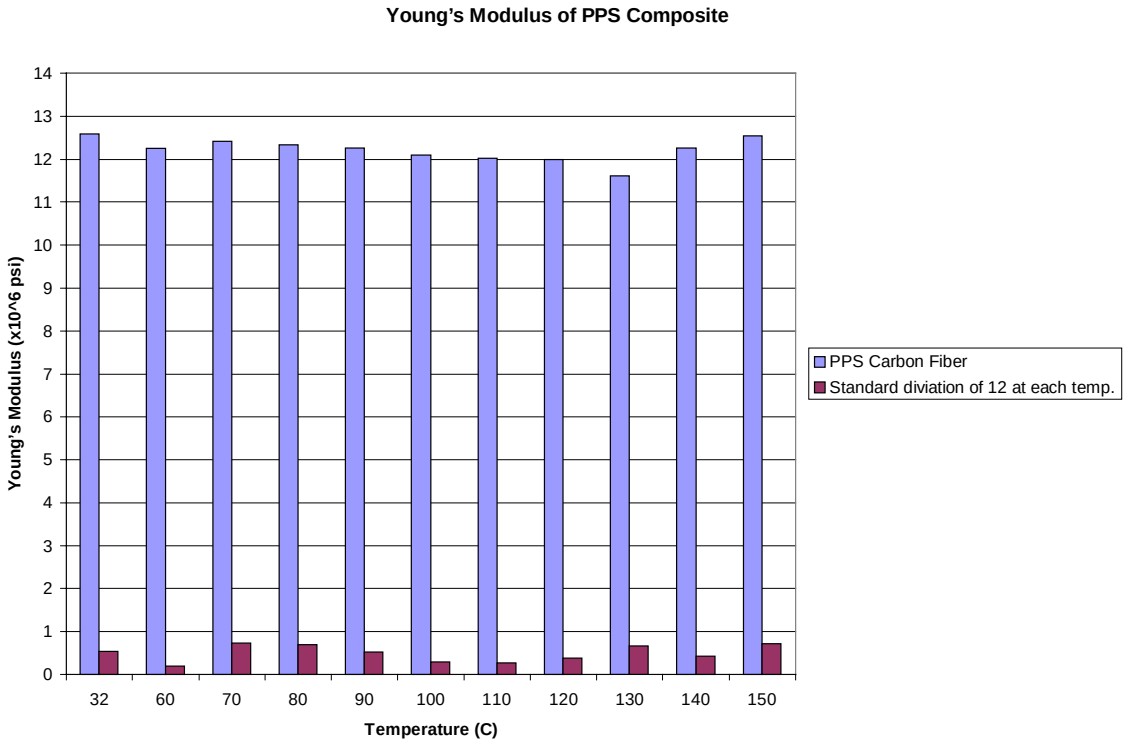

Figure 3.07 A bar graph of Young's modulus for the PPS carbon fiber composite.

All of the above data were evaluated with all three loading rates. This testing was intended to explore the visco-elastic properties of composites. The combination of different strain rates and elevated temperatures may influence the strength of the composite. This behavior was interrogated using different loading rates on the material at the temperatures. The results are given in Figure 3.08.

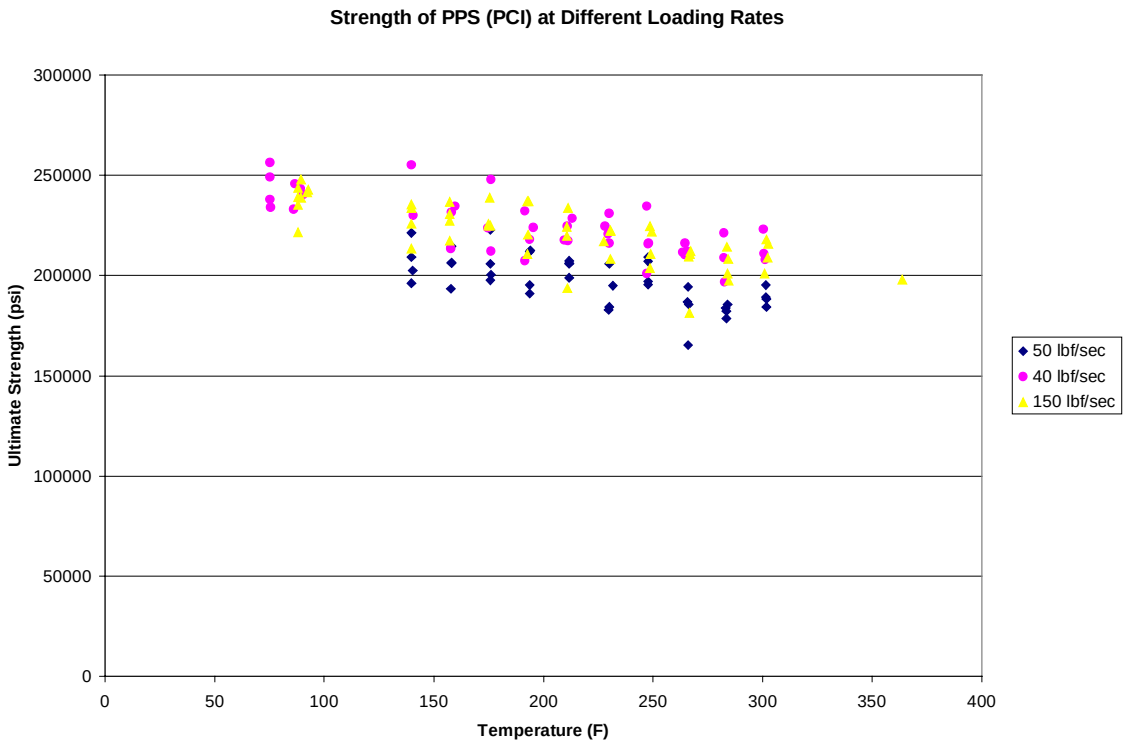

Figure 3.08 The strength of PPS composite differentiating load rates of 40,50, and 150 pounds per sec.

The visco-elastic response is difficult to explore. For amorphous polymers, the principles of linear viscoelasticity can be applied. However for semi-crystalline polymers these techniques can not be applied. Semi-crystalline polymers maintain a higher modulus over a wider range of temperatures. Additionally, the fiber dominance of this system may off set any visco-elastic response. A difference in strength is seen between

the rates of 40 and 50 pounds per second. However, the rate of 150 lbf/sec is within the scatter of 40 and 50 lbf/sec.

In addition to the above data points, more data were collected on strength at higher temperatures. Only the strength was collected at these temperatures because they were beyond the range of the extensometer. Figure 3.09 reports points above 150 degrees Celsius.

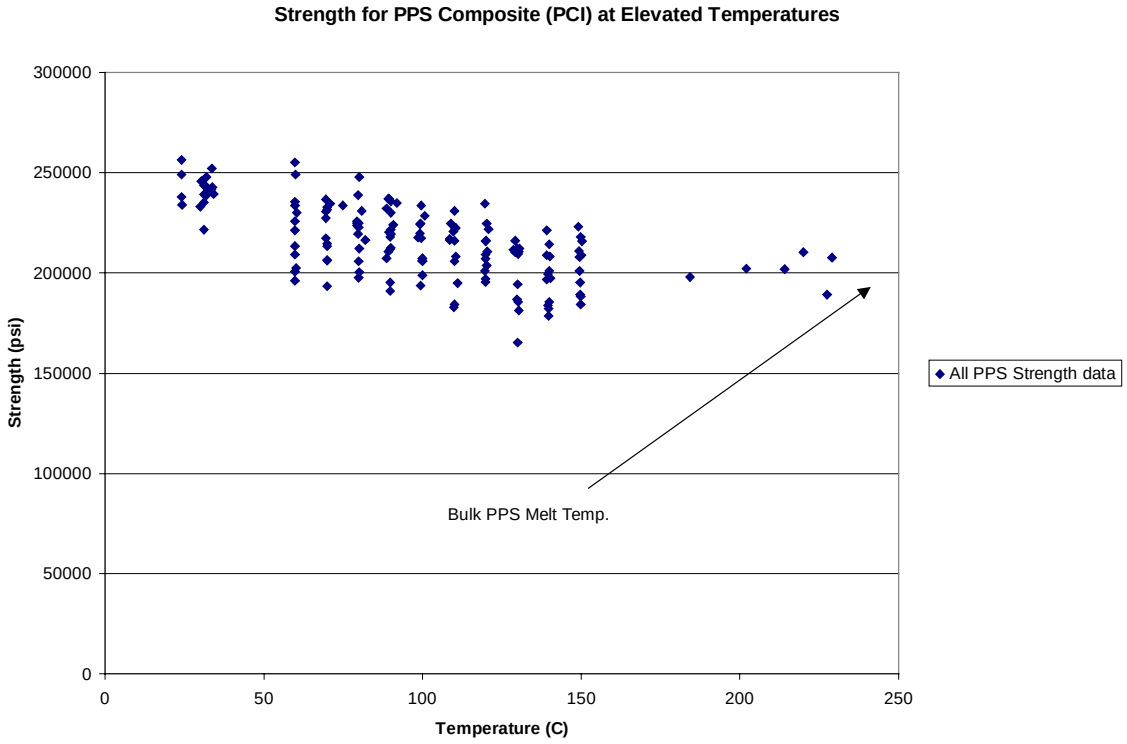

Figure 3.09 All strength data on PPS composite, data without strain measurements.

The strength does not appear to decline dramatically as the melt temperature for PPS is approached. The melt temperature for bulk PPS is approximately 285 degrees Celsius. However, the strength may have a dramatic decline as the test temperature

approaches the melt temperature. This relatively small decrease indicates that this composite's tensile strength is a fiber-dominated property.

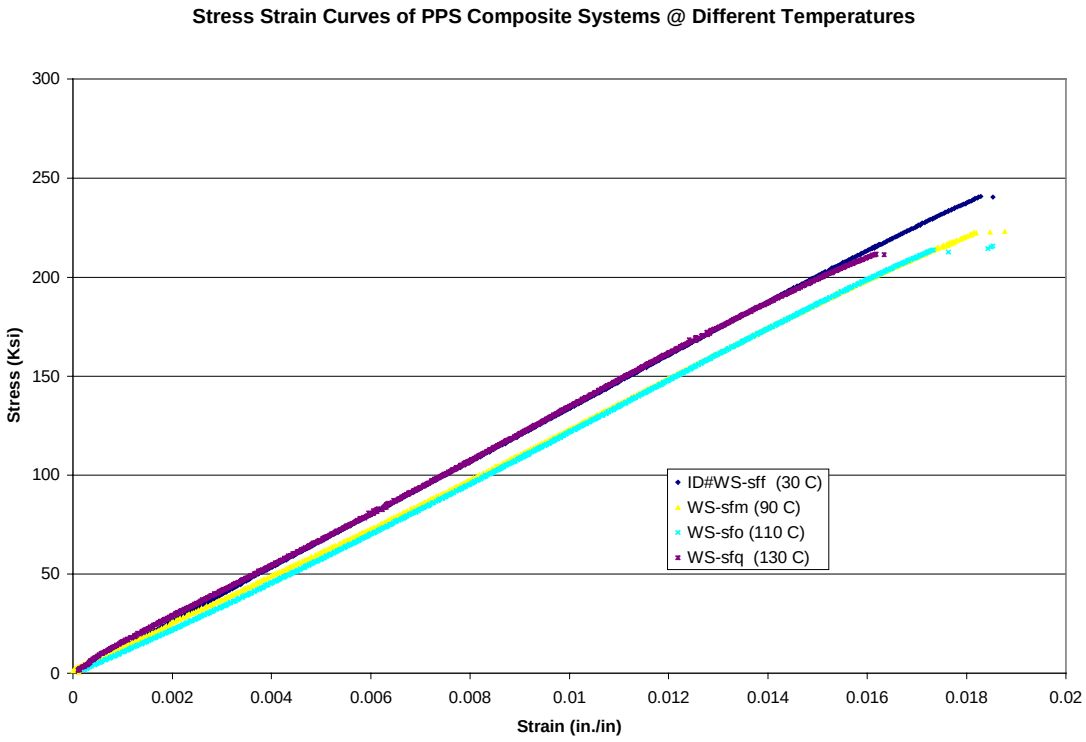

Figure 3.10 A family of stress-strain curves for PPS composites at four different temperatures (30, 90, 110, and 130 degrees Celsius).

Representative stress-strain curves are shown in Figure 3.10, to illustrate how the stiffness is decreasing as a function of temperature. The family of curves is not a collection of the averages at these temperatures (contains the stress strain curves of four individual specimens).

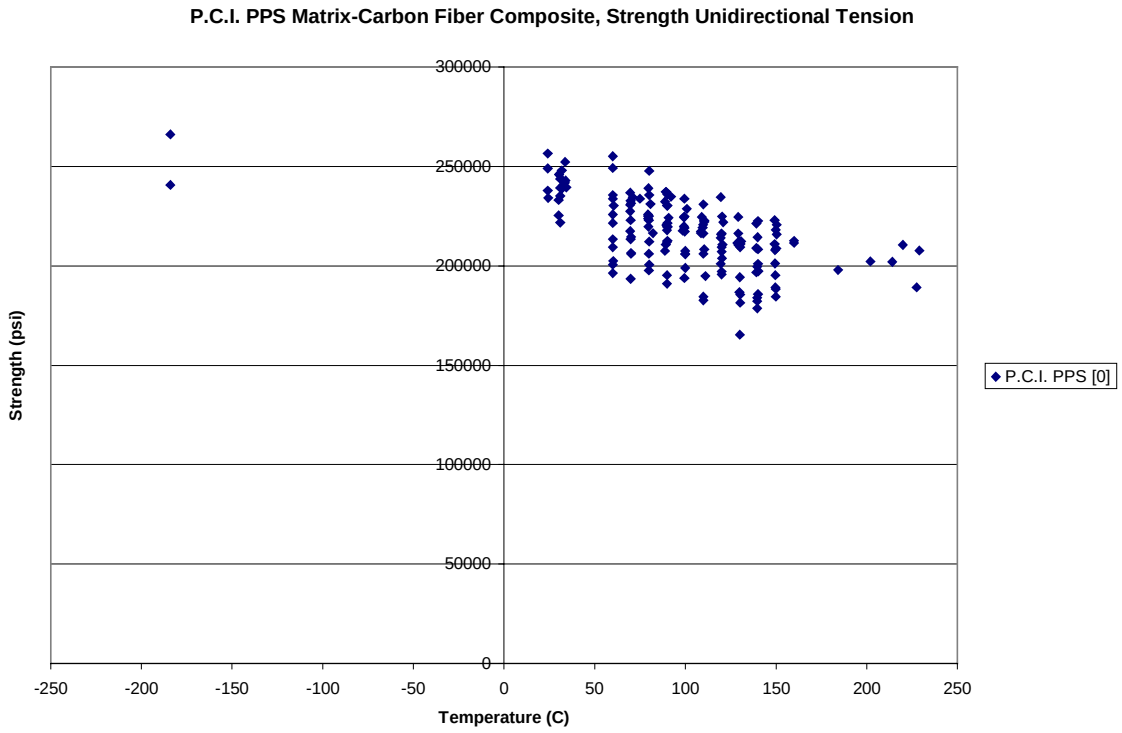

Figure 3.11 Strength of PPS composite at elevated temperatures and cryogenic temperatures.

In addition to the elevated temperature tests, the system was also evaluated at cryogenic temperatures. The evaluation was not as extensive as the elevated temperatures; nevertheless, some data was obtained (Figure 3.11). It appears that the PPS composite gains strength at cryogenic temperatures when compared to room temperature strength values. No strain measurements were made of the cryogenically tested specimens. Future testing should be conducted in this area.

Fracture Modes

The failure mode for the PPS composite was of the type XGM (X-explosive, G-gage, M-middle) according to the ASTM Standards D 3039 [12]. They had excessive

longitudinal splitting making the failure surfaces highly irregular and jagged. These types of failures are sometimes defined as being a “plastic” failure. Plastic failure occurs when the fiber debonds from the matrix prior to overall failure of the composite. The failures of two specimens are shown in Figure 3.12 and Figure 3.13. Figure 3.12 shows the failure at 31.1 degrees Celsius and Figure 3.13 shows the failure at 229 degrees Celsius. At the elevated temperature, the matrix appears to be curling or pealing back at failure.

Figure 3.12 Fracture of PPS specimen at 31.1 degrees Celsius (Front and Side Views).

Figure 3.13 Fracture of PPS specimen at 229 degrees Celsius (Front and Side Views).

Vinyl Ester

Fiber Volume Fraction

Table 3.03 Volume fracture measurements for vinyl ester matrix composite with an epoxy fiber-matrix interface.

Specimen #	Dry Weight (gr.)	Wet Weight (gr.)	Density of Vinyl Ester	Volume Fraction of Fiber
1	0.4155	0.2137	1.6101	0.6461
2	0.4362	0.2263	1.6251	0.6773
3	0.6199	0.3193	1.6126	0.6513
4	0.6144	0.3179	1.6204	0.6676
5	0.4531	0.2340	1.6172	0.6608

As shown in Table 3.03, the average percent fiber in the Vinyl Ester Composite was 66 percent. This is for the vinyl ester composite with the epoxy fiber-matrix interface. Fiber volume fraction tests were not preformed on the vinyl ester composite with a polyurethane fiber-matrix interface because the both composite systems were products of the same pultrution method. Also for this calculation the composite was assumed to consist of only vinyl ester and carbon fiber (no interphase effect was included). The fiber-matrix interface material should be in low concentrations. Therefore, the percent fiber volume fraction should be the same for both systems.

Results of Macro-Mechanical Test

In addition to the PPS composite system, a thermosetting plastic matrix was studied at elevated temperatures. The matrix is made of vinyl ester with two different fiber-matrix interfaces, epoxy and polyurethane. Epoxy is a thermosetting polymer and polyurethane is a thermoplastic. The fiber is made of carbon, however, it was not determined what specific type of fiber was in the composite. Only some statistical analysis was determined for this composite system because the supply of material was low (Tables 3.04 and 3.05).

Table 3.04 Strength and stiffness results of vinyl ester composite with an epoxy fiber-matrix interface.

Test Temperature (C)	# of Specimens	Average Strength (ksi)	Standard Deviation for Strength	Average Stiffness (x10^6 psi)	Standard Deviation for Stiffness
35	2	109.5	12.1	16.23	0
70	2	106.3	1.90	14.66	0
90	2	101.8	3.80	15.39	0.62
110	2	89.0	0.99	14.40	0.40
130	1	83.6	N/A	14.60	N/A
140	1	76.1	N/A	14.60	N/A
-123.3	1	131.5	N/A	N/A	N/A

Table 3.05 Strength and stiffness results of vinyl ester composite with a polyurethane fiber-matrix interface.

Test Temperature (C)	# of Specimens	Average Strength (ksi)	Standard Deviation for Strength	Average Stiffness (x10^ psi)	Standard Deviation for Stiffness
34	2	160.3	1.11	18.1	0.50
90	1	124.8	N/A	17.1	N/A
110	1	129.9	N/A	16.8	N/A
130	1	121.7	N/A	16.3	N/A
150	1	108.8	N/A	N/A	N/A
-189.4	3	175.6	8.83	18.7	0.65
-101.0	1	156.0	N/A	17.7	N/A

.

Figures 3.14 and 3.15 show a typical stress-strain curve for the vinyl ester system. The strain was measured by the extensometer for all of the specimens in this family. The stiffness of young's modulus was measured from the stress strain curve using the slope of the curve up to 40 percent of the failure strength.

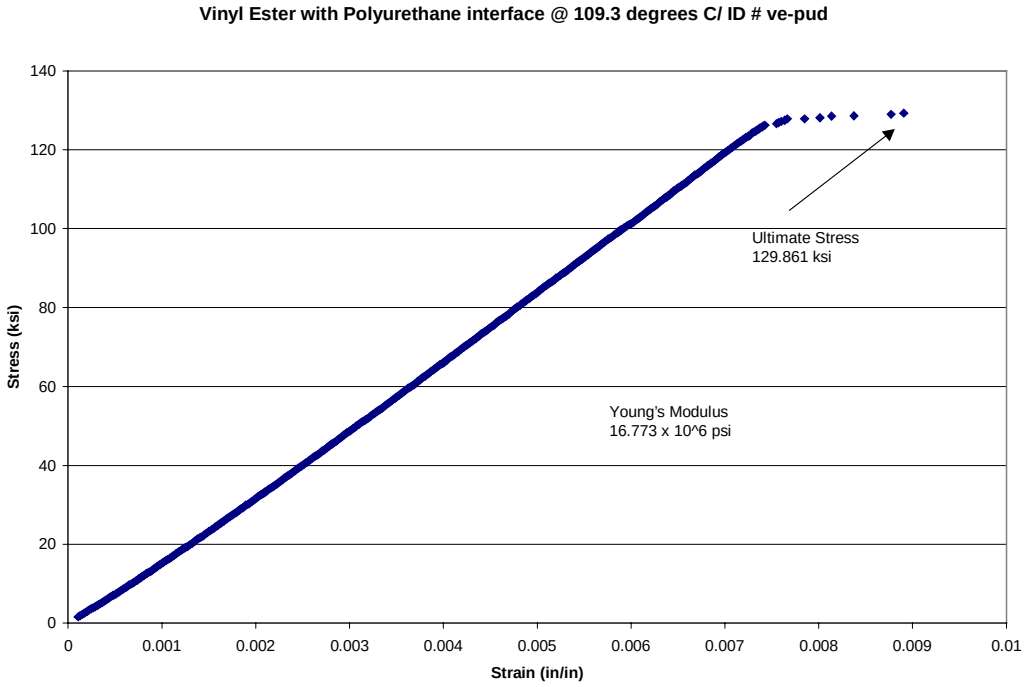

Figure 3.14: Stress-strain curve for vinyl ester with polyurethane interface.

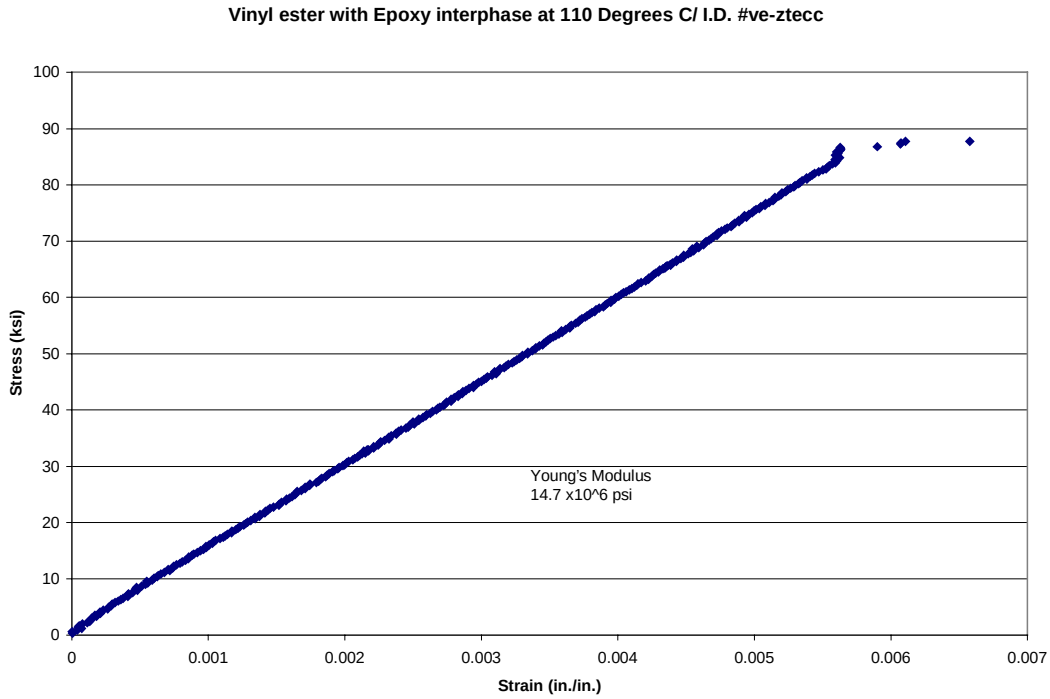

Figure 3.15 Stress-strain curve for vinyl ester with epoxy interface.

As with the PPS composite system, the strength of the vinyl ester composite system declines with elevated temperatures (Figure 3.16). The decline in strength for the vinyl ester system, from 30 degrees to 140 degrees Celsius, is about 30 percent. Both of the different fiber-matrix interfaces demonstrated this decline.

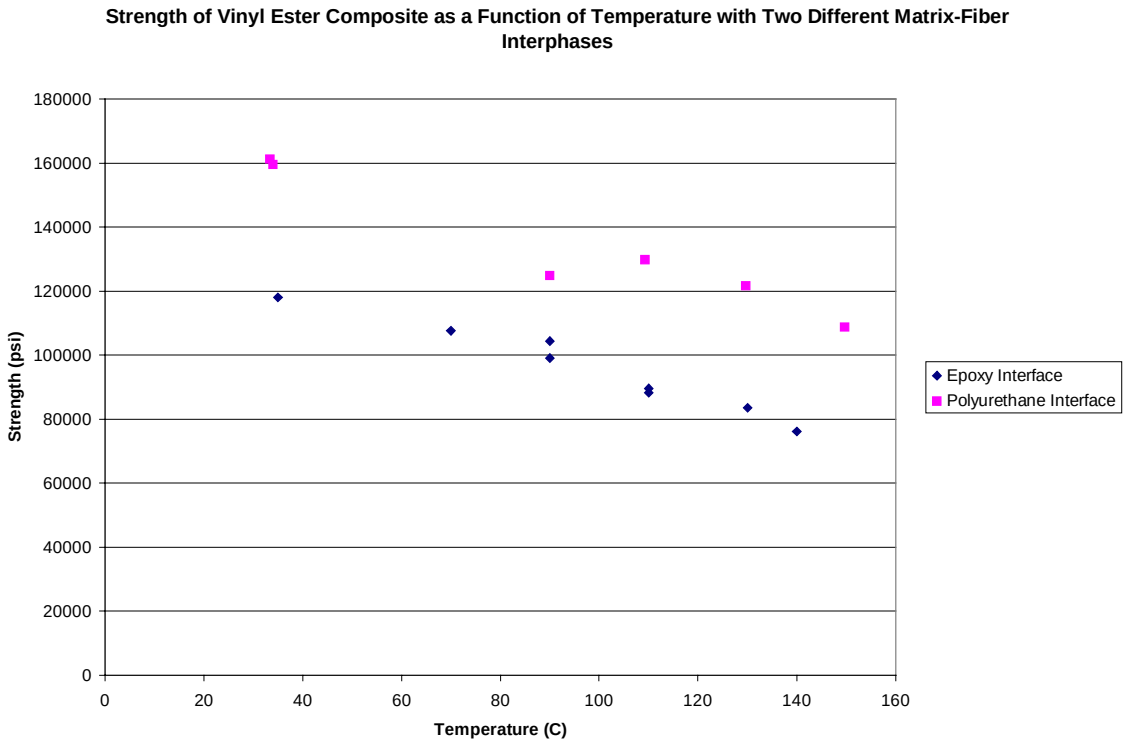

Figure 3.16 Strength of vinyl ester composite as a function of temperature and two different interfaces.

The stiffness was measured for this material at the elevated temperatures. The results are expressed in Figure 3.17. Again, like the PPS composite, the stiffness does not decline at the same rate of as the strength declines at the elevated temperatures. The decline in stiffness (young's modulus) from 30 degrees to 150 degrees Celsius was measured to be approximately 13 percent. However, more specimens must be tested in order to make more accurate conclusions.

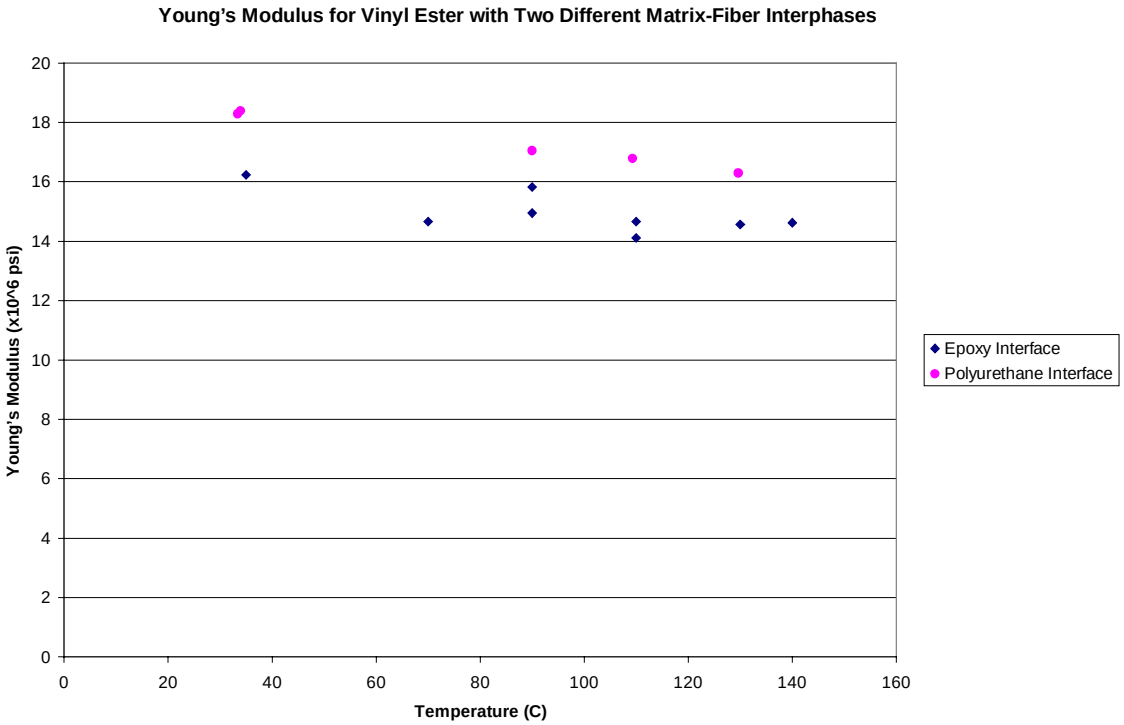

Figure 3.17 Stiffness of vinyl ester composite as a function of temperature and two different interfaces.

Representative stress-strain curves are shown in Figure 3.18. This figure shows the strength and stiffness changes as a function of temperature. This figure illustrates that temperature does not effect the elastic region of the stiffness; however, the temperature effect is in the inelastic region.

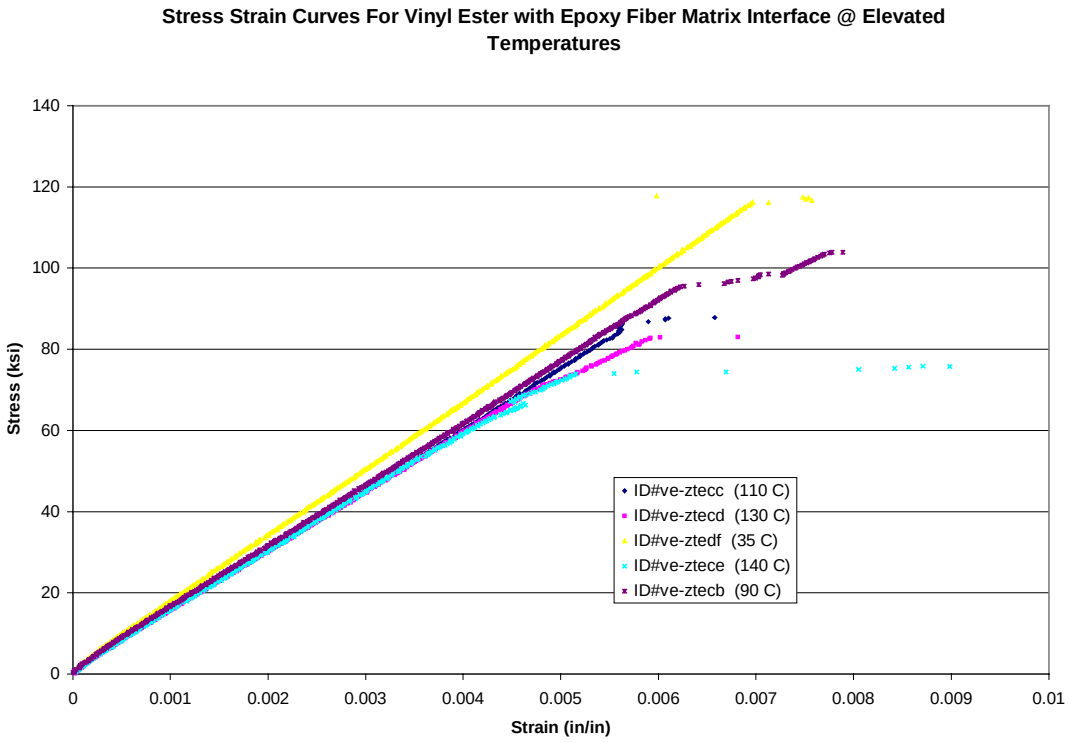

Figure 3.18 A family of stress-strain curves for vinyl ester composite with an epoxy fiber-matrix interface at different temperatures (90, 140,35,110, and 130 Degrees C).

In addition to the elevated temperature strength values, cryogenic temperature tests were conducted on the vinyl ester system. As with the PPS system, the strength of the system appears to increase at the cryogenic temperatures compared with the room temperature values. The results of these tests are added to the elevated temperature results and shown in Figure 3.19.

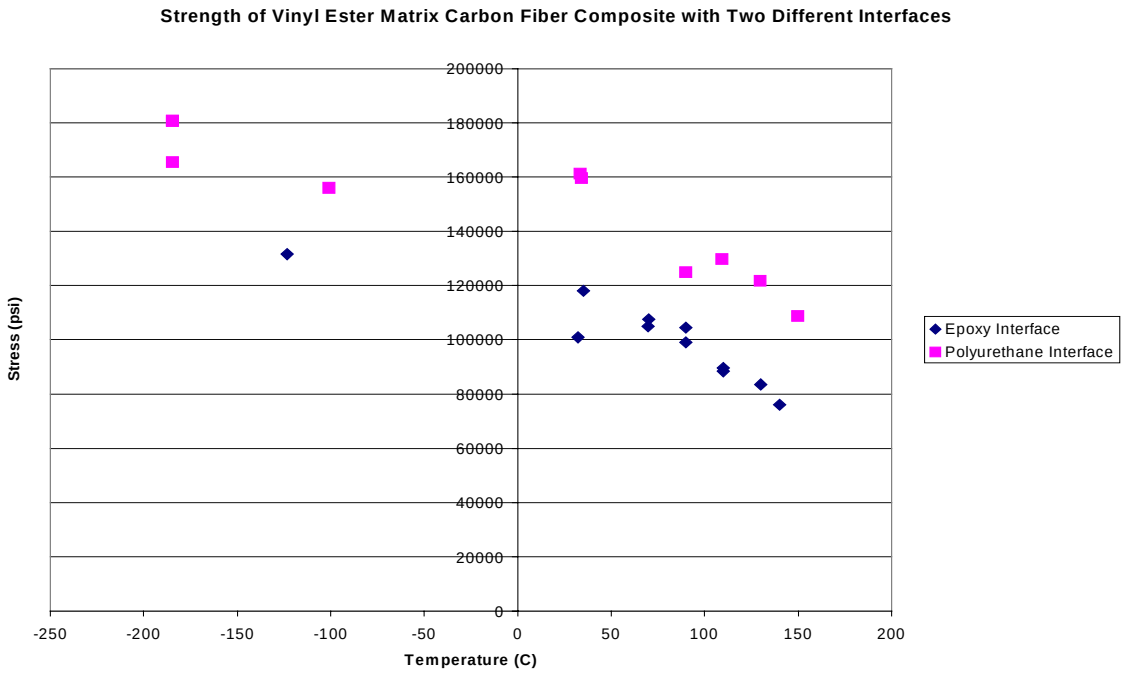

Figure 3.19 Strength for vinyl ester composite with both interfaces at elevated temperatures and cryogenic temperatures.

In addition to the strength at cryogenic temperatures, the stiffness was measured on the vinyl ester system with strain gages. Table 3.04 and Table 3.05 report the stiffness values at these temperatures, and Figure 3.20 shows these stiffness values added to the elevated temperature values. The system appears to gain stiffness at the cryogenic temperatures compared to the room temperature values. The testing at these temperatures was not as extensive as the elevated temperature tests.

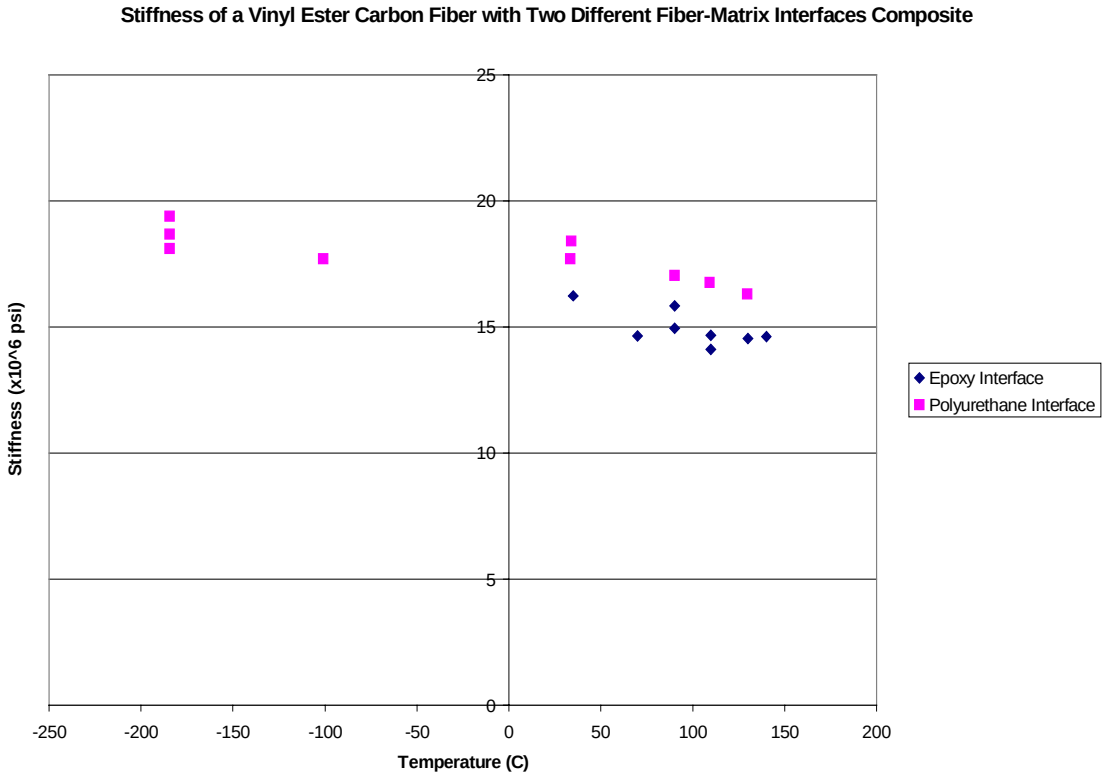

Figure 3.20 Stiffness values of the vinyl ester composite with both fiber-matrix interfaces at elevated temperature and cryogenic temperatures.

Fracture Modes

The failure mode for both vinyl ester systems were characterized as type XGM (X-explosive, G-gage, M-middle) according to the ASTM Standard D 3039/D 3039M-93 [12]. The vinyl ester system with the polyurethane fiber-matrix interface offers a failure mode change. This is shown in Figure 3.21 to Figure 3.22. The room temperature failure (Figure 3.21) has splitting of the matrix with clumps of fiber. However the failure at 150 degrees Celsius (Figure 3.22) is more of a "fluffy" failure of the composite. In explanation of this difference, the elevated temperature appears to be debonding from the fibers. At lower temperatures a more brittle failure in the matrix occurs making the

failure to have clumps of fibers. In the elevated temperature the matrix is less stiff and the failure is not clumped with groups of fibers. This also gets back to the discussion of ineffective length. At the higher temperatures the matrix is less stiff and this causes the ineffective length to become larger. With the large ineffective length, the stress is only gradually transferred to other fibers. Therefore, the fiber fracture regions are able to interact and connect together over long distances to cause failure. This is why the failure is more "fluffy" and more fibers are involved in the failure. Figures 3.23, 3.24, and 3.25 show other temperature fractures.

Figure 3.21 Fracture of a vinyl ester specimen with polyurethane fiber-matrix interface at 33.4 degrees Celsius (Front and Side Views).

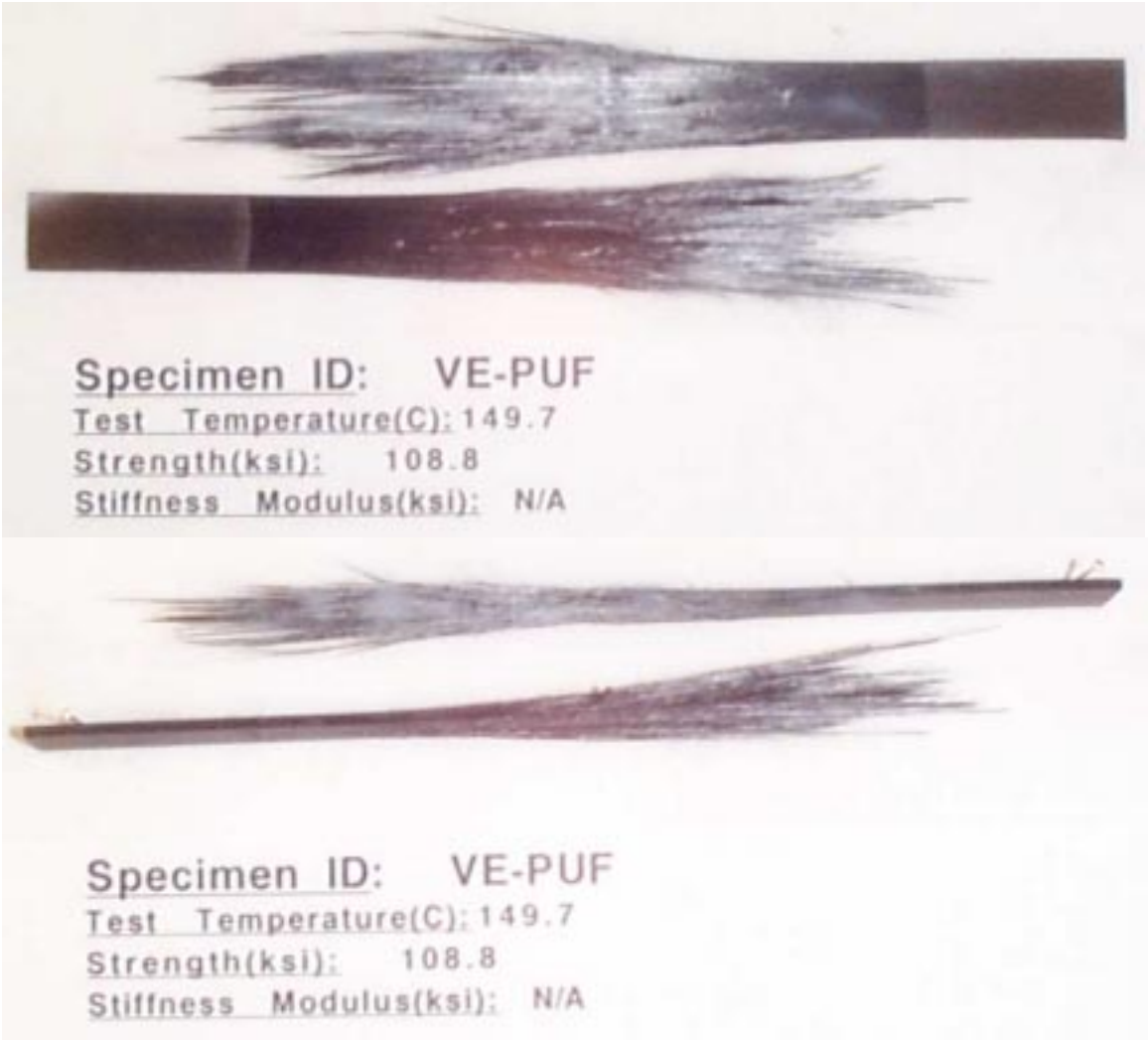

Figure 3.22 Fracture of a vinyl ester specimen with polyurethane fiber-matrix interface at 149.7 degrees Celsius (Front and Side Views).

Figure 3.23 Fracture of a vinyl ester specimen with polyurethane fiber-matrix interface at -184.4 degrees Celsius (Front and Side Views).

Figure 3.24 Fracture of a vinyl ester specimen with epoxy fiber-matrix interface at 35 degrees Celsius (Front and Side Views).

Figure 3.25 Fracture of a vinyl ester specimen with epoxy fiber-matrix interface at 140 degrees Celsius (Front and Side Views).

PEEK

Fiber Volume Fraction

Table 3.06 Results of fiber volume fraction test for PEEK matrix composite.

Specimen #	Dry Weight (gr.)	Wet Weight (gr.)	Density of PEEK	Volume Fraction of Fiber
1	0.3536	0.1824	1.6152	0.7333
2	0.4801	0.2433	1.5855	0.6852
3	0.4697	0.2380	1.5853	0.6849
4	0.4617	0.2349	1.5919	0.6957
5	0.4423	0.2258	1.5976	0.7048
6	0.4471	0.2277	1.5936	0.6984

The average fiber volume fraction of the PEEK matrix composite was 69 percent carbon fiber (Table 3.06).

C-Scans Results

The C-Scan was nondestructive evaluation used to detect any major flaws in the panel formation. Three 10 inch by 10 inch panels were C-Scanned for flaws. No detectable flaws were found in any of the panels. Figure 3.26 is an example of a C-Scan on one of the panels.

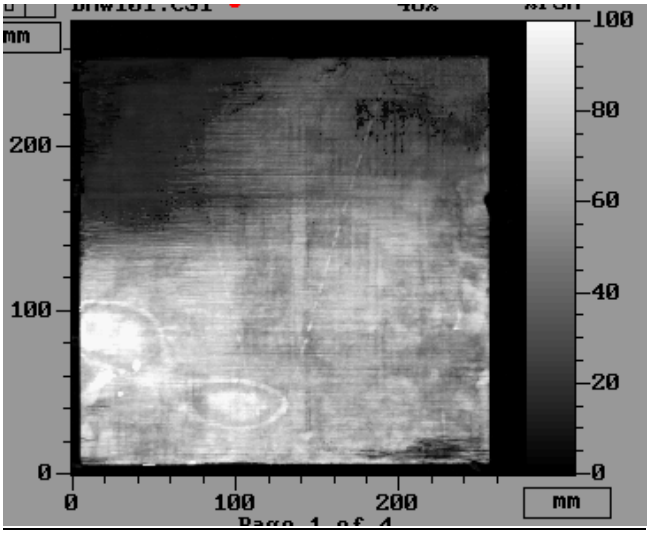

Figure 3.26 C-Scan of PEEK matrix composite.

Results of Macro-Mechanical Test

Thirty specimens were tested for ultimate strength on the MTS at a loading rate of 50 lb./sec. Strain was also measured for many of the specimens with both a strain gage and an extensometer. The stiffness was measured on the linear domain of the stress-strain curve. This slope was calculated up to approximently 50 % of the failure strength. The results of this analysis are given in Table 3.07.

Table 3.07 Strength and stiffness results for PEEK matrix composite.

Test Temper-ature (C)	# of Speci-mens	Average Strength (ksi)	Standard Deviation of Strength	Average Stiffness from Extensometer (x10^6 psi)	Standard Deviation for Extensometer Stiffness	Average Stiffness from Strain Gage (x10^6 psi)	Standard Deviation for Strain Gage Stiffness
27.7	6	333.2	24.2	22.2	0.76	21.7	0.22
60	3	308.3	34.0	21.4	1.2	20.4	1.31
70	3	312.0	15.6	22.5	0.87	21.7	0.25
80	3	317.3	26.1	21.9	0.71	21.2	0.71
90	1	318	0	23.3	0	21.5	0
100	2	295.5	68.5	22.5	0.49	21.3	0
110	1	283	0	N/A	N/A	19.0	0
120	2	301.5	12.0	22.1	0.33	21.9	0.14
140	1	343	0	22.7	0	22.1	0
150	1	302	0	21.5	0	21	0
160	3	299.7	9.3	23.6	1.41	20.9	1.11
170	1	297	0	23.7	0	21.5	0
180	2	282.5	2.12	N/A	N/A	N/A	N/A
190	1	269	0	N/A	N/A	N/A	N/A

Figures 3.27, 3.28, and 3.29 show typical stress strain curves for the PEEK matrix composite at 150, 100, and 27.7 degrees Celsius. All of the plots contain both the extensometer and the strain gage measurements of strain. In each case the extensometer measures a higher strain then the strain gage. However, the stiffness up to 50% of failure is in good agreement between the two measurement devices. The extensometer begins to measure a relatively higher modulus than the strain gage after 150 degrees Celsius (Table 3.07). This is most likely due to the fact that the MTS extensometer is only temperature compensated up to 150 degrees Celsius according to the manufacture.

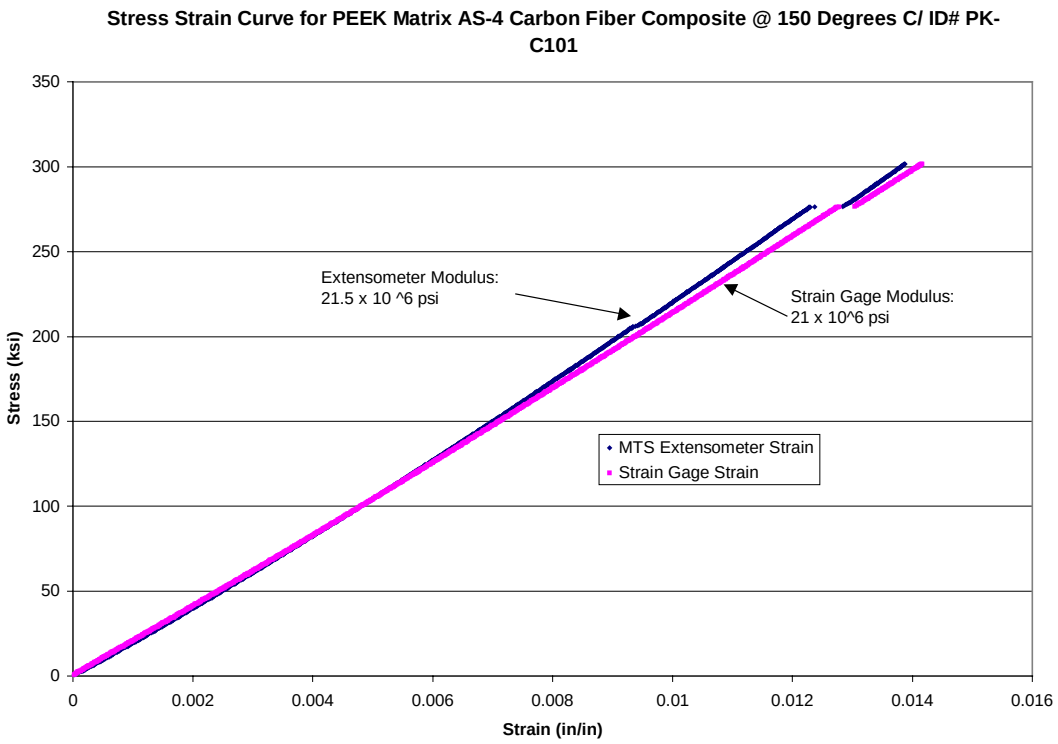

Figure 3.27 Stress-strain curve for PEEK matrix composite at 150 degrees C.

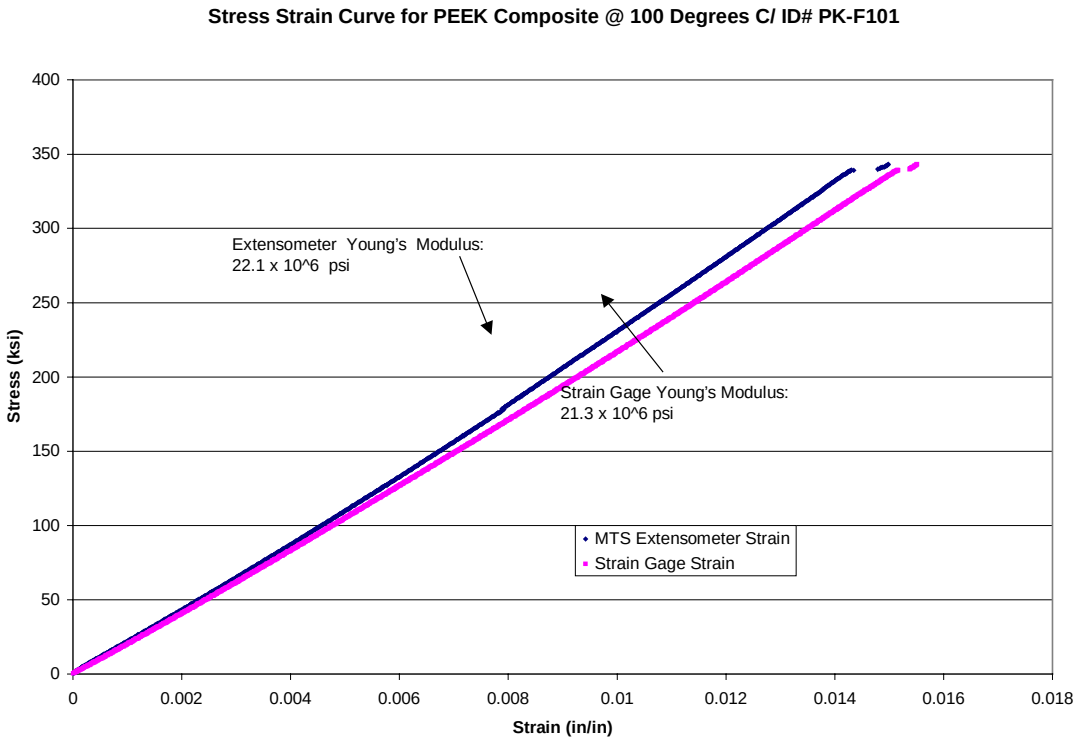

Figure 3.28 Stress-strain curve of a PEEK matrix composite at 100 degrees C.

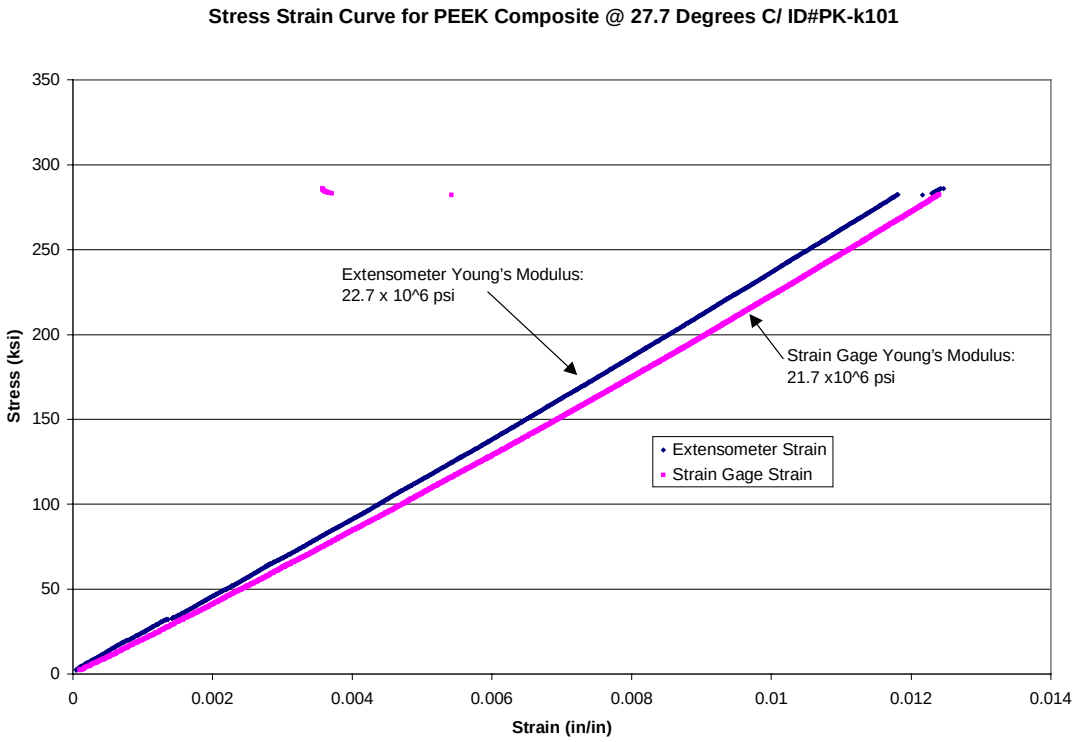

Figure 3.29 Stress-strain curve for PEEK matrix composite at 27 degrees C.

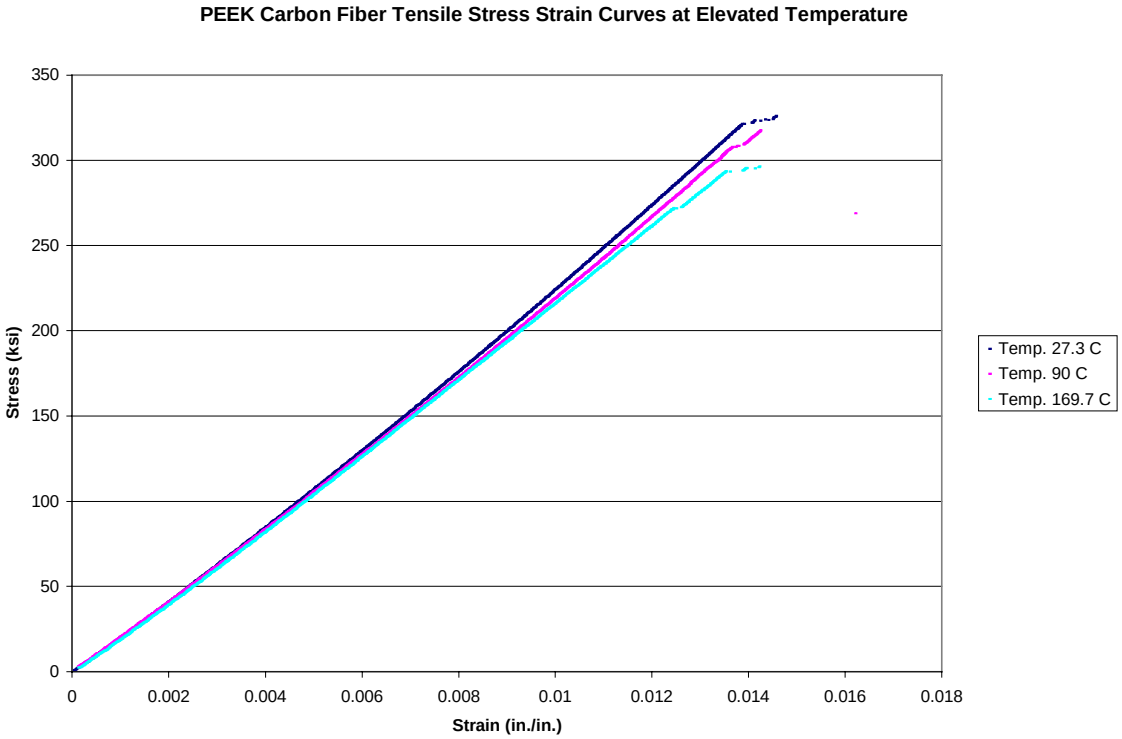

Figure 3.30 A family of stress-strain curves for PEEK matrix at different temperatures (27, 90, and 170 Degrees C).

Figure 3.30 shows a family of stress-strain curves that indicate the behavior of these curves for different temperatures. The stiffness of this material (measured to 50% before failure) does not seem to change as a function temperature. However this is misleading because the stiffness was estimated up to 50% of the failure strength. The stiffness does not change in this domain at the different temperatures. This figure also indicates the small change in the strength of this material in this temperature range. The family of curves also shows that the failure strain remains about the same at the different temperatures. The first 50% of the curve can be approximated by a linear line; however the other 50% is non-linear.

The failure strength decreases about 20% from 30 degrees Celsius to 190 degrees Celsius. This is shown in Figure 3.31. However the stiffness, measured by both a strain gage and extensometer, remains essentially constant from this temperature range. This is shown in Figure 3.32 and Figure 3.33.

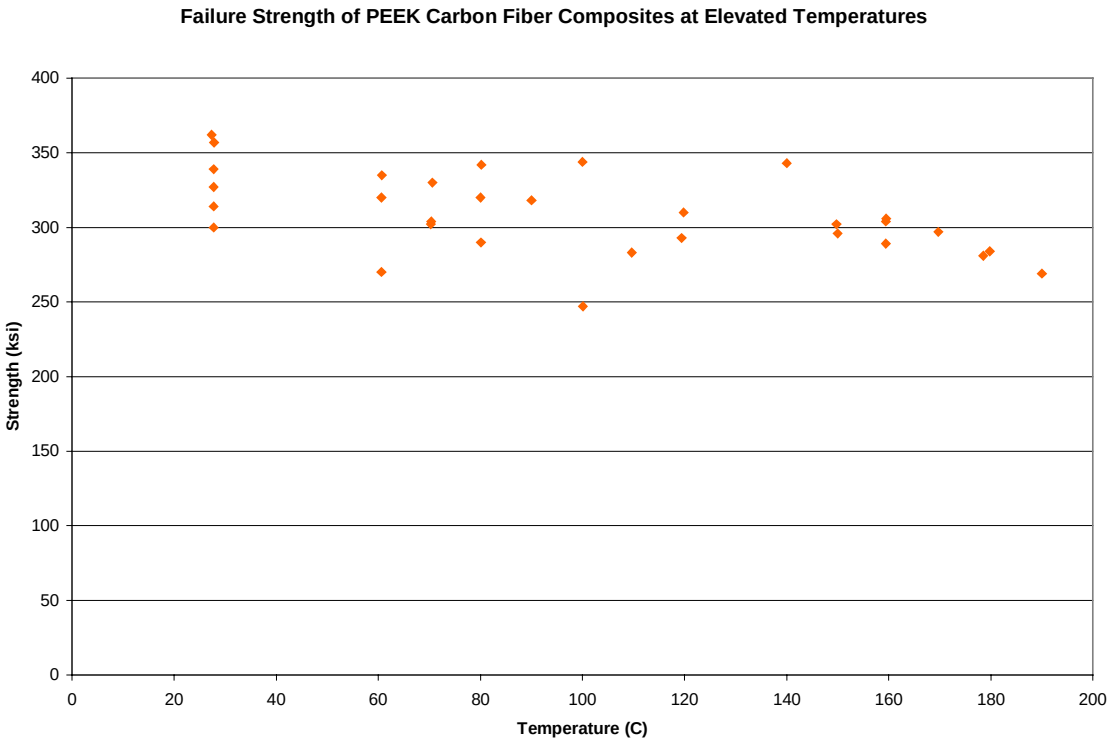

Figure 3.31 Strength values of PEEK matrix composite at elevated temperatures.

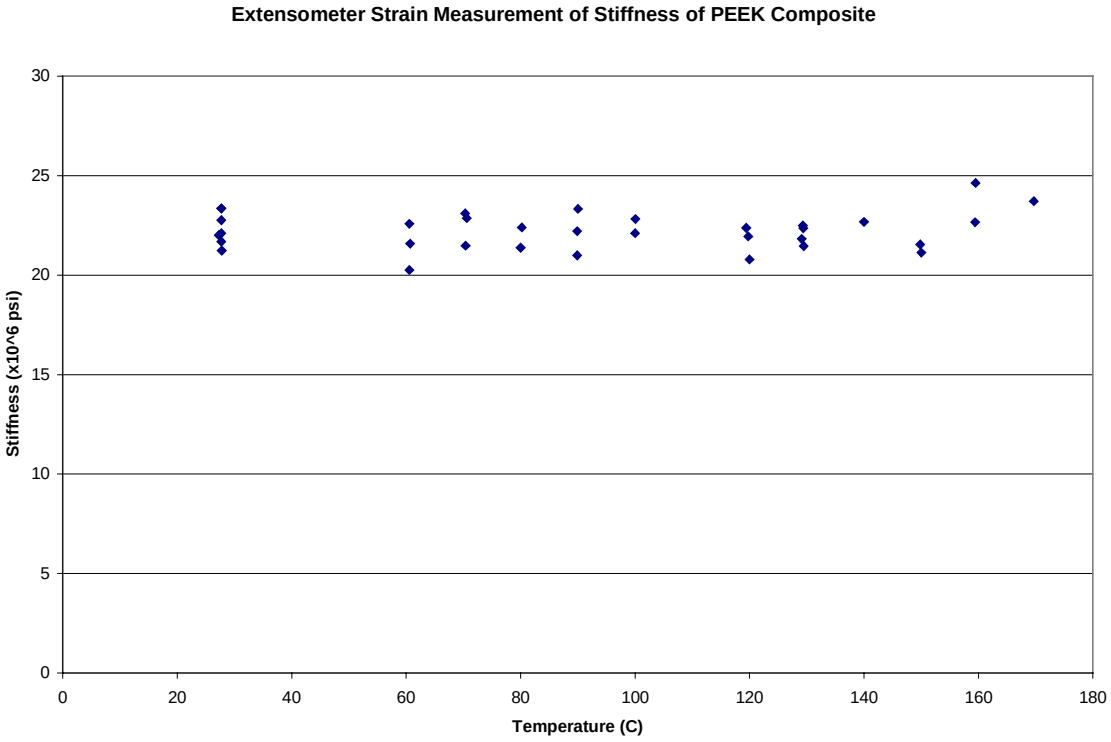

Figure 3.32 Stiffness values for PEEK matrix composite measured with an extensometer.

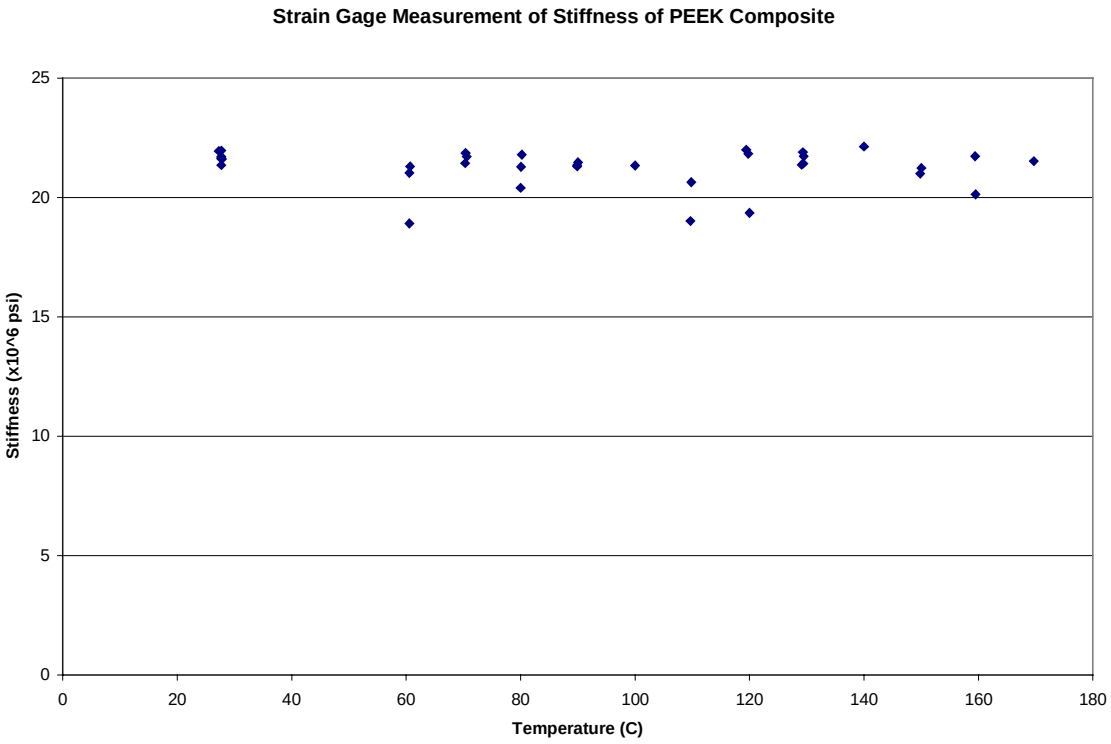

Figure 3.33 Stiffness of PEEK matrix composite measured with a strain gage.

The average strength and the standard deviation of these values are shown in Figure 3.34. This data set is not as extensive as the PPS system; however, it is more extensive than the vinyl ester set. The deviation at the lower temperatures appears to be more extensive than at the higher temperatures. However this might be just the scatter of the material and more specimens should be tested at these temperatures for the complete picture.

In addition to the strength, the average stiffness and the standard deviation of these values are shown in Figure 3.35. This figure compares the extensometer and strain gage strain for the stiffness calculation. As mentioned above, the extensometer measured a higher stiffness than the strain gage.

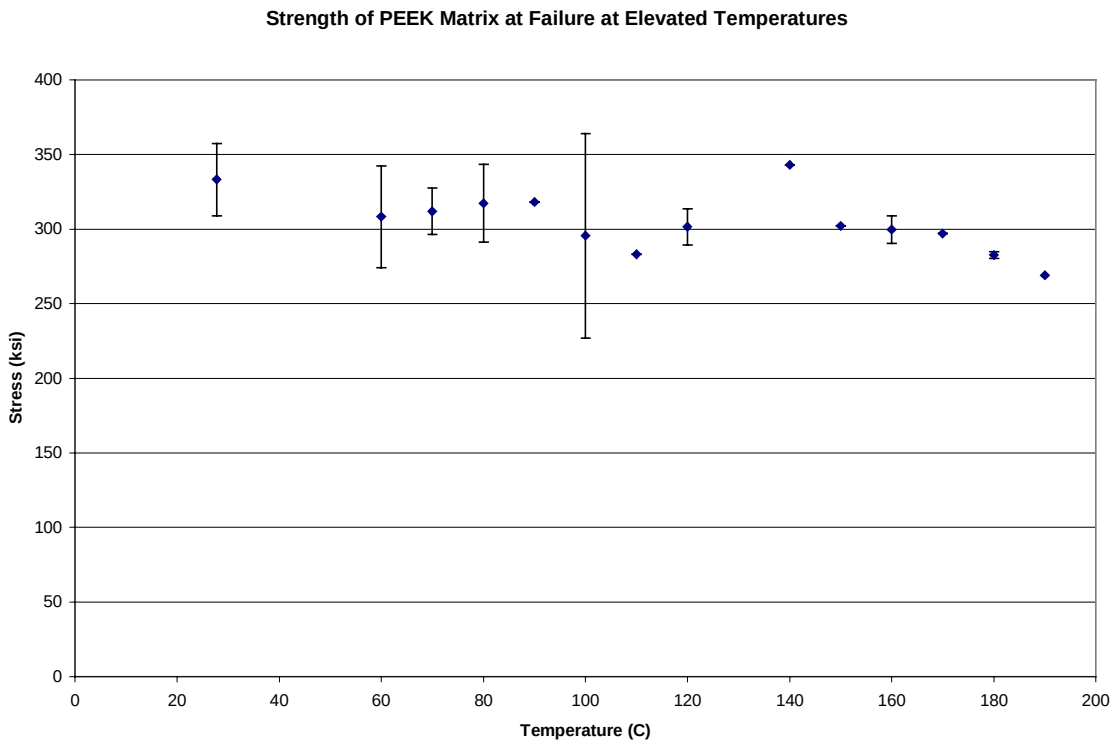

Figure 3.34 Average strength of PEEK matrix composite with standard deviations.

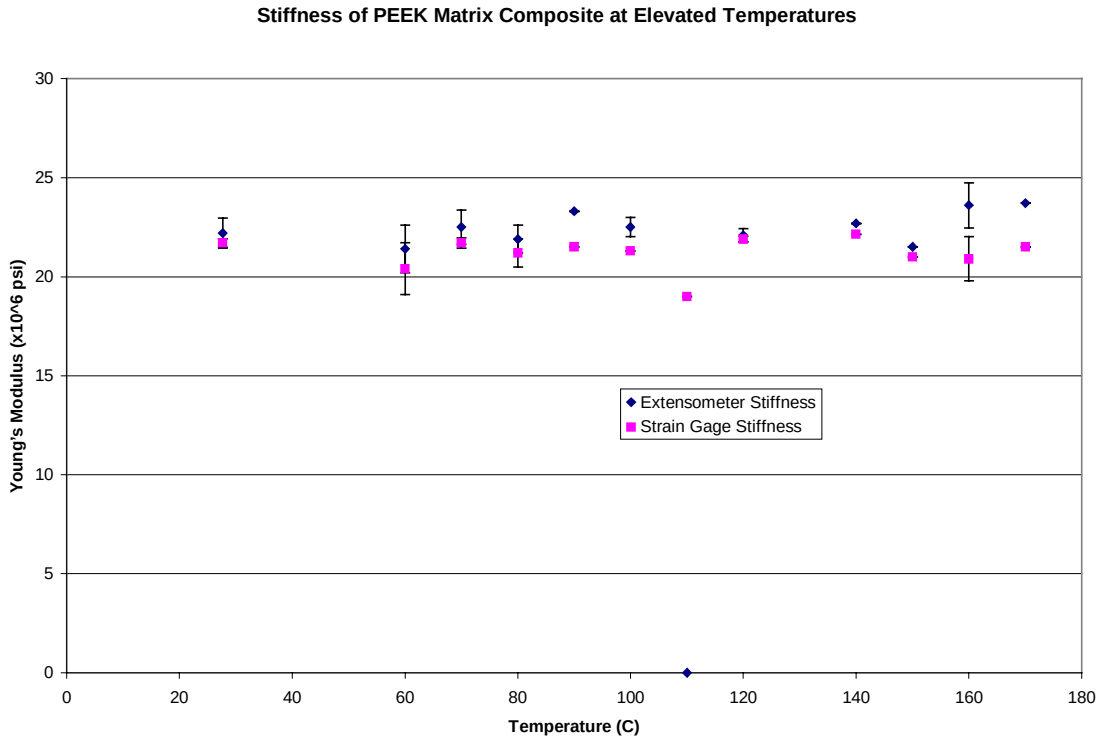

Figure 3.35 Stiffness of PEEK matrix composite with standard deviations.

Fracture Modes

The failure mode for this system is not fully characterized in the ASTM Standards. The failure was a complete "explosion" of the material. Many times after failure the only material left in the MTS were the glass epoxy tabs in the grips. This could be a result of the high volume fraction of fiber.

Summary of Experimental Results

The unidirectional tensile strength of the PPS composite system decreased by 17 percent from 30 degrees Celsius to 140 degrees Celsius. The unidirectional stiffness of this same system decreased 7.7 percent between 30 and 130 degrees Celsius. These changes appear to occur near two distinct points, at the bulk PPS glass transition temperature and the PPS composite glass transition. The loading rate did not affect the strength of this system over the ranges of 40 to 150 pounds per second. The strength of the system slightly increases at -180 degrees Celsius compared to room temperature.

The unidirectional tensile strength of the vinyl ester composite with two different fiber-matrix interfaces decreased by 30 percent from 30 to 140 degrees Celsius. The unidirectional stiffness of these systems decreased by 13 percent from 30 to 150 degrees Celsius. The strength of those systems slightly increased at -180 degrees Celsius compared to room temperature strength. The stiffness of the vinyl ester composite with the polyurethane interface slightly increased at -180 degrees Celsius. A failure mode change in the vinyl ester composite with the polyurethane interface was found between 150 and 30 degrees Celsius.

The unidirectional tensile strength of the PEEK composite decreased by 20 percent from 30 to 190 degrees Celsius. The unidirectional elastic stiffness was essentially constant in this temperature range. However, the temperature did affect the inelastic region of the stiffness for this system.

IV. Model Development and Prediction of Experimental Results

Parametric Study

In order to examine how the interfacial shear strength affects the strength of the composite, a parametric study was preformed with the two models discussed in the literature review. Both interfacial shear strength and the polymer shear modulus were studied parametrically to examine how they effect the composite strength. After the shear modulus parametric study, it was determined that this parameter does not effect the strength of the composite as much as the interfacial shear strength effects the composite strength. Figure 4.01 shows how the interfacial shear strength effects the strength values as it is decreased from 8000 (psi). Typical values of the interfacial shear strength are in this range. This parametric study did not take in account the fact that both the shear modulus and strength are changing. However, it did demonstrate that the composite strength, based on the models, does change by large amounts as the interfacial shear strength is changed.

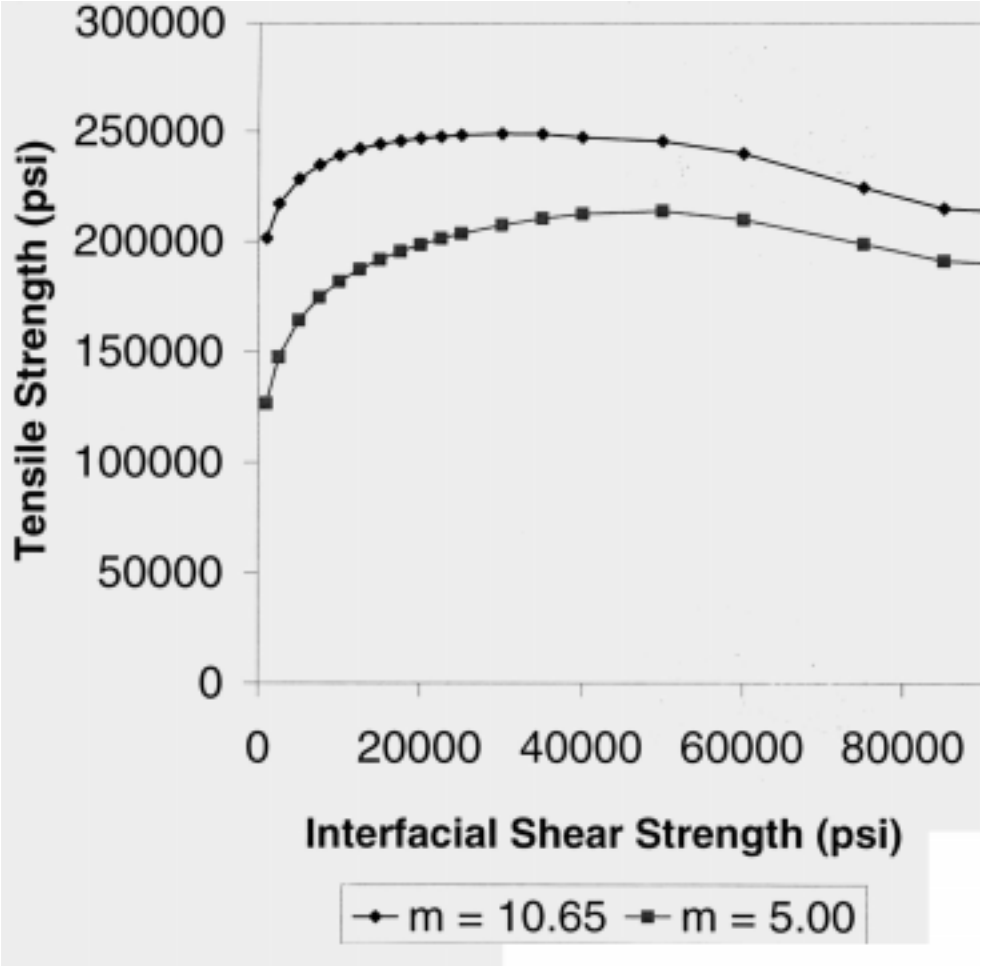

Figure 4.01 Parametric study of the interfacial shear strength effect on strength of a composite.

Changes to Model Parameters for Elevated Temperature

As Figure 1.06 indicated, the interfacial shear strength should be some function of temperature. No specific measurement was made on the interfacial shear strength with PPS and a carbon fiber at elevated temperatures. Assuming this trend would apply to the PPS system, an approximation was generated of the interfacial shear strength as a function of elevated temperatures. This is shown in Figure 4.02. The approximation used a value of room temperature interfacial shear strength for PPS with a carbon fiber found in the literature [13]. Using the room temperature as one reference point and the melt

temperature of PPS as the other reference point, a straight line was fitted. At melt temperature, the interfacial shear strength was assumed to be zero.

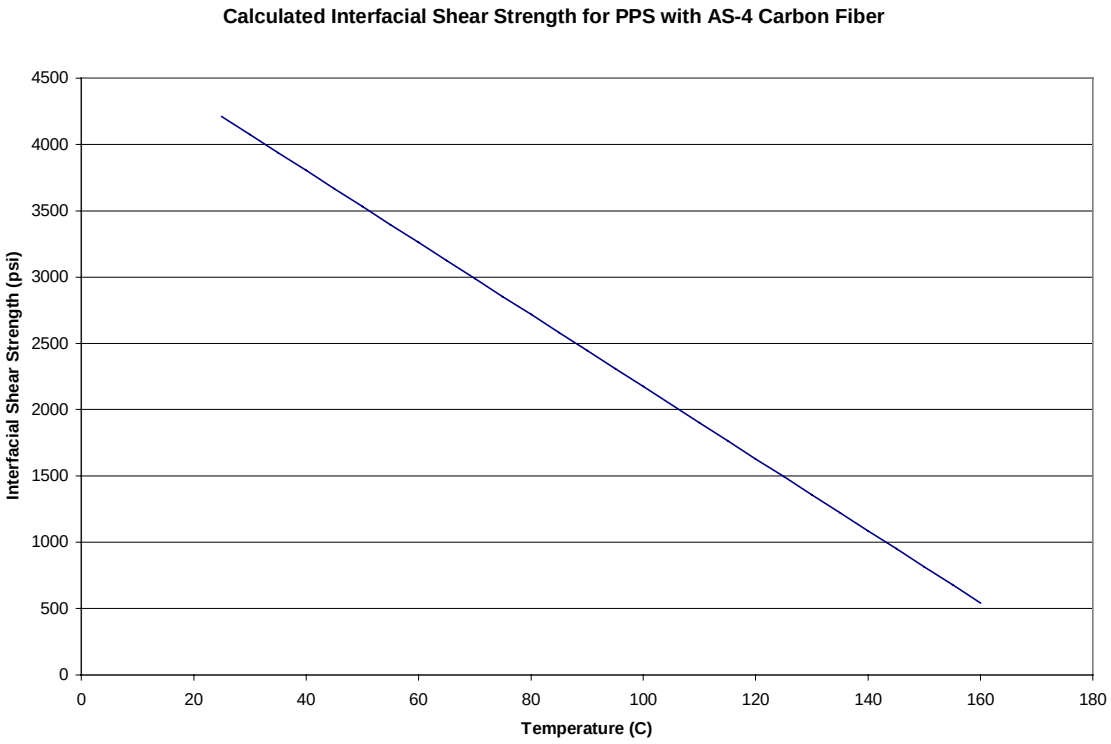

Figure 4.02 Approximation of the interfacial shear strength as a function of temperature for a PPS composite system.

In addition to the interfacial shear strength, Figure 1.08 indicated that the stiffness of the matrix material should be some function of temperature. No specific measurement was made on the stiffness of the PPS polymer. So assuming this trend would apply to the PPS polymer, an approximation was generated of the stiffness as a function of elevated temperatures. This is shown in Figure 4.03. The approximation used a value of the stiffness a room temperature of the PPS found in the literature [9]. Using the room temperature of PPS as one reference point and the melt temperature of PPS as the other

reference point a straight line was fitted. At melt temperature, the stiffness of PPS was assumed to be zero.

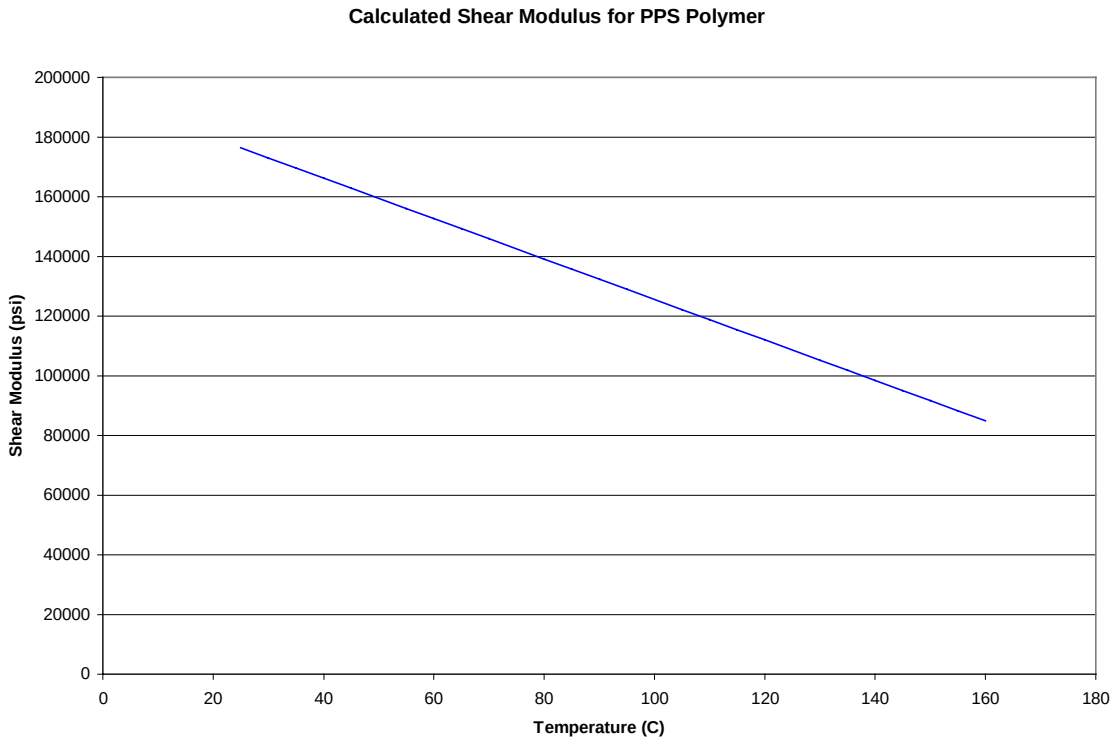

Figure 4.03 Approximation of the shear modulus as a function of temperature for the PPS matrix.

In addition to the PPS system, the interfacial shear strength of the PEEK system should be some function of temperature. No specific measurement was made on the interfacial shear strength with PEEK and a carbon fiber at elevated temperatures. So assuming that a trend similar to Figure1.06 applies to the PEEK system, an approximation was generated of the interfacial shear strength as a function of elevated temperatures. This is shown in Figure 4.04. The approximation was generated by using a value of interfacial shear strength at room temperature for PEEK with a carbon fiber found in the literature [13]. Using the room temperature as one reference point and the

melt temperature of the PEEK matrix as the other reference point a linear line was fitted as the approximation. At melt temperature, the interfacial shear strength was assumed to be zero.

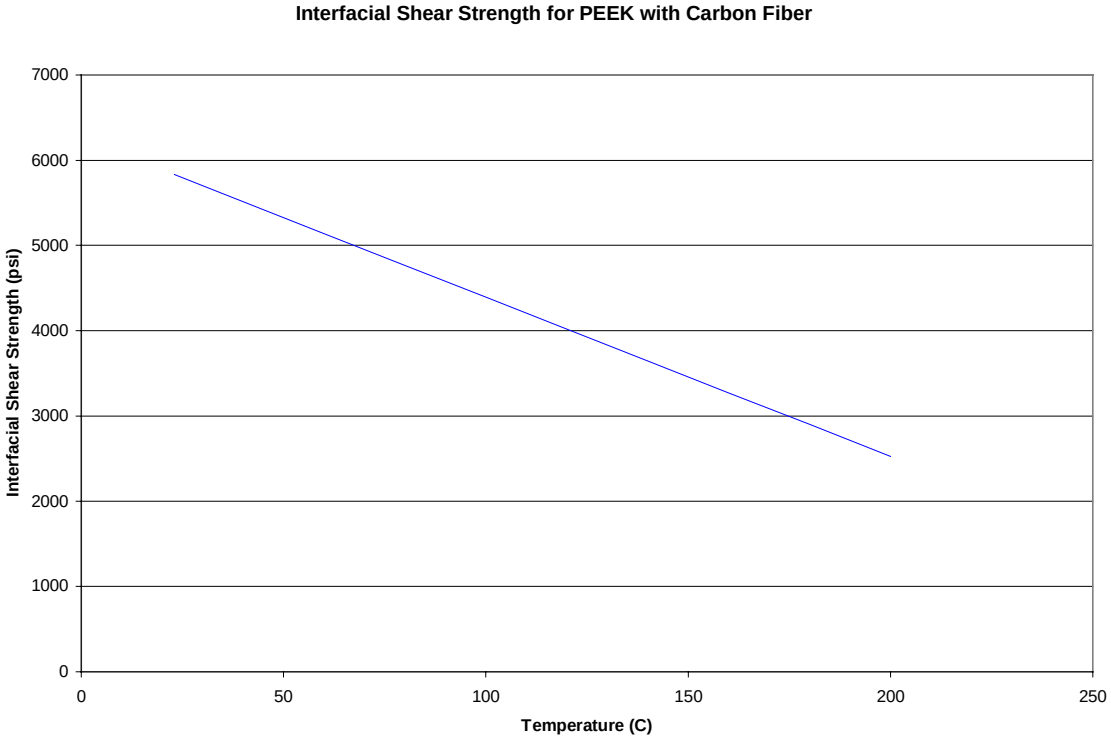

Figure 4.04 Approximation to the interfacial shear strength as a function of temperature for PEEK composite system.

As mentioned above, Figure 1.08 indicated that the stiffness of a polymer material should be some function of temperature. No specific measurement was made on the stiffness of PEEK at elevated temperature. However, by using the room temperature value found in the literature, an approximation was generated assuming the trend indicated by Figure 1.08 [10]. A linear fit was used as the trend with one reference point at room temperature and the other at melt temperature. At melt temperature, the stiffness of the PEEK was assumed to be zero. This approximation is shown in Figure 4.05.

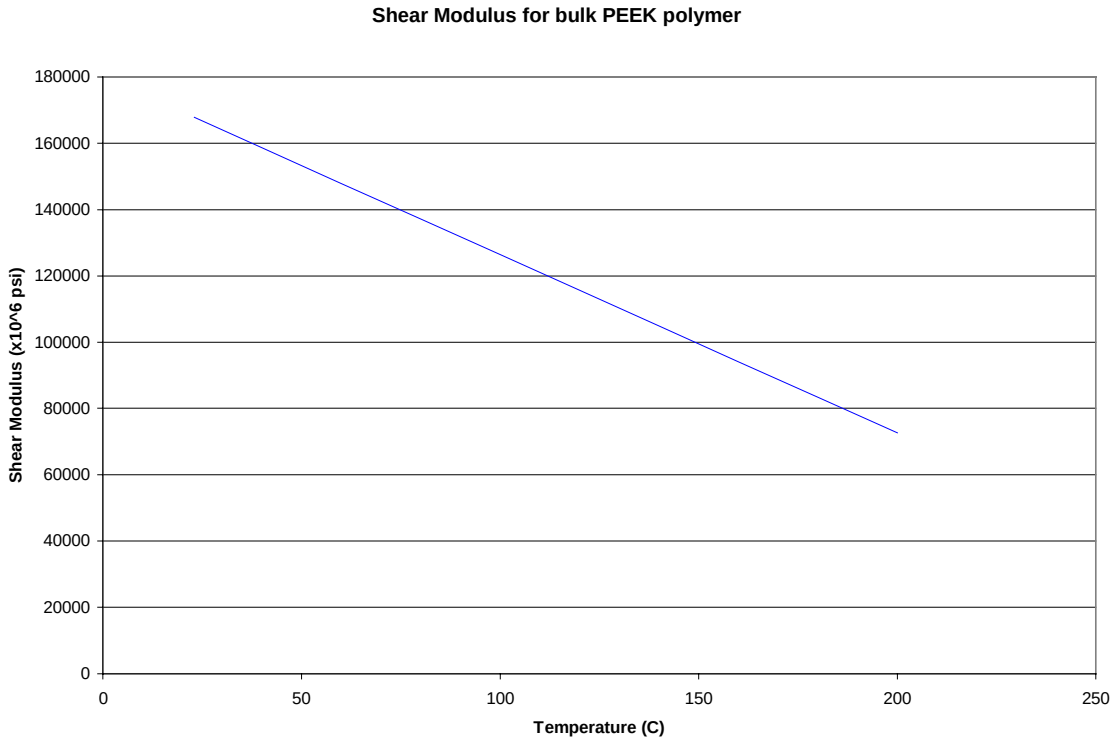

Figure 4.05 Approximation of the shear modulus for PEEK as a function of temperature.

Model Predictions of Strength at Elevated Temperatures

The above variables were put into both models as a function of temperature. The other variables for the PPS and PEEK systems that were used in the models are given in Table 4.01 and 4.02 (also given in Table 1.02). The fiber properties used in the models are given in Table 4.01 and 4.02 (also given in Table 1.01). These are the main variables that must be determined and inserted into both models. The predicted results from the models are shown in Table 4.03 and 4.04 for both the PPS and PEEK systems.

Table 4.01 Input variables for the micro-mechanical models for PPS composite.

Variable Description	Variable Symbol	Value
Matrix Shear Modulus	G_m	180,000 PSI at Room Temperature; Then the function developed above
Interfacial Shear Strength	Tau_m	4407 PSI at Room Temperature; then the function developed above
Fiber Modulus	e_{f2}	34x10^6 PSI
Fiber Volume Fraction	v_f	0.40
Radius of a Single Fiber	r_f	1.378 x 10^-4 in
Total # of Fibers in Composite	n	83627
Fiber Strength Location Parameter	Sig_o	786000 PSI
Efficiency Factor	η	1
Fiber Strength Shape Factor	M	10.65

Table 4.02 Input variables for the micro-mechanical models for PEEK composite.

Variable Description	Variable Symbol	Value
Matrix Shear Modulus	G_m	167,825 PSI at Room Temperature; Then the function developed above
Interfacial Shear Strength	Tau_m	5831 PSI at Room Temperature; then the function developed above
Fiber Modulus	e_{f2}	34x10^6 PSI
Fiber Volume Fraction	v_f	0.39
Radius of a Single Fiber	r_f	1.378 x 10^-4 in
Total # of Fibers in Composite	n	231,329
Fiber Strength Location Parameter	Sig_o	786000 PSI
Efficiency Factor	η	1
Fiber Strength Shape Factor	M	10.65

These inputs were used in the two models along with the derived temperature functions for the interfacial shear strength and the stiffness of the matrix. The predictions from both models can be found in Table 4.03 and 4.04.

Table 4.03 Model strength results for the PPS composite system.

Test Temperature (C)	Average Strength from figure 3.xx (ksi)	Predicted Strength (Model 1 Reifsnider and Gao) (ksi)	Predicted Strength (Model 2 Reifsnider and Subramanian) (ksi)
23-30	241	221	213
60	223	216	208
80	221	213	205
100	220	209	201
120	212	204	198
140	198	197	191

Table 4.04 Model strength results for the PEEK composite system.

Test Temperature (C)	Average Strength from figure 3.xx (ksi)	Predicted Strength (Model 1 Reifsnider and Gao) (ksi)	Predicted Strength (Model 2 Reifsnider and Subramanian) (ksi)
23-27	333	393	367
60	308	389	363
80	317	386	361
100	296	383	359
120	301	381	357
160	299	374	349

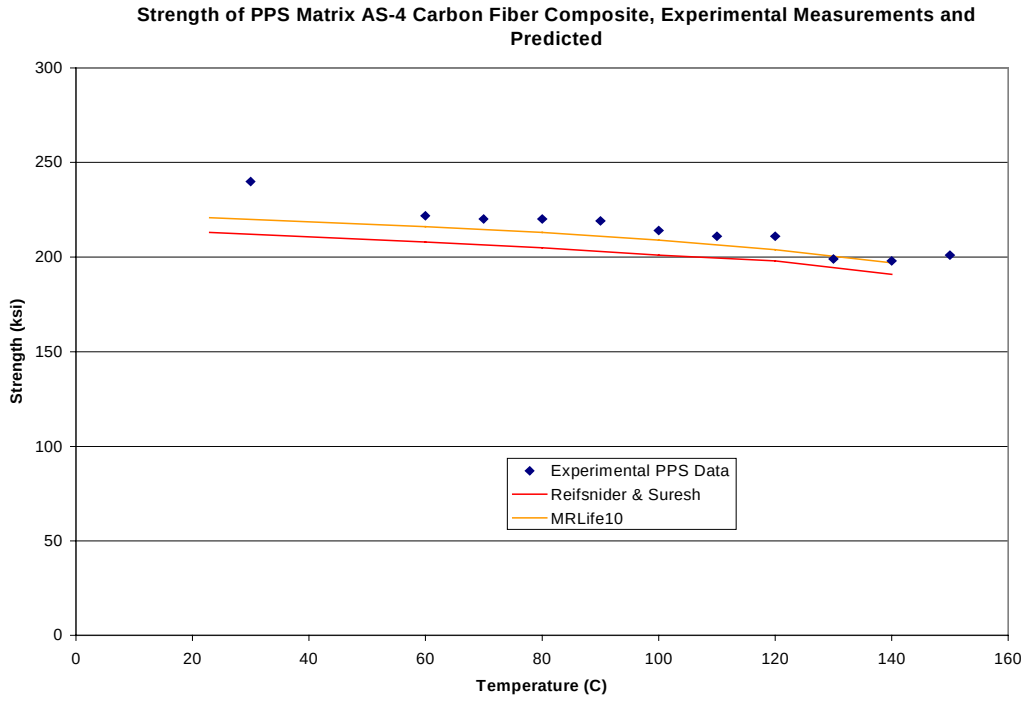

Figure 4.06 Experimental data for PPS compared to model predictions of strength.

As shown in Figure 4.06, both models under-predict the average strength of the PPS composite system. However, both of the models' predictions are within the experimental scatter of this system. Both models predict a 10 percent decrease in strength from room temperature to 140 degrees Celsius. A R-squared linear fit for model #2 gave a slope of -0.18 and a R-square value of 0.96. The same fit for model #1 gave a slope of -0.19 and a R-square value of 0.96. The experimental results showed a 17 percent decrease in this temperature range for the PPS composite system. A R-squared linear fit for the average experimental data gave a slope of 0.32 and a R-square value of 0.93. This difference could be a result of several factors. One such factor is that the interfacial shear strength and the shear modulus assumptions in Figures 4.02 and 4.03 are not accurate. More information must be determined to eliminate the guesswork for these variables. Another factor could be due to the fact that the temperature is effecting more variables than the interfacial shear strength and the matrix stiffness. Maybe the models have not taken into account all the variables that control the strength.

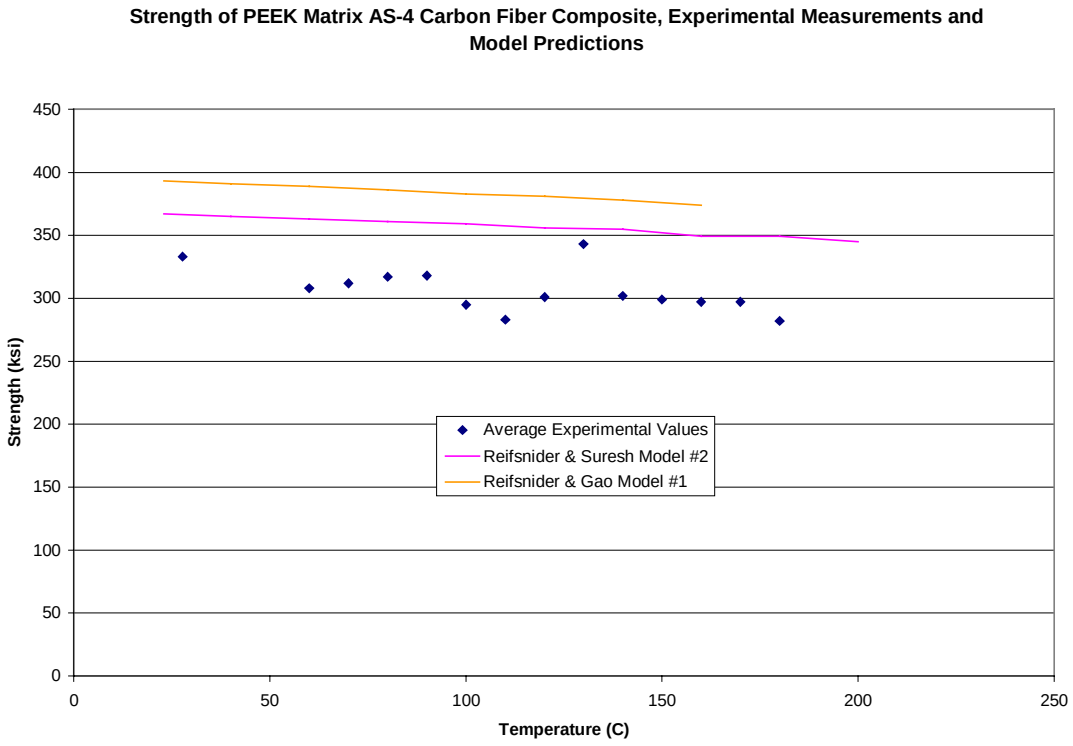

Figure 4.07 Experimental data for PEEK composite compared to model predictions of strength.

For the PEEK, both models over estimated the average experimental strength value (Figure 4.07). Both of the models' predictions did not fall within the experimental values for this system. Additionally, both models predict a 5 percent decrease in strength from room temperature to 160 degrease Celsius for this system. A R-squared linear fit for model #2 gave a slope of -0.12 and a R-square value of 0.98. The same fit was applied to model #1 gave a slope of -0.13 and a R-square value of 0.99. The experimental results showed a 10 percent decrease in strength. A R-squared linear fit for the average experimental data gave a slope of -0.20 and a R-square value of 0.29. This could be due to the same factors discussed for the PPS system.

V. Summary, Conclusions, and Future Work

Summary of Method

In order to predict the strength of a polymer composite in an environment of elevated temperature, the temperature dependence of the two main variables must be determined. These variables are the interfacial shear strength and the shear modulus of the matrix material. If the information is not available then an approximation can be used for these values. After these variables are determined, the micro-mechanical models can be used to predict the temperature response of the composite system.

Conclusions

Based on these three systems, the strength of unidirectional polymer composite systems can be expected to decrease with elevated temperatures between room temperature and the glass transitional temperature. In addition to the strength the stiffness of these systems can also be expected to decrease. The strength decrease can be expected to be more than the stiffness decrease. For each of these materials, the ineffective length is being increased as the temperature is elevated. This is concluded because the matrix stiffness decreases. The change in the fracture mode of vinyl ester also leads to this conclusion.

The vinyl ester system at the lower temperatures failed with more of the fibers grouped together. At the higher temperatures, the fracture was less clumped with groups of fibers and consisted more of single fibers. In this case, ineffective lengths were larger and fiber fracture regions interacted more readily to cause failure.

Based on recent research efforts, the interfacial shear strength of a polymer matrix and a carbon fiber can be expected to decrease with elevated temperatures. The interfacial strength and stiffness also controls the ineffective length. In addition to the interfacial shear strength, the stiffness of a polymer can be expected to decrease with elevated temperatures. The combination of these effects can be placed in micro-mechanical models to give a reasonable prediction. Therefore, this method is a viable for predicting the failure strength of unidirectional polymer carbon fiber composite systems.

Future Work

More work should be done on the interfacial shear strengths as a function of temperature. The accuracy of this parameter can make models more accurate in their predictions. In addition, the stiffness as a function of temperature of PPS and PEEK must be more accurately determined. These variables should also be explored for cryogenic temperatures.

The study involved the response of strength in the tensile fiber direction. Additional information of the effect of elevated temperatures should be explored for off-axis (+45/-45) orientations. This type of test would produce the macro-mechanical shear modulus of the composite as a function of temperature. It also will produce a shear strength of the composite as a function of temperature. A panel of the same PEEK (AS-

4) in this study has been produced with this lay-up. The lay-up of this panel is a symmetric sixteen-ply +45/-45 orientation. CEA-06-125UW-350 strain gages have been placed on the specimens with M-Bond 600.

This same method should apply to the cryogenic temperatures. More data should be obtained at these temperatures. The chamber for this environment should be further advanced and better controlled. At cryogenic temperatures, the ineffective length should be small and this will cause higher stress concentrations.

An additional material should be investigated for its response at elevated temperatures. This material should be an epoxy system with carbon fibers (AS-4). This system is ideal to test this method due to the fact that the interfacial shear strength is given for this particular system as a function of temperature (Figure 1.06). In addition to the known interfacial shear strength, the stiffness of this material is known as a function of temperature. For this study, two different panels have been produced with different cure cycles. These different processes are given in Figures 5.01 and 5.02. The material was donated by Adhesive Prepregs for Composites Manufacturers. It is identified by the name DA 4518U and is a toughened modified epoxy resin system. This material was processed in the platen hot press with a lay-up of seven-ply unidirectional fiber orientation.

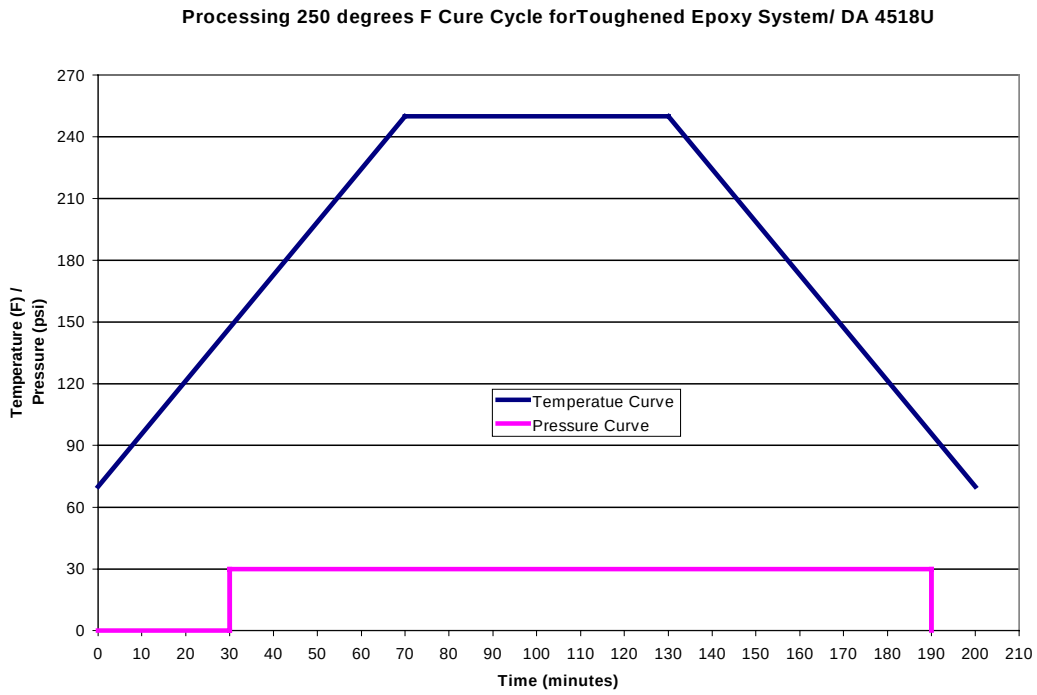

Figure 5.01 Processing for 350 degrees F cure cycle for toughened epoxy.

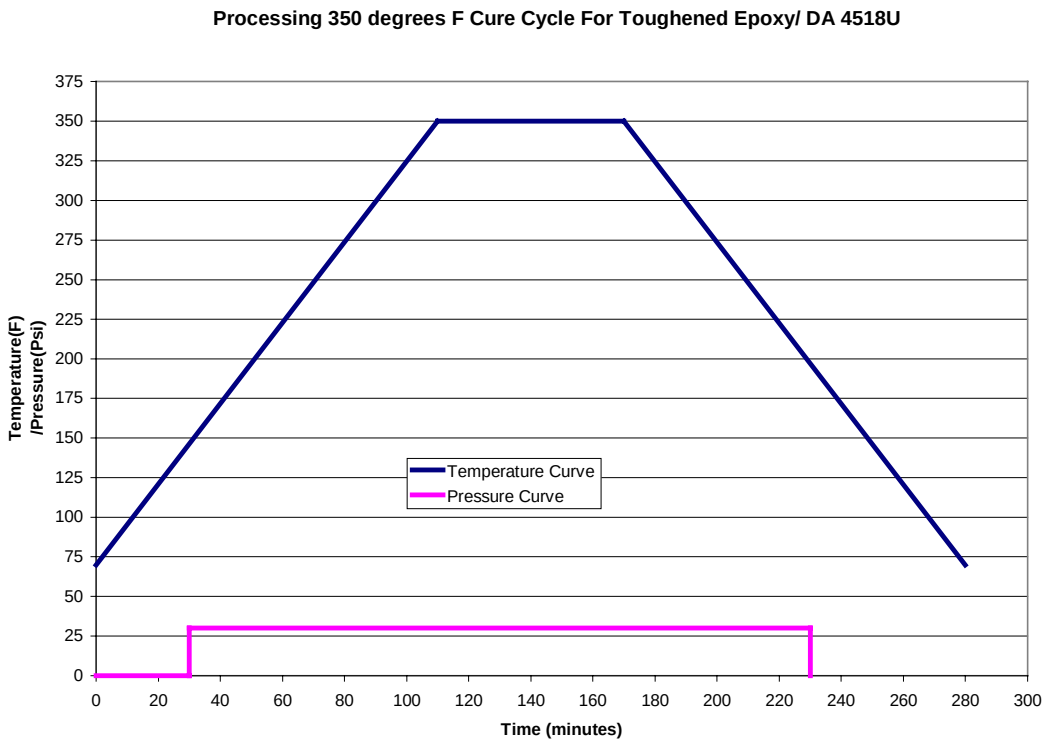

Figure 5.02 Processing for 250 degrees F cure cycle for toughened epoxy.

REFERENCES:

1. Subramanian, S., Reifsnider, K.L., and Stinchcomb, W.W., “Tensile Strength of Unidirection Composites: The Role of Efficiency and Strength of Fiber-Matrix Interface,” *Journal of Composites Technology & Research*, JCTRER, Vol.17,No. 4, October 1995, pp. 239-300.

2. MRLife10, *"A Strength and Life Prediction Code for Laminated Composite Materials,"* S. Case and K.L. Reifsnider, Materials Response Group, Virginia Polytechnic Institute and State University, 1997.

3. Gao, Z., and Reifsnider, K.L., “Micromechanics of Tensile Strength in Composite Systems,” *Composite Materials: Fatigue and Fracture, Fourth Volume,* ASTM STP 1156, W.W. Stinchcomb and N.E. Ashbaugh, Eds., American Society for Testing and Materials, Philadelphia, 1993, pp. 453-470.

4. Reifsnider K.L., ESM 6104 Class Notes, Department of Engineering Science and Mechanics, Virginia Polytechnic Institute & State University.

5. Reifsnider, K.L., Case, Scott, “Mechanics of Temperature-Driven Long-Term Environmental Degradation of Polymer-Based Composite Systems,” Department of Engineering Science and Mechanics, *Virginia Polytechnic Institute and State University*, Blacksburg, Virginia.

6. NASA Contractor Report # 178272, *"Time-Temperature-Stress Capabilities of Composite Materials for Advanced Supersonic Technology Application,"* J.R. Kerr and J.F. Haskins, NASA, May 1987.

7. H. Zhuang and J.P. Wightman, "The Influence of Surface Properties on Carbon Fiber / Epoxy Matrix Interfacial Adhesion," *Journal of Adhesion*, 1996, Vol. 62, pp. 213-245.

8. A.S. Wimolkiatisak and J. P. Bell, "Interfacial Shear Strength and Failure Modes of Interphase-Modified Graphite-Epoxy Composites," *Polymer Composites*, June 1989, Vol. 10, No.3, pp. 162-172.

9. Charles A. Harper, "Handbook of Plastics, Elastomers, and Composites," Third Edition, McGraw-Hill Companies, Inc., 1996.

10. P.K. Mallick, "Fiber-Reinforced Composites," Second Edition, Marcel Dekker, Inc., 1993.

11. A.J. Kinloch, *"Adhesion and Adhesives,"* Chapman & Hall, London, 1987

12. ASTM Designation D 3039/D 3039M - 93, "*Standard Test Method for Tensile Properties of Polymer Matrix Composite Materials,"* 1993

13. S. L. Chuang and Ning-Jo Chu, "Effect of Polyamic Acids on Interfacial Shear Strength in Carbon Fiber / Aromatic Thermoplastics," *Journal of Applied Polymer Science,* Vol. 41, 1990, pp. 373-382.

APPENDIX A: PPS RAW DATA

Specimen Name	Temperature Tested (C)	Temperature (F)	Strength Psi	Gage Modulus (10^6 psi)	Ex. Modulus (10^6 psi)	Loading Rate (lbs/sec)	Tab Type
ws-a60a	60.2	140.36	202437.5		Did not me	50	Glass
ws-b60b	59.9	139.82	209205		Did not me	50	Glass
ws-c60c	59.9	139.82	221413.1		Did not me	50	Glass
ws-d60d	59.9	139.82	196244.5		Did not me	50	Glass
ws-e70a	70	158	206065.6		Did not me	50	Glass
ws-f70b	70	158	206346.6		Did not me	50	Glass
ws-g70c	70	158	214607		Did not me	50	Glass
ws-h70d	69.9	157.82	193349.2		Did not me	50	Glass
ws-i80a	79.9	175.82	205992.8		Did not me	50	Glass
ws-j80b	80	176	200483.3		Did not me	50	Glass
ws-k80c	79.9	175.82	222948.1		Did not me	50	Glass
ws-l80d	79.9	175.82	197695.2		Did not me	50	Glass
ws-m90a	89.9	193.82	195169.6		Did not me	50	Glass
ws-n90b	89.9	193.82	190907.6		Did not me	50	Glass
ws-o90c	89.9	193.82	211974.9		Did not me	50	Glass
ws-p90d	90	194	212501		Did not me	50	Glass
ws-q100a	99.9	211.82	198961		Did not me	50	Glass
ws-r100b	99.9	211.82	207380.1		Did not me	50	Glass
ws-s100c	99.9	211.82	205883		Did not me	50	Glass
ws-t100d	99.9	211.82	206040.8		Did not me	50	Glass
ws-u110a	111	231.8	194857.6		Did not me	50	Glass
ws-v110b	109.9	229.82	182705.8		Did not me	50	Glass
ws-w110c	110	230	205955.5		Did not me	50	Glass
ws-x110d	110	230	184403.9		Did not me	50	Glass
ws-y120a	119.9	247.82	197180.8		Did not me	50	Glass
ws-z120b	119.9	247.82	206970		Did not me	50	Glass
ws-aa120c	119.9	247.82	209216.7		Did not me	50	Glass
ws-bb120d	119.9	247.82	195640.5		Did not me	50	Glass
ws-cc130a	130	266	165271.2		Did not me	50	Glass
ws-dd130b	129.8	265.64	186699.5		Did not me	50	Glass
ws-ee130c	130	266	194263.4		Did not me	50	Glass
ws-ff130d	130.2	266.36	185471.2		Did not me	50	Glass
ws-gg140a	140	284	185640.6		Did not me	50	Glass
ws-hh140b	139.7	283.46	182226.3		Did not me	50	Glass
ws-ii140c	139.6	283.28	183875		Did not me	50	Glass
ws-jj140d	139.7	283.46	178481		Did not me	50	Glass
ws-kk150a	149.7	301.46	189139.1		Did not me	50	Glass
ws-ll150b	149.8	301.64	184408.8		Did not me	50	Glass
ws-mm150	149.9	301.82	188391.4		Did not me	50	Glass

Specimen Name	Temperature Tested (C)	Temperature (F)	Strength Psi	Gage Modulus (10^6 psi)	Ex. Modulus (10^6 psi)	Loading Rate (lbs/sec)	Tab Type
ws-nn150d	149.7	301.46	195223		Did not me	50	Glass
ws-sfa	33.6	92.48	252263			NA	AL-Screen void
ws-sfb	75	167	233632			NA	AL-Screen void
ws-sfc	92	197.6	234766.9			NA	AL-Screen void
ws-sfd	90	194	219610.9			NA	AL-Screen void
ws-sfe	34.3	93.74	239417			NA	AL-Screen void
ws-sff	31.7	89.06	243357		13.525	40	AL-Screen
ws-sfg	30	86	233125		13.19	40	AL-Screen
ws-sfh	30.4	86.72	245829			NA	AL-Screen
ws-sfi	30.4	86.72	245876.5		13.32	40	AL-Screen
ws-sfj	60.4	140.72	230172		12.354	40	AL-Screen
ws-sfk	71	159.8	234608		13.069	40	AL-Screen
ws-sfl	80	176	247824		13.138	40	AL-Screen
ws-sfm	90.8	195.44	224084		12.366	40	AL-Screen
ws-sfn	100.7	213.26	228530		11.937	40	AL-Screen
ws-sfo	110	230	216137		11.784	40	AL-Screen
ws-sfp	120	248	216260		11.417	40	AL-Screen
ws-sfq	129.7	265.46	212301		12.918	40	AL-Screen
ws-sfr	139.6	283.28	199424		12.163	100	AL-Screen void
ws-sfs	80.8	177.44	231083			NA	AL-Screen void
ws-sft	82	179.6	216435		13.372	100	AL-Screen
ws-sfu	90	194	230179		13.372	100	AL-Screen
ws-sfv	90	194	219480		12.019	100	AL-Screen
ws-sfx	90	194	221564			NA	AL-Screen
ws-23a	24	75.2	256424			40	AL-Screen
ws-23b	24	75.2	249005			40	AL-Screen
ws-23c	24	75.2	237827			40	AL-Screen
ws-23d	24.2	75.56	234080			40	AL-Screen
ws-90nt	89.9	193.82	217912			40	AL-Screen
ws-110nt	110	230	230841			40	AL-Screen
ws-78ppsa	59.9	139.82	200558		12.529	100	AL-Screen
ws-78ppsb	60	140	249231		12.562	100	AL-Screen
ws-78ppsc	59.9	139.82	255095		12.058	40	AL-Screen
ws-78ppsd	69.9	157.82	213353		12.296	40	AL-Screen
ws-78ppsf	70	158	231468		11.62	40	AL-Screen
ws-78ppsg	80	176	212138		12.265	40	AL-Screen
ws-78ppsh	79.3	174.74	223720		11.98	40	AL-Screen
ws-78ppsi	88.7	191.66	207451		11.561	40	AL-Screen
ws-78ppsj	88.7	191.66	232306		12.288	40	AL-Screen
ws-78ppsk	99.6	211.28	217247		12.176	40	AL-Screen

Specimen Name	Temperature Tested (C)	Temperature (F)	Strength Psi	Gage Modulus (10^6 psi)	Ex. Modulus (10^6 psi)	Loading Rate (lbs/sec)	Tab Type
ws-78ppsl	98.6	209.48	217673		11.959	40	AL-Screen
ws-78ppsm	108.6	227.48	216316		n/a	40	AL-Screen
ws-78ppsn	109	228.2	224554		12.067	40	AL-Screen
ws-78ppso	119.6	247.28	234583		12.112	40	AL-Screen
ws-78ppsp	119.6	247.28	200936		12.401	40	AL-Screen
ws-78ppsq	128.6	263.48	211534		11.862	40	AL-Screen
ws-78ppsr	129.2	264.56	210438		12.165	40	AL-Screen
ws-78ppss	139.1	282.38	208816		12.126	40	AL-Screen
ws-78ppst	139.2	282.56	196695		12.832	40	AL-Screen
ws-718a	69.9	157.82	232685		11.954	100	Glass
ws-718b	79.7	175.46	219568		12.342	100	Glass
ws-718c	90	194	235871		12.383	100	Glass
ws-718d	99.4	210.92	224690		12.605	40	Glass
ws-718e	109.7	229.46	220594		12.394	40	Glass
ws-718f	119.8	247.64	215739		11.844	40	Glass
ws-718g	129.2	264.56	216234		10.288	40	Glass
ws-718h	139.1	282.38	221262		n/a	40	Glass
ws-718i	149.5	301.1	207845		12.301	40	Glass
ws-718j	32.5	90.5	240505		12.192	40	Glass
ws-78ppsv	149.2	300.56	210904		13.917	40	AL-Screen
ws-78ppsx	149.1	300.38	222977		13.577	40	AL-Screen
ws-81a	31.1	87.98	221697		12.053	150	AL-Screen
ws-81b	31.1	87.98	235144		12.12	150	AL-Screen
ws-81c	31.1	87.98	239167		11.73	150	AL-Screen
ws-81d	31.1	87.98	243687		12.62	150	AL-Screen
ws-81e	59.9	139.82	225760		12.206	150	AL-Screen
ws-81f	59.9	139.82	235443		12.357	150	AL-Screen
ws-81g	59.9	139.82	233709		11.918	150	AL-Screen
ws-81h	59.9	139.82	213313		12.253	150	AL-Screen
ws-81i	69.5	157.1	217467		12.358	150	AL-Screen
ws-81j	69.6	157.28	227339		12.214	150	AL-Screen
ws-81k	69.6	157.28	236750		13.893	150	AL-Screen
ws-81l	69.5	157.1	230590		11.89	150	AL-Screen
ws-81m	79.4	174.92	225825		12.023	150	AL-Screen
ws-81n	79.4	174.92	224869		12.87	150	AL-Screen
ws-81o	79.7	175.46	238901		11.181	150	AL-Screen
ws-81p	79.9	175.82	225000		11.789	150	AL-Screen
ws-81q	89.5	193.1	237083		12.772	150	AL-Screen
ws-81r	89.2	192.56	237164		12.116	150	AL-Screen
ws-81s	89.4	192.92	220410		11.997	150	AL-Screen

Specimen Name	Temperature Tested (C)	Temperature (F)	Strength Psi	Gage Modulus (10^6 psi)	Ex. Modulus (10^6 psi)	Loading Rate (lbs/sec)	Tab Type
ws-81t	89.3	192.74	210621		11.706	150	AL-Screen
ws-81u	99.5	211.1	233791		11.944	150	AL-Screen
ws-81v	99.4	210.92	193856		n/a	150	AL-Screen
ws-81w	99.2	210.56	219858		11.726	150	AL-Screen
ws-81x	99.2	210.56	224435		12.212	150	AL-Screen
ws-81y	108.6	227.48	217192		11.745	150	AL-Screen
ws-81z	110.4	230.72	208218		12.08	150	AL-Screen
ws-81aa	110.4	230.72	222638		11.781	150	AL-Screen
ws-81bb	110.3	230.54	222071		12.345	150	AL-Screen
ws-81cc	120.4	248.72	210631		12.357	150	AL-Screen
ws-81dd	120.8	249.44	221972		12.428	150	AL-Screen
ws-81ee	120.3	248.54	203869		11.62	150	AL-Screen
ws-81ff	120.3	248.54	224656		11.832	150	AL-Screen
ws-81gg	130.4	266.72	210819		11.735	150	AL-Screen
ws-81hh	130.2	266.36	209351		n/a	150	AL-Screen
ws-81ii	130.6	267.08	212332		11.893	150	AL-Screen
ws-81jj	130.3	266.54	181338		11.959	150	AL-Screen
ws-81kk	140.3	284.54	197345		12.337	150	AL-Screen
ws-81LL	140	284	200964		12.721	150	AL-Screen
ws-81mm	140.1	284.18	208300		12.099	150	AL-Screen
ws-81nn	139.9	283.82	214339		11.588	150	AL-Screen
ws-81oo	150.3	302.54	215732		12.246	150	AL-Screen
ws-81pp	150.1	302.18	208753		11.914	150	AL-Screen
ws-81qq	149.9	301.82	218083		12.776	150	AL-Screen
ws-81rr	149.4	300.92	201064		12.153	150	AL-Screen
ws81ss	33.4	92.12	241576	12.313	12.056	150	AL-Screen
ws-81tt	33.8	92.84	242819	12.243	11.514	150	AL-Screen
ws-81uu	31.9	89.42	238823	12.983		150	AL-Screen
ws-81vv	31.9	89.42	247867	12.449		150	AL-Screen
ws-81ww	184.3	363.74	197868			150	AL-Screen
ws-81xx	202	395.6	202189			80	AL-Screen
ws-81yy	214	417.2	201908			40	AL-Screen
ws-81zz	220	428	210493			40	AL-Screen
ws-81aaa	227.4	441.32	189166			80	AL-Screen
ws-81bbb	229	444.2	207601			80	AL-Screen
ws-912b	30	86	225344			50	AL-Screen
ws-912c	140	284	222529			50	AL-Screen

Specimen Name	Temperature Tested (C)	Temperature (F)	Strength Psi	Gage Modulus (10^6 psi)	Ex. Modulus (10^6 psi)	Loading Rate (lbs/sec)	Tab Type
ws-912d	159.9	319.82	212621			50	AL-Screen
ws-912e	119.5	247.1	213968	11.767		50	AL-Screen
ws-912f	99.5	211.1	219003	11.919		50	AL-Screen
ws-912g	150.3	302.54	220627			50	AL-Screen
ws-912h	89.8	193.64	230160	12.491		50	AL-Screen
ws-912k	159.9	319.82	211474			50	AL-Screen
ws-912l	109.6	229.28	219153	12.216		50	AL-Screen
ws-912m	129.2	264.56	224527	12.773		50	AL-Screen
ws-912n	80	176	235518	12.597		50	AL-Screen
ws-912o	60	140		12.528		50	AL-Screen
ws-912p	69.9	157.82	222953	11.826		50	AL-Screen
ws-cl1	-142.7	-225	176000	NA		100	AL-Screen
ws-cl2	-184	-300	240700	NA		50	AL-Screen
ws-cl3	-184	-300	266000	NA		50	AL-Screen

APPENDIX B: PEEK RAW DATA

Specimen name	Temperature (C)	Strain Gage of Modulus(x10^6) psi	Extensometer Modulus (x10^6) psi	Ultimate Stress (ksi)	Load Rate (lbs/sec)	Tab Type	Grip Pressure psi	Strain@ Failure
PK-A101	60.6	18.908	20.262	270	50	Glass	1000	0.0143
PK-B101	60.6	21.031	22.584	320	50	Glass	1000	0.0145
PK-C101	149.8	21.001	21.534	302	50	Glass	1000	0.0142
PK-D101	150	21.242	21.13	296	50	Glass	1000	0.0137
PK-E101	100.1	NA	22.821	247	50	Glass	1000	NA
PK-F101	100	21.338	22.113	344	50	Glass	1000	0.0155
PK-G101	140	22.132	22.68	343	50	Glass	1000	0.0155
PK-H101	159.4	21.733	22.654	289	50	Glass	1000	0.0154
PK-I101	159.5	20.136	24.631	306	50	Glass	1000	NA
PK-J101	169.7	21.518	23.712	297	50	Glass	1000	0.0142
PK-K101	27.7	21.711	22.758	300	50	Glass	1000	NA
PK-L101	80.2	21.79	22.389	342	50	Glass	1000	0.0157
PK-H103	119.4	22.007	22.373	293	50	Glass	NA	NA
PK-G103	119.8	21.833	21.941	310	50	Glass	NA	0.0139
PK-E103	60.7	21.303	21.58	335	50	Glass	NA	0.0147
PK-D103	27.7	21.958	21.687	327	50	Glass	NA	0.0146
PK-C103	27.3	21.943	22.008	362	50	Glass	NA	0.0154
PK-B103	27.8	21.614	21.224	357	50	Glass	NA	0.0157
PK-A103	27.7	21.639	23.349	339	50	Glass	NA	0.0142
PK-O101	178.5			281	50	Glass	1000	
PK-P101	159.4			304	50	Glass	1000	
PK-A102	109.7	19.018	NA	283	50	Glass	1000	0.0144
PK-B102	80	20.415	21.379	320	50	Glass	1000	0.0147
PK-C102	80.1	21.295	NA	290	50	Glass	1000	0.0131
PK-D102	70.3	21.433	23.105	302	50	Glass	1000	0.014
PK-E102	70.4	21.861	21.484	304	50	Glass	1000	0.0135
PK-F102	27.7	21.349	22.106	314	50	Glass	1000	0.0139
PK-G102	70.6	21.708	22.857	330	50	Glass	1000	0.0144
PK-H102	90	21.475	23.326	318	50	Glass	1000	0.0142
PK-I102	179.8	NA	NA	284	50	Glass	1000	NA
PK-J102	190	NA	NA	269	50	Glass	1000	NA

APPENDIX C: VINYL ESTER RAW DATA

Specimen name	Temperature (C)	Ultimate Stress (psi)	Load Rate (lbs/sec)	Modulus (x10^6) psi	Tab Type
ve-zteca	70	107663	100	14.659	Al-Wire
ve-ztecb	90	104445	100	14.956	Al-Wire
ve-ztecc	110	88302	100	14.669	Al-Wire
ve-ztecd	130	83556	100	14.558	Al-Wire
ve-ztece	140	76157	100	14.618	Al-Wire
ve-ztecf	35	118092	100	16.23	Al-Wire
ve-ztech	90	99144	100	15.826	Al-Wire
ve-zteci	110	89696	100	14.11	Al-Wire
ve-ztecm	-123.3	131522	100	NA	Al-Wire
ve-ztecl	69.8	104961	40	NA	Al-Wire
ve-ztecj	32.2	100977	40	NA	Al-Wire
ve-puc	90	124828	100	17.052	Al-Wire
ve-pud	109.3	129861	100	16.773	Al-Wire
ve-pue	129.7	121691	100	16.303	Al-Wire
ve-puf	149.7	108788	100	NA	Al-Wire
ve-pug	-101	155987	100	17.695	Al-Wire
ve-pui	-184.4	165400	100	18.109	Al-Wire
ve-puj	-184.4	180600	100	18.68	Al-Wire
ve-puk	-184.4	180800	100	19.4	Al-Wire
ve-pua	33.4	161167	100	17.7	Al-Wire
ve-pub	34	159591	100	18.4	Al-Wire

VITA

Brady M. Walther was born on August 17, 1971 to Jane and Phillip M. Walther in Columbus, OH. After eighteen years in Gahanna Ohio, he graduated from Gahanna Lincoln High School in spring of 1990. Brady then went to Emory & Henry College in Emory Virginia in the fall of 1990. He also enrolled at the University of Tennessee at Knoxville in the fall of 1992. Mr. Walther graduated with Bachelor of Science degree from institutions in spring 1996. He majored in Physics, Mathematics, and Engineering Science and Mechanics. In the fall of 1996, Brady enrolled in the Graduate School of Virginia Polytechnic Institute and State University under the program of Engineering Mechanics. In the summer of 1998, Mr. Walther graduated with a Master of Science degree.